THE UNIVERSITY OF OKLAHOMA

GRADUATE COLLEGE

SAND MOVEMENT IN HORIZONTAL FRACTURES

A DISSERTATION

SUBMITTED TO THE GRADUATE FACULTY

in partial fulfillment of the requirements for the

degree of

DOCTOR OF PHILOSOPHY

BY

HARRY ALBERT WAHL

Norman, Oklahoma

1963

SAND MOVEMENT IN HORIZONTAL FRACTURES

APPROVED BY

J. W. Campbell

A. L. Hamilton

L. W. Reid

Richard Fowler

and

William N. Tuffle

DISSERTATION COMMITTEE

ACKNOWLEDGMENT

Special appreciation is expressed to Dr. John M. Campbell, chairman of the doctoral committee, for his encouragement, suggestions, and advice.

The author gratefully acknowledges the management of Continental Oil Company for providing support of the thesis work and permission to release the work.

The author is indebted to The Shell Oil Company for their financial support of this work on campus.

The assistance of Bill Moyer and Ralph Strode in the construction and operation of the test equipment is particularly appreciated.

Harry Albert Wahl

TABLE OF CONTENTS

LIST OF TABLES

LIST OF ILLUSTRATIONS

SAND MOVEMENT IN HORIZONTAL FRACTURES

CHAPTER I

INTRODUCTION AND LITERATURE REVIEW

This study was initiated to provide important information on the flow of solid-liquid slurries in horizontal fractures. Data obtained on rate of sand advance and pressure behavior will prove valuable in the design of hydraulically induced formation fractures. A comprehensive photographic study was undertaken in a 10-foot long transparent flow cell to provide an insight into the basic flow mechanisms involved.

Hydraulic fracturing is the most successful well stimulation technique in the oil industry. This process was introduced in 1948 and has increased the oil reserves in the Western Hemisphere by approximately 5 1/2 billion barrels. The key to its success is not just the hydraulic disruption of the oil bearing formations but lies in the ability to prop the fracture and keep it open after the pressure is released. The pressure parting of formations has been observed in water injection wells since the 1920's. However, below a given pressure the formation heals and essentially no residual permeability due to the splitting of the rock remains.

Despite this dependency upon propping agents, very little is known about the mechanics of sand placement. There are numerous

theories on the optimum distribution of the propping agent within the fracture. Although these are used in designing fracture treatments, the conditions required to actually achieve the various sand packs have not been determined.

All concepts in fracture propping have one thing in common—the total fracture area created must be propped to obtain maximum treatment efficiency. Although engineering techniques are available to estimate the areal extent of fractures from treatment conditions and properties of the fracture fluid and formation (14,32), there is no method available to estimate the portion of this area that is propped.

The complexity and scope of the problem have deterred research efforts in this area. Difficulties in obtaining consistent data for slurry flow in circular pipes have been shown by Durand (8) and Newitt et al. (22) Sand transport in fractures is more difficult because the dimensions of the conduit are unknown. Even the general configuration of the fracture is a source of disagreement.

In this study, only flow through horizontal fractures is considered. Of the two extremes of fracture orientation, this is the more difficult case. Sand transport within a vertical fracture may be estimated by considering a thin vertical segment of a rectangular conduit in which a slurry is flowing. This approach, however, cannot be applied to a horizontal segment because of the variation in solids concentration in the vertical direction.

Fracturing fluid loss to the formation and variations in fracture thickness affect velocity distribution. For horizontal fractures the velocity distribution is further complicated by the geometry

of the system. If the fractures are created in a more or less radial pattern, velocity at a given point will also be a function of the distance from the well bore.

Because of the complexity of the problem, any single study of slurry flow in fractures must, by necessity, be limited in scope. The fact that very limited data are available on sand transport in fractures increases the importance of the literature search in this and associated fields.

Fluid Flow Between Parallel Plates

Although little basic work has been reported on the flow of fluids in fractures, a real insight into the problem may be afforded by a review of available data for flow between parallel plates. The geometric similarity between the systems would indicate that the two systems have at least some factors in common. Davis and White (6) investigated the flow of water in rectangular pipes of various dimensions. Their study covered a Reynolds number range from 60 to 4,500. Page et al (24), studying temperature gradients in gas streams flowing between parallel glass plates, reported flow data in the Reynolds number range of 7,000 to 60,000. Whan and Rothfus (34), using broad parallel plates, studied the characteristics of flow during the transition from fully laminar to fully turbulent flow. The combined scope and range of these three studies are normally sufficient to adequately describe isothermal single phase fluid flow in smooth fractures. If it is assumed that horizontal fractures are extended in all directions in a general radial pattern, very low velocities can exist at the fracture extremities. Although little experimental data are available for low Reynolds numbers,

expressions describing laminar flow between parallel plates may be developed from theoretical considerations.

Isothermal laminar flow between two infinite parallel planes is described by the following differential equation:

$$g_c \frac{\partial P}{\partial x} = \mu \frac{\partial^2 v}{\partial y_c^2} \tag{1}$$

In Figure 1, flow is in the x direction with the mid-plane between the bounding planes coinciding with the horizontal xz plane. If the distance between the planes is b, the following boundary conditions exist:

$$\text{At } y_c = 0 \quad \frac{\partial v}{\partial y_c} = 0 \tag{2a}$$

$$\text{At } y_c = \frac{b}{2} \quad v = 0 \tag{2b}$$

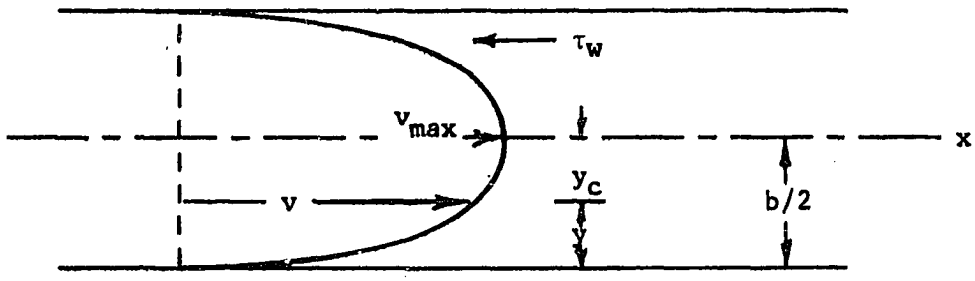

Figure 1 - Velocity Distribution for Laminar Flow Between Parallel Plates

Integrating equation (1) and using the boundary conditions given above:

$$v = -\frac{g_c}{2\mu} \frac{\partial P}{\partial x} \left[\left(\frac{b}{2} \right)^2 - y_c^2 \right] \tag{3}$$

The average bulk velocity v_B is obtained by integrating equation (3) between the limits $y_c = 0$ and $y_c = b/2$ and dividing the result by b/2:

$$v_B = -\frac{g_c}{3\mu} \frac{\partial P}{\partial x} \left(\frac{b}{2} \right)^2 \tag{4}$$

Equations (3) and (4) may be solved to yield:

$$v = \frac{3v_B}{2}\left[1 - \frac{y_c^2}{(b/2)^2}\right] \tag{5}$$

Since the maximum point velocity occurs at $y_c = 0$:

$$v_{max} = \frac{3v_B}{2} \tag{6}$$

Equation (5) expresses the point velocity between the two planes as a function of the average velocity of flow and the thickness of the simulated fracture. The solution to this equation is given by the velocity distribution curve in Figure 1. Equation (6) shows that the maximum velocity occurring at $y_c = 0$ is equal to 1.5 times the average or bulk velocity.

For a Newtonian fluid, the shear stress on the fluid is:

$$\tau = -\frac{\mu}{g_c}\frac{dv}{dy} \tag{7}$$

Differentiating equation (5) with respect to y_c and combining with equation (7):

$$\tau = \frac{3\mu v_B y_c}{g_c(b/2)^2} \tag{8a}$$

and

$$\tau_w = \frac{3\mu v_B}{g_c(b/2)} \tag{8b}$$

The pressure loss due to friction can be related to the shear at the wall by:

$$\frac{-dP}{dx} = \frac{\tau_w}{(b/2)} \tag{9}$$

Combining the last two equations,

$$-\frac{dP}{dx} = \frac{12\mu v_B}{g_c b^2} \tag{10}$$

The Fanning friction factor is defined as

$$f = \frac{g_c D_e}{2\rho v_B^2} \frac{-dP_f}{dx} \tag{11}$$

where D_e is the equivalent diameter of the conduit. The equivalent diameter normally is defined as four times the cross-sectional area occupied by the flowing fluid divided by the wetted perimeter. Thus, for infinite parallel planes, $D_e = 2b$. The Reynolds number for this system is:

$$Re = \frac{2bv\rho}{\mu} \tag{12}$$

Therefore,

$$f = \frac{24\mu}{2bv_B\rho} = \frac{24}{Re} \tag{13}$$

Equation (13) is the theoretical equation expressing the friction factor as a function of the Reynolds number for laminar single phase fluid flow. This expression has been verified experimentally. The equivalent expression for smooth circular conduits differs only in that the value of the constant is 16 instead of 24.

Although this study is primarily focused on the laminar flow range, it is probable that turbulent flow exists in the vicinity of the well bore during the creation of a horizontal fracture. Using the equivalent diameter concept, friction factors for turbulent flow between smooth parallel plates have been shown to be the same as those for smooth circular tubes. The following equation expresses the friction factor as a function of Re for Reynolds numbers from 3,000 to 100,000:

$$f = 0.079\ (Re)^{-0.25} \tag{14}$$

Equation (14) has been shown to predict friction factors in both circular

and noncircular conduits with excellent accuracy within this range of Re. (20)

Fluid Flow in Simulated Fractures

The effect of surface roughness on flow in simulated fractures has been investigated by Huitt. (16) The fractures were constructed by coating steel plates which formed the boundary of the flow cell with Shellac and sprinkling sieved sand on the surfaces. Flow data were obtained for fracture widths of 1.58 to 3.74 mm with relative surface roughness (Z/b) of 0.0446 to 0.156.

Nikuradse (23), who investigated the relative roughness effects of artificially roughened pipe, found that for viscous flow the equation for smooth surface pipe was adequate. Huitt showed that this also applied to fractures. At large Reynolds numbers where f is dependent only on Z/b, the following empirical relationship was developed from flow data on fractures:

$$f = 0.055\ (Z/b)^{0.472} \qquad (15)$$

The f values calculated using this equation are within 15 per cent of the data obtained by Nikuradse for flow under similar conditions in circular pipes. However, this equation is not valid when the friction factor is dependent on both relative roughness and the Reynolds number. This occurs at low Reynolds numbers in the turbulent region of flow when the relative surface roughness is small.

Solids Transport in Circular Pipes

A search of the literature reveals numerous sources of information on the simultaneous flow of solids and fluids. The technique

of hydraulic and pneumatic conveying is quite old. Despite the amount of effort expended in this field, the design of fluidized solids transport systems is still an "art". However, the results of these studies do afford an insight into the flow characteristics of sand in fractures. Their main limitation is that emphasis is placed on suspended flow of the two phases. For the most part, the sand in horizontal fractures should be transported in the deposit flow regime due to the low velocities. In addition, this study is interested in the flow under unsteady state conditions that exist before the sand reaches the end of the model.

Early tests in hydraulic conveying were carried out by Blatch (3) who studied the flow characteristics of 20-40 mesh sand and water in one-inch diameter pipes. This and many subsequent studies are limited in scope and are valid only within the particular set of test conditions.

Durant (8) has attempted to organize and systematically investigate the variables involved in hydraulic solids transport. He correlated the three basic modes of solids transport with the size of particles in the mixture. The transport mechanisms are: (1) homogeneous mixtures, (2) intermediary mixtures, and (3) heterogeneous mixtures.

With the usual solids concentration and flow rates encountered in hydraulic transportation, grains with diameters less than 20 or 30 microns are considered as forming practically homogeneous mixtures with water. Actually, under laminar flow conditions, even fine solids tend to settle out. Homogeneous mixtures, commonly called muds,

possess plastic properties which have been studied by Bingham (2) and others.

Intermediary mixtures are formed with particles from 25 to 50 microns in diameter and are classified in the transition zone between homogeneous and heterogeneous flow. Silt is an example of this particle size range.

Mixtures containing solids over 50 microns in diameter cannot attain total homogeneity even under turbulent flow conditions. Heterogeneous mixtures in turn may be subdivided into three groups. Particles from 50μ to 0.2 mm may be transported in fully suspended flow at normal transport velocities although the concentration in the vertical plane is not uniform. Heterogeneous mixtures transported in the deposit flow regime are formed with solids such as gravel and pebbles above 2 millimeters in diameter. The transition between suspended and deposit flow occurs with particles with diameters from 0.2 to 2 millimeters. The sand sizes normally used in fracturing fall within this range.

It should be noted that the grain size range designated by Durand for the transition from suspended flow to deposit flow closely corresponds to the transition zone between the laws governing the maximum settling velocity of quartz grains in calm water. Grains with diameters less than 0.15 mm settle according to Stokes' law:

$$v_t = \frac{(\rho_p - \rho_l)gd^2}{18\mu} \tag{16}$$

Grains with diameters greater than 1.5 mm follow Newton's law:

$$v_t = \left[\frac{4(\rho_p - \rho_l)gd}{3\rho_l (f_D)}\right]^{1/2} \tag{17}$$

where f_D approaches 0.5 as the Reynolds number, based on particle size, increases.

In designing hydraulic conveying systems, pressure is an important factor. All investigators measured this quantity. A typical curve of head loss versus bulk flow velocity is given in Figure 2.

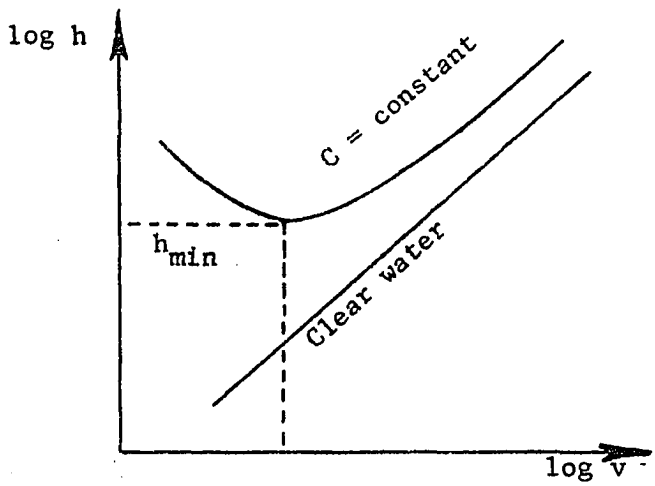

Figure 2 - Typical Pressure Behavior for Slurry Flow in Pipes

The head losses of clear water result in essentially a straight line when logarithmic coordinates are used. The curve for water containing a given concentration of solids diverges more and more from the straight line as velocity decreases. Considering concentration constant, the power requirements to transport a given volume of solids are at a minimum when the head losses are at the minimum. This minimum roughly corresponds to the point separating flow with and without deposits on the bottom of the pipe.

The velocity required to induce this change in flow regime is called the minimum velocity. As the velocity increases, the head loss curves for fine sands transported in suspension approach the clear

water curve. The point at which this occurs is called the standard velocity. Above this velocity, the slurry behaves as a homogeneous liquid. Under these conditions, friction head losses may be calculated using the Fanning equation for turbulent flow. However, the density and viscosity of the suspension should be used in determining the Reynolds number. Head losses incurred in transporting coarse sands and gravel approach a parallel asymptote of the clear water line.

Spells (27) studied the flow of slurries containing solid particles with diameters less than one millimeter. He applied dimensional analysis to the problem of determining the minimum and standard velocities. This indicated that both transitional velocities depend upon a balance between the turbulent forces tending to disperse the solids and the effect of gravity at the bottom of the pipe. The Reynolds number, $\rho vD/\mu$, representing the ratio of inertial to viscous forces, and the Froude number, v^2/dg, representing the ratio of inertial to gravitational forces, were the dimensionless groups used. The inertia of a moving fluid depends upon its absolute density, while the gravitational force acting on the solid particles depends upon the difference between density of the solid and the density of the liquid. Spells modified the Froude number to include the ratio of densities, $\frac{\rho_l}{\rho_p - \rho_l}$. Thus, a dimensionless equation of the form

$$\frac{v^2}{gd}\left(\frac{\rho_l}{\rho_p - \rho_l}\right) = f\left(\frac{vD\rho_s}{\mu_l}\right) \tag{18}$$

was used for the correlation of both the minimum and standard velocities.

Using the data of Blatch and others, he obtained the empirical equation:

$$\frac{v^2}{gd}\left(\frac{\rho_l}{\rho_p - \rho_l}\right) = K\left(\frac{vD\rho_s}{\mu_l}\right)^{0.775} \tag{19}$$

where K = 0.0251 for the minimum velocity and 0.0741 for the standard velocity.

Durand determined the minimum velocity of aqueous mixtures in pipes with diameters from 40 to 700 mm and particles from 0 to 3 mm in diameter. He presented his results by plotting F_L versus grain diameter at various constant concentrations, where:

$$F_L = \frac{v_m}{\sqrt{2gD\left(\frac{\rho_p - \rho_l}{\rho_l}\right)}} \tag{20}$$

For fine and average sized sand (0.05 mm to 1 mm), increases in concentration and grain size tend to increase the value of the minimum velocity. The value of F_L varies from 0.9 to 1.5 within this range. For coarse sand and pebbles (above 1 mm), concentration and grain diameter have practically no influence on the value of F_L. The constant concentration lines rapidly converge to a single horizontal line with a F_L value of 1.34. Therefore, for particles with diameters over 1 mm transported in water:

$$\frac{v_m^2}{gD}\left(\frac{\rho_l}{\rho_p - \rho_l}\right) = 3.59 \tag{21}$$

The dimensionless group in the equation above differs from the left side of equation (19) in that the diameter of the pipe is used in the former while particle diameter is included in the latter.

A more general method of predicting the velocity required to initiate suspended flow in circular pipes is proposed by Thomas. (30) His test results and the data of others indicate that suspended flow

is attained when the ratio of the particle settling velocity to friction velocity at the wall, v_t/v_w^*, is less than 0.20. This criterion is estimated to correspond within 10 per cent of Durand's correlation for suspended flow in sand-water systems under normal transport conditions. Tests were performed under turbulent conditions with solid particles sufficiently large to extend into the turbulent core of the flow stream when resting on the pipe wall. Turbulent fluctuations are considered the primary factor in distributing the solids vertically in the pipe. This correlation was verified for air and water suspensions. No data were obtained for solids suspended in viscous liquids.

Dimensional analysis may be applied to the problem of the friction resistance of slurries. Reynolds number and the modified Froude number used by Spells are pertinent dimensionless groupings. In addition, the laws of settling of particles in calm liquid introduce another dimensionless group. For Stokes' law of settling:

$$K_1 = \frac{gd(\rho_p - \rho_1)}{v_t \mu} \tag{22}$$

or for Newton's law:

$$K_2 = \frac{v_t^2 \rho_1}{gd(\rho_p - \rho_1)} \tag{23}$$

The final group is the concentration of the slurry, C, expressing the volumetric fraction of solids.

Letting Δh_s represent the head loss of the slurry per unit length of pipe, the generalized dimensionless equation for frictional resistance may be written as:

$$\frac{\Delta h_s}{v^2} = f\left(C, \frac{\rho_s v D}{\mu}, \frac{\rho_1 v^2}{gD(\rho_p - \rho_1)}, K\right) \tag{24}$$

where K is K_1 or K_2 depending on which settling law is applicable.

It is convenient to compare the friction loss encountered in pumping a slurry to the loss at the same bulk velocity incurred while handling the pure liquid, Δh. Since $\Delta h = f\ (\rho_1 vD/\mu)$ and $\rho_s/\rho_1 = f\ (C)$, equation (24) may be written as:

$$\frac{\Delta h_s}{\Delta h} = f\left(C,\ \frac{\rho_1 v^2}{gD(\rho_p - \rho_1)},\ K\right) \tag{24a}$$

Durand studied head losses of heterogeneous mixtures in the deposit and suspended flow regime. The results were correlated in terms of a function $\psi = \frac{\Delta h_s - \Delta h}{\Delta h}$. An empirical equation for aqueous slurries was obtained, which may be written as:

$$\psi = 121\ C\left(\frac{gD(\rho_p - \rho_1)}{v_B{}^2}\right)^{1.5}\left(\frac{v_t{}^2}{gd(\rho_p - \rho_1)}\right)^{0.75} \tag{25}$$

Equation (25) has the same form as equation (24) since $\rho_1 = 1$ and $K = K_2 = \frac{v_t{}^2}{gd(\rho_p - \rho_1)}$. Even though his experiments included fine slurries which should obey Stokes' law of settling, Durand's correlation is based upon the assumption that Newton's law governs settling. This may be valid because of the degree of turbulence already existing in the liquid at normal pumping velocities.

Newitt et al (22) also investigated head losses incurred when pumping heterogeneous suspensions. He found that the equation for ψ given below described his test results:

$$\psi = 1100\ C\left(\frac{\rho_p - \rho_1}{\rho_1}\right)\left(\frac{v_t}{v_B}\right)\left(\frac{gD}{v_B{}^2}\right) \tag{26}$$

In the range of Newitt's work, the agreement between equations (25) and (26) is so close that differences are within

experimental error. However, for the larger diameter pipes used by Durand, considerable discrepancy exists. Both equations show that ψ is inversely to the cube of the mean velocity. The two equations differ principally on the role played by pipe diameter. Since Newitt's experiments are performed only in 1-inch diameter pipe, he could not evaluate the effect of this variable.

In addition, Newitt analytically derived an expression for the frictional resistance encountered in flow with a moving bed. Correlation of experimental results gave:

$$\psi = 66\, C \left(\frac{\rho_p - \rho_1}{\rho_1}\right)\left(\frac{gD}{v_B^2}\right) \tag{27}$$

Particle diameter is not a variable in this equation. Under normal transport conditions, flow with a moving bed does not occur for particles with diameters less than 2 mm. Durand and others have shown that for pebbles and gravel the frictional resistance is independent of diameter. However, Durand concludes that this occurs because the drag coefficient for large particles is constant, i.e.,

$$v_t = B\sqrt{d\,\frac{\rho_p - \rho_1}{\rho_1}} \tag{28}$$

Substituting equation (28) into equation (25) yields for aqueous slurries:

$$\psi = 252\, C \left[\frac{gD(\rho_p - \rho_1)}{v_B^2}\right]^{1.5} \tag{29}$$

The discrepancy between equations (27) and (29) has not been resolved by the two investigators. However, by the shear bulk of supporting data, equation (29) should be the more reliable. The difference between the two equations may be due to the assumption made by

Newitt that the particles travel at a speed which is equal to, or a constant ratio of, the bulk velocity. Several investigators have observed that this is false. The causes of particle speed variation are unknown.

Sand Movement in Vertical Fractures

The movement of sand during fracturing has been studied for vertical fracture systems. Kern et al (19) investigated sand movement in a simulated fracture, 1/4 inch wide, formed between two plexiglas plates 22 inches long and 7 1/2 inches high. Although the authors considered the work preliminary, the study did describe sand movement in a semiquantitative sense. The top and bottom of the fracture were sealed so that fluid flowed horizontally. Sand-liquid slurries were injected at constant rates into the vertical slit representing the well bore.

It was observed that the sand settled to the bottom of the fracture before moving very far. When the fluid velocity exceeded a certain critical value, all of the sand injected began moving through the crack even though it had settled to the bottom.

If the fluid velocity initially was less than this value, most of the sand deposited in the fracture remained in place until the fluid velocity in the open flow channel above the deposit attained the critical value. All sand subsequently injected moved through the crack while the initial sand deposit remained in place. Increasing or decreasing the injection rate altered the area of the fracture open to flow. In other words, the system automatically sought to maintain an equilibrium or critical velocity.

Water was used as the fracturing fluid. Viscosity was increased by adding CMC (carboxymethylcellulose). The results of these tests indicated that the equilibrium velocity is not very sensitive to sand size, fracturing fluid viscosity, or sand injection rate except at very low rates. For fluid viscosities from 1 to 18 centipoises and sand injection rates from 5 to 50 pounds per minute, the average equilibrium velocity for sand was approximately 5 feet per second. Two graded sands of 10-20 and 20-40 mesh were used. A series of tests using 20-40 mesh steel shot indicated that the equilibrium velocity is fairly sensitive to density differences between the propping agent and the transporting fluid.

One run was made with gelled water at zero sand injection rate. Here the fracture was filled with sand and gelled water was injected until no more sand was washed out. The equilibrium velocity obtained was 9.2 feet per second, the highest value obtained in these tests. This indicated that the equilibrium velocity for gelled fluids is considerably greater than for Newtonian fluids. The higher velocity requirements are attributed to the high flow rates necessary to induce turbulence in the gel.

It should be pointed out that vertical fractures, if confined to a single stratum, will maintain a relatively high constant velocity throughout the fracturing treatment. For horizontal fractures, velocity should be a function of distance from the well bore. Actually, fluid loss or leak-off to the formation rock will result in some decrease in velocity in both cases.

If the slurry velocity is less than the equilibrium value,

a bed of settled sand will build up at the bottom of the fracture. The authors related the rate at which the height of the settled sand bed grows $\frac{dH_s}{dt}$ to the terminal velocity of the sand and to sand concentration being pumped:

$$\frac{dH_s}{dt} = v_t C \frac{1}{1 - \phi} \tag{30}$$

The distance the sand deposit extends from the well bore while it is growing is:

$$S = \frac{Q_B}{2bv_t} \tag{31}$$

where b, the thickness of the fracture, is assumed to be constant. The effect of fracturing fluid leak-off has been neglected in both equations (30) and (31). Fluid loss will increase the rate of growth of the settled bed height and decrease the distance the settled sand bed extends from the well bore.

In many cases, injection is stopped before the sand deposit height reaches the value required to establish the equilibrium velocity. However, the height of the open section above the settled sand pack necessary to yield the equilibrium velocity may be calculated from the following equation:

$$H_o = \frac{Q_B}{2bv_e} \tag{32}$$

Again, it is assumed that the crack has a rectangular cross-section.

If the equilibrium velocity is established and the treatment continued, all additional sand injected would be washed over the top of the settled sand deposit. Leak-off reduces the total flow rate in the fracture which in turn decreases the height of the open section away from the well bore.

Sand Movement in Horizontal Fractures

Izyumove and Shan'gin (17) investigated the movement of sand in horizontal fractures using a transparent pie-shaped flow model, representing a segment of a radial flow system. The model was made with two trapezoidal plexiglas plates 89 inches long, 0.91 inch wide at the inlet side, and 46 inches wide at the outlet.

Flow rates of 35 to 1000 cc/sec (0.41 bpm) were used in the experiments. This corresponded to injection rates in the entire radial pattern of up to 2000 cubic meters per day (8.9 bpm). The majority of tests was made with 20-40 mesh sand as the propping agent. Water and a 60-centistoke viscosity oil were the fracturing fluids employed.

The movement of the sand transported by water followed a characteristic pattern which was essentially unchanged at the various test conditions. In the vicinity of the inlet where the fluid velocity was high, the sand moved as individual particles with roughly the same concentration as the injected slurry. As the distance from the inlet increased the velocity decreased and the sand concentration increased. Although the sand was transported in the suspended state, an accumulation of particles took place. Eventually the reduction of velocity became so pronounced that the stream could not retain all of the sand in suspension. Part of the sand fell to the bottom of the model and formed bodies resembling the "shallows" of a river bed which were separated by open "channels". After the shallows had formed, sand movement took place mainly in the channels. They observed that for a given flow rate the amount of sand deposited remained unchanged regardless of how the sand was introduced into the model.

The interest was focused primarily on determining the amount and configuration of the sand deposited in the fracture after several fracture volumes of slurry had been pumped through the model. No data were presented on the rate of advance of the sand before a steady-state flow condition was attained. Pressure measurements were also primarily restricted to the static flow conditions. These data were presented as a ratio of the permeability of the fracture containing sand to that of the fracture without sand deposits. The change in this ratio with respect to time was presented graphically for five tests.

Experiments with water-sand slurries flowing through a 3 mm (0.12 inch) thick fracture showed that:

(a) At constant sand concentrations, a decrease in flow rate resulted in sand deposition nearer to the inlet of the model and a greater amount of sand in the model when flow was stopped.

(b) At a constant flow rate, an increase in sand concentration in the slurry caused an increase in the amount of sand in the model when the test was terminated.

Several of these runs were repeated using oil as the carrying fluid. With the increase in viscosity, the region of sand deposition was displaced from the inlet of the model. The general conclusions regarding the effects of concentration and flow rate on sand deposition were similar to those obtained for water-sand slurries.

Several tests were made to determine the effect of over-flushing with clear liquid on the permeability of the sand filled

fractures. This was not stressed since high permeability ratios, between 0.45 and 0.85, were reported. It was observed that overflushing removed the dispersed sand in the flow channels and increased the flow capacity of the simulated fracture. It was also observed that there was a critical amount of overflush after which sand displacement no longer occurred.

Doroshkin, Zheltov and Zheltov (7) studied the flow of sand-liquid slurries in a horizontal linear model. The initial phase of the study was the determination of the effective viscosity of sand-liquid slurries, μ_s. Einstein (9,10), assuming that the particles were spherical and did not interfere with each other, developed the following expression for the effective viscosity of a suspension in terms of the viscosity of the carrying liquid, μ_l, and the concentration of sand, C:

$$\mu_s = \mu_l (1 + 2.5C) \tag{33}$$

It has been established that equation (33) is rigorous when C is less than 0.01.

Tests were performed in a vertical pipe at various concentrations using several liquids and sand sizes. Although there was some degree of scattering in the experimental data, the application of the method of least squares yielded:

$$\frac{\mu_s}{\mu_l} = e^{3.18C} \tag{34}$$

Flow rates were sufficiently low to insure that laminar flow conditions existed during these tests. The effective viscosities predicted by equation (34) are generally high compared to previously observed values. (31)

The dimensions of the simulated fracture in the flow model were: fracture thickness = 5 mm, length = 6000 mm, and width = 90 mm. The top of the model was made of plexiglas while a synthetic sandstone was constructed and used for the bottom.

Glycerine, diluted with water to obtain viscosities from 50 to 600 centipoises, was used as the carrying fluid. The propping agent was 20-40 mesh sand. Since all tests were performed under laminar flow conditions, the low velocities resulted in the formation of a sand deposit at the bottom of the flow model. During a given test, deposit thickness was essentially uniform. The parameters measured were the viscosity of the carrying fluid, the concentration of the sand in the flow stream, and the thickness of the sand deposit. The measurements were made after steady state deposit flow conditions were established.

The reference study shows that at low input sand concentrations C, an increase in C increases the sand concentration in the bottom layer until a value of approximately 0.45 is reached, while the height of the layer does not increase. When the sand concentration in the layer reaches 0.4 to 0.5, an increase in C causes an increase in the thickness of the sand layer while the sand concentration in the layer remains practically unchanged.

CHAPTER II

EXPERIMENTAL DESIGN

The literature search revealed that only limited information applicable to slurry flow in horizontal fractures was available. This lack of basic information on the problem stressed the necessity of approaching the problem on a sound, fundamental basis. It was deemed advisable that a linear flow system be studied rather than the more complex radial patterns. In addition it was considered imperative that the model be transparent so that the mechanics of the sand movement could be observed during the test. The definition of the regimes of flow involved in sand transport, related to the test parameters, was considered an important contribution and was important in correlating the quantitative results.

Test Design

The quantitative results desired from the experimental work were (1) pressure behavior along the line of flow and (2) rate of advance of the solid particles in the slurry. Interest was primarily focused on sand movement during the sand placement phase of the tests, i.e., the interval of time preceding steady state sand flow conditions in the model. However, the effects of overflushing with clear fluid would also be studied.

Because of the large number of parameters affecting sand movement in slurries, it was necessary to limit the scope of the study. While the effects of the majority of the variables on sand transport could be scanned, only three could be examined in detail.

Prior to making the selection, the parameters were divided in four groups—fracturing fluid characteristics, characteristics of the propping agents, flow conditions, and physical dimensions and characteristics of the fracture. Selection was based not only on the magnitude of effect the parameters would have on sand movement but also on their degree of variance in actual hydraulic fracturing treatments in the field. Thus, variables overlooked in the basic test series may, in fact, be extremely important in the general problem of sand transport in slurries.

The physical dimensions and characteristics of the fracture were set during the design and construction of the flow model. Briefly, the configuration of the model defined a linear flow system as well as the length-to-width ratio of the flow channel. Although provisions were made to vary fracture thickness, this dimension was constant with respect to length. In addition, the simulated fracture surfaces were smooth and horizontal. A detailed description of the simulated fracture is given in the following section.

Propping agent characteristics were eliminated from consideration since the majority of fracturing treatments are performed using 20-40 mesh Ottawa sand. The propping agent selected for the basic tests was 20-40 mesh glass beads. Such beads have approximately the same density as sand. In addition they have a sphericity of almost 1.0.

This is shown in Figure 3, enlarged photographs of 20-40 mesh glass beads, 20-40 mesh round Ottawa sand, and a 20-40 mesh angular sand. The natural occurring sands are samples of propping agents commonly used in the field.

Similarly, if only sand-oil slurries are considered, fracturing fluid density may be eliminated as a variable because of the limited range of values normally encountered.

The remaining pertinent variables were oil viscosity (fracturing fluid characteristics), fluid flow rate and concentration of the propping agent (flow conditions), and fracture thickness (fracture characteristics).

Through necessity, one of these parameters was eliminated. The one selected was fracture thickness. In the basic test series, the fracture thickness was set at 1/4 inch. It is probable that a horizontal fracture does not have a uniform thickness. Fracture width should be at a maximum at the well bore with only a very fine separation at the fracture extremity. However, material balances on the amount of sand and oil pumped and the amount of fracturing fluid lost to the formation during actual field treatments indicate the average thickness is on the order of 1/4 inch.

Flow Cell Design

The dimensions of the model were important in obtaining reliable results. Since interest was focused on the mechanics of sand movement during the unsteady state sand placement phase, the model had to be relatively long to obtain usable results. This was particularly

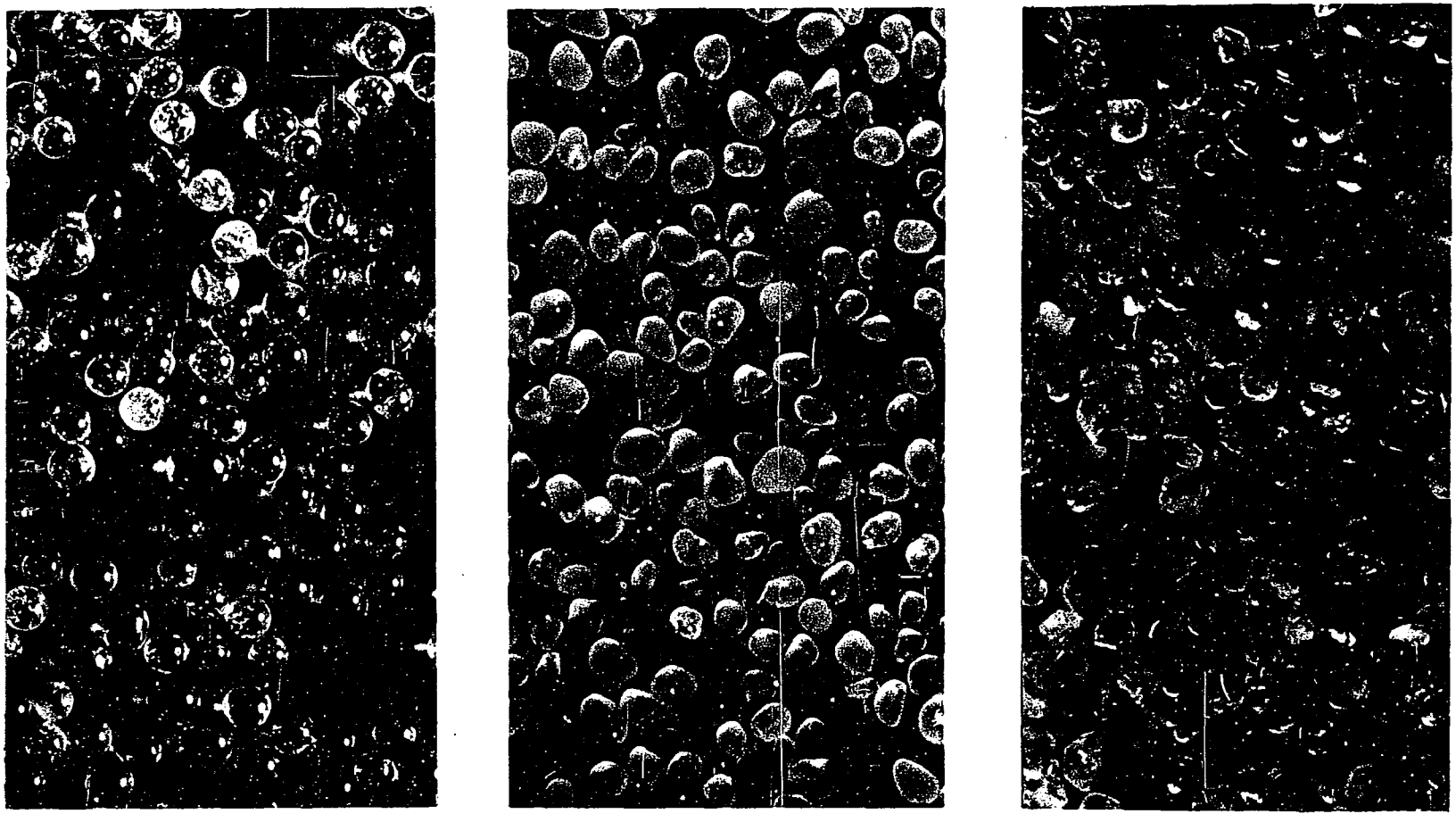

(a) GLASS BEADS (b) OTTAWA SAND (c) ANGULAR SAND

FIGURE 3 MAGNIFICATION OF 20-40 MESH PROPPING AGENTS

critical since both entrance effects and end effects could shorten the effective test length. Within the normal range of fracture thickness, the model had to be sufficiently wide to approximate infinite parallel plates, thus reducing the boundary effects along the sides of the simulated fracture. Provisions for varying fracture thickness had to be included in the design.

In view of these considerations, a 10 1/2-foot long flow cell was constructed in four sections. Each section consisted of five 1-foot square plate glass windows set in a metal frame. The resulting areal extent of the fracture flow channel was 1.0 by 10.53 feet. Steel spacers were used to obtain the desired separation between the plates. A continuous O-ring around three sides of the model was used to obtain a fluid seal when the top and the bottom sections were bolted together.

Plate glass was selected over other transparent materials since it is relatively inexpensive and is scratch resistant. Because of the scouring action expected, the commonly available plastics were eliminated from consideration. Tempered glass frequently used for windows in high pressure cells was not used because very slight scratches could cause failure below the limit of ordinary plate glass.

Section frames were constructed from a single sheet of steel plate 1 1/2 inches thick. Most of the excess material was removed by a cutting torch. The remaining material was milled out to meet specifications as shown in Figure 4. From the published data on slurry flow in pipe lines, it was estimated that a pressure of 25 psi was more than sufficient to obtain suspended flow in the simulated fracture. This figure was used as the design pressure. In designing the flow cell it was

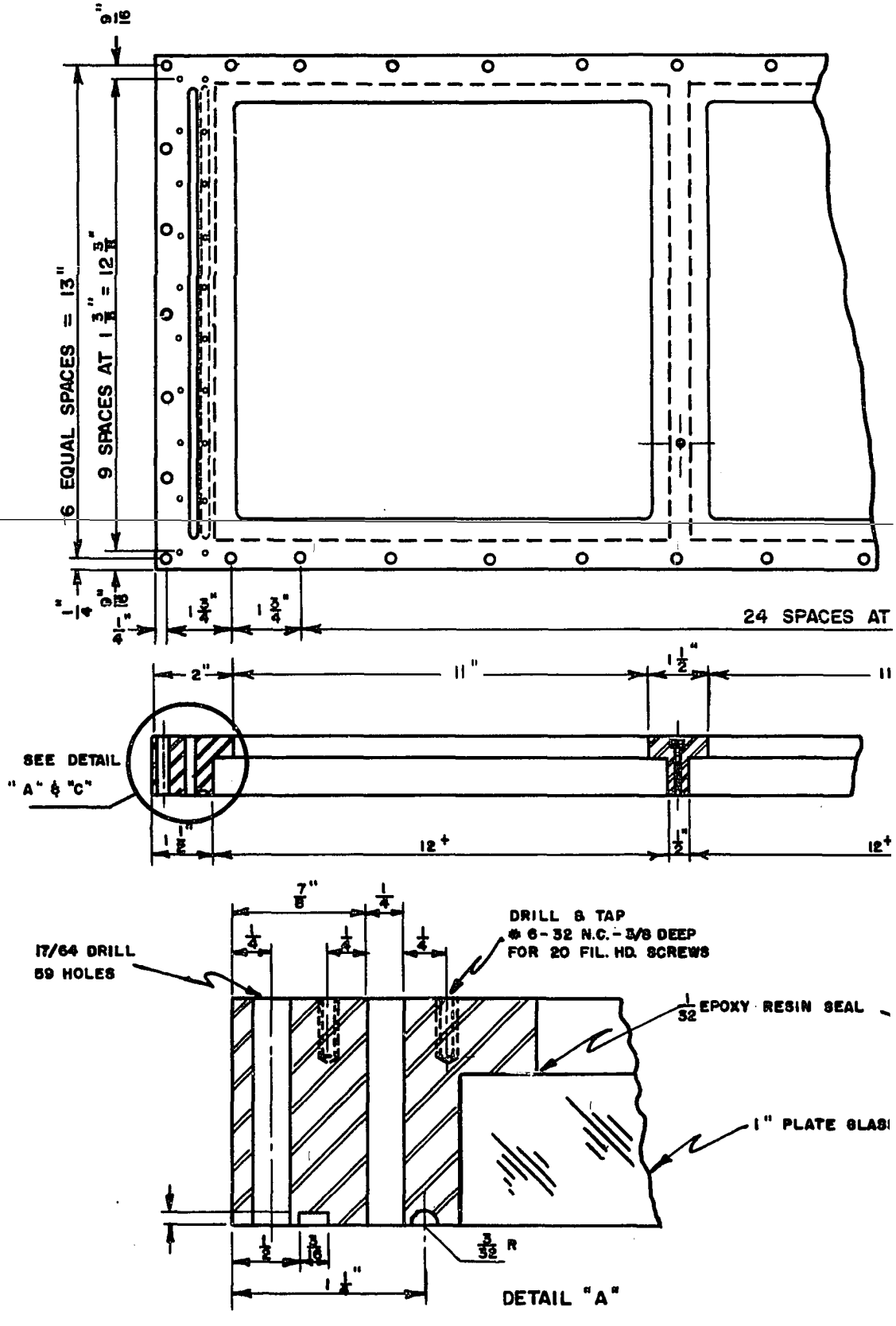
6 EQUAL SPACES = 13"
9 SPACES AT 1 3/8" = 12 3/8"
1 3/4"
1 3/4"
24 SPACES AT
2"
11"
1 1/2"
SEE DETAIL
" A " & "C"
12+
DRILL & TAP
6-32 N.C. - 3/8 DEEP
FOR 20 FIL. HD. SCREWS
17/64 DRILL
59 HOLES
1/32 EPOXY RESIN SEAL
1" PLATE GLAS
3/32 R
DETAIL "A"

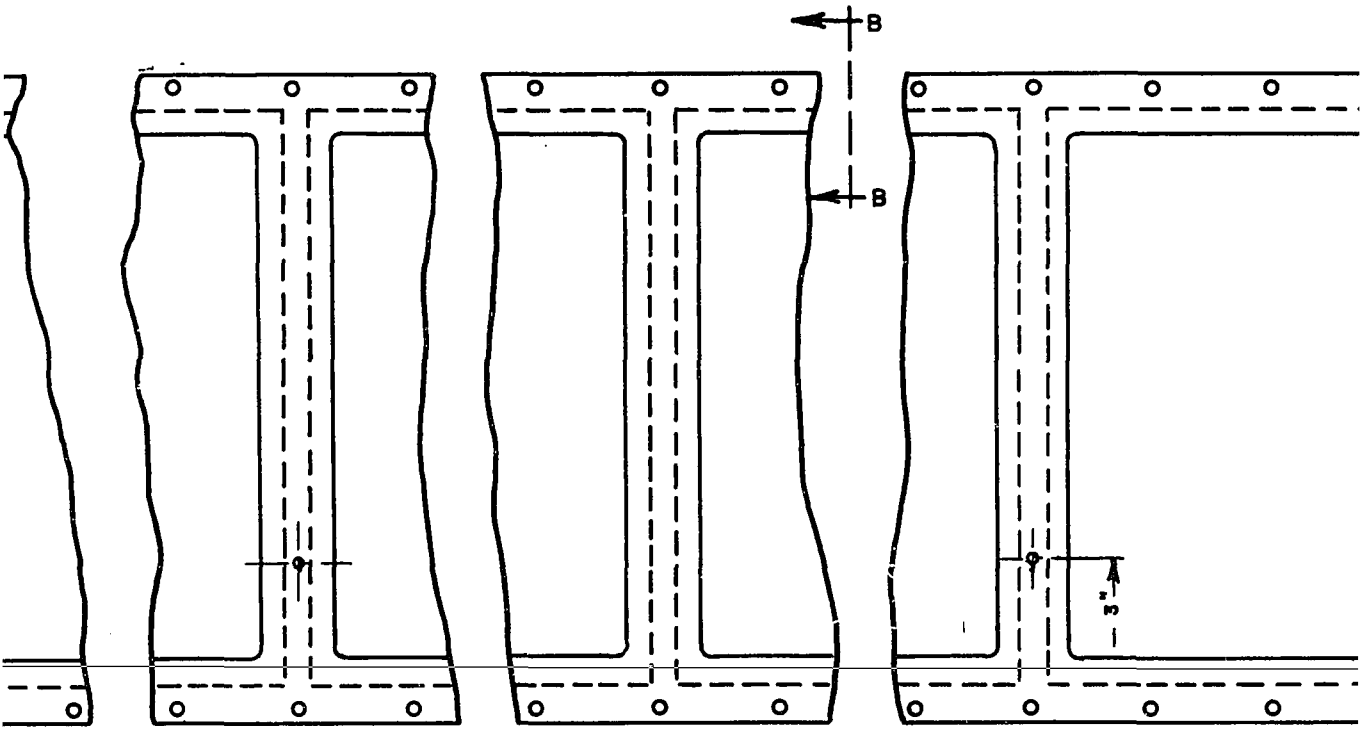

ACES AT $2\frac{1}{2}$" = 60"

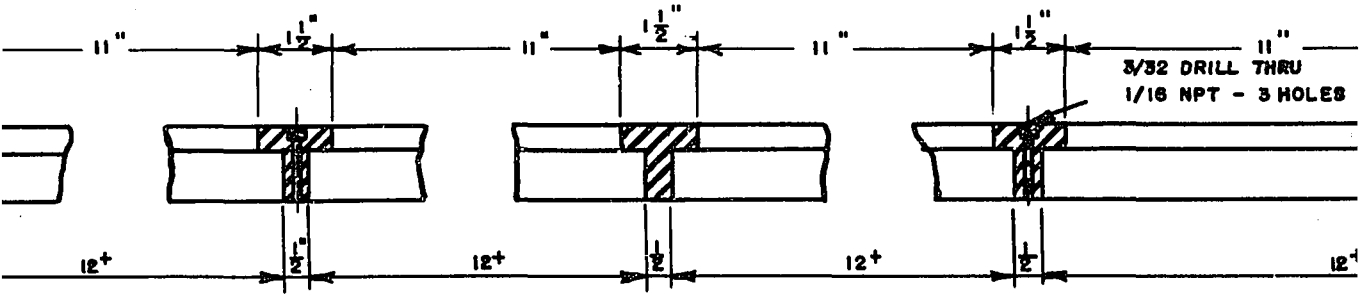

N SEAL

ATE GLASS

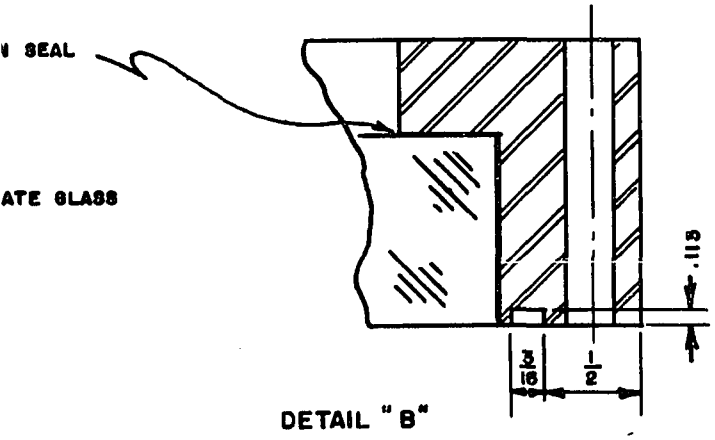

DETAIL "B"

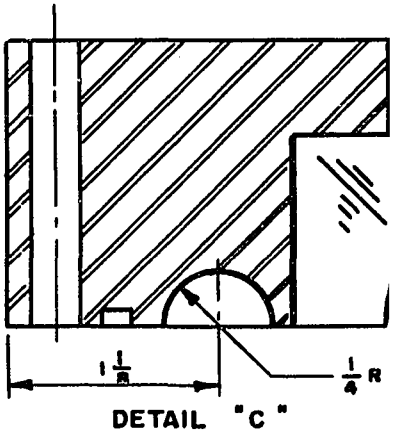

DETAIL "C"

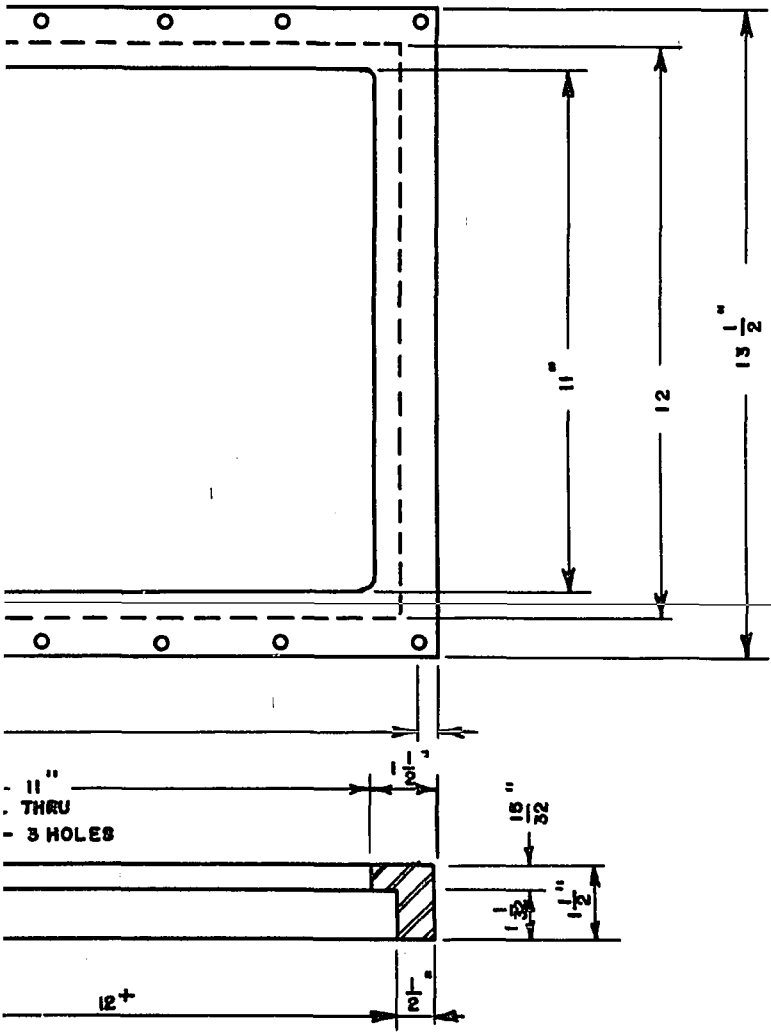

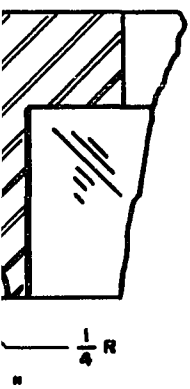

FIGURE 4
DETAIL DRAWING OF SAND FLOW MODEL

also stipulated that the maximum permissible deflection at the design pressure be less than 1/100 inch. One-inch thick plate glass fitted in the frame shown in Figure 4 satisfies both of these requirements.

Flow Cell Fabrication

It was important that the simulated fracture face be smooth and flat. Extreme care was taken in the fabrication of each section. The procedure consisted of inserting the glass plates into the frame with the simulated fracture surface on top. Short metal tabs were bolted at the corner of each window. The entire section was then raised and supported by columns contacting only the glass plates. A flat surface was obtained by loosening or tightening the bolts connecting the metal tabs to the frame. Discontinuity between the glass plates and the frame was checked both longitudinally and laterally using a machinists straight edge. A few of the metal crossbars had to be ground and polished. In this position the glass plates were not contacting the frame at any point. Approximately 1/32-inch clearance existed. To affix the plates permanently in the frame an epoxy resin was used. The gap between the glass plates and the metal frame was sealed from below with plastic tape. The epoxy resin and catalyst were heated to 140°F to increase fluidity. The plastic was then poured in the gaps along the simulated fracture-formation interface. Care was exercised so that air bubbles were not entrained during this step. The plastic became tacky between two and three hours and cured overnight. Considerable shrinkage occurred and additional epoxy resin was applied to completely fill the gaps around each plate. This presented no problem since this plastic forms an excellent bond to itself. The most satisfactory method of insuring the

smooth surface was the use of excess plastic in the second application. After curing, the excess material was scraped off with a razor blade held perpendicular to the model surface.

To assemble the flow model, the two lower sections were placed on a metal stand 18 inches high and were bolted together to form the lower fracture surface. Bolts were inserted in the 113 holes drilled in the frame on three sides of the model. The end of the model was unobstructed so that slurry discharged to the atmosphere would not be hampered. A continuous O-ring groove was provided in the metal frame between the bolts and the glass. One-quarter inch diameter polyethylene welding material was then inserted in the groove and the steel spacer was placed in position. The steel spacers used to separate the upper and lower fracture surfaces were constructed from 3/4-inch precision bar stock. The two remaining sections bolted together formed the upper fracture surface. The gasket material was placed in the O-ring groove. It was held in place by strips of masking tape. The bolt holes in the upper section were aligned with the bolts protruding from below, and the section was dropped into place. The masking tape was removed and the steel, glass and polyethylene sandwich was bolted together. Care was taken to insure that the gasket material was not pinched during this operation. A uniform torque of 100 inch-pounds was applied to each bolt.

A view of the assembled flow model is found in Figure 5.

Model Entrance

As stated previously, the slurry flowed vertically downward to reach the model entrance. This flow path was selected because it approximated conditions in the prototype and aided in the distribution of

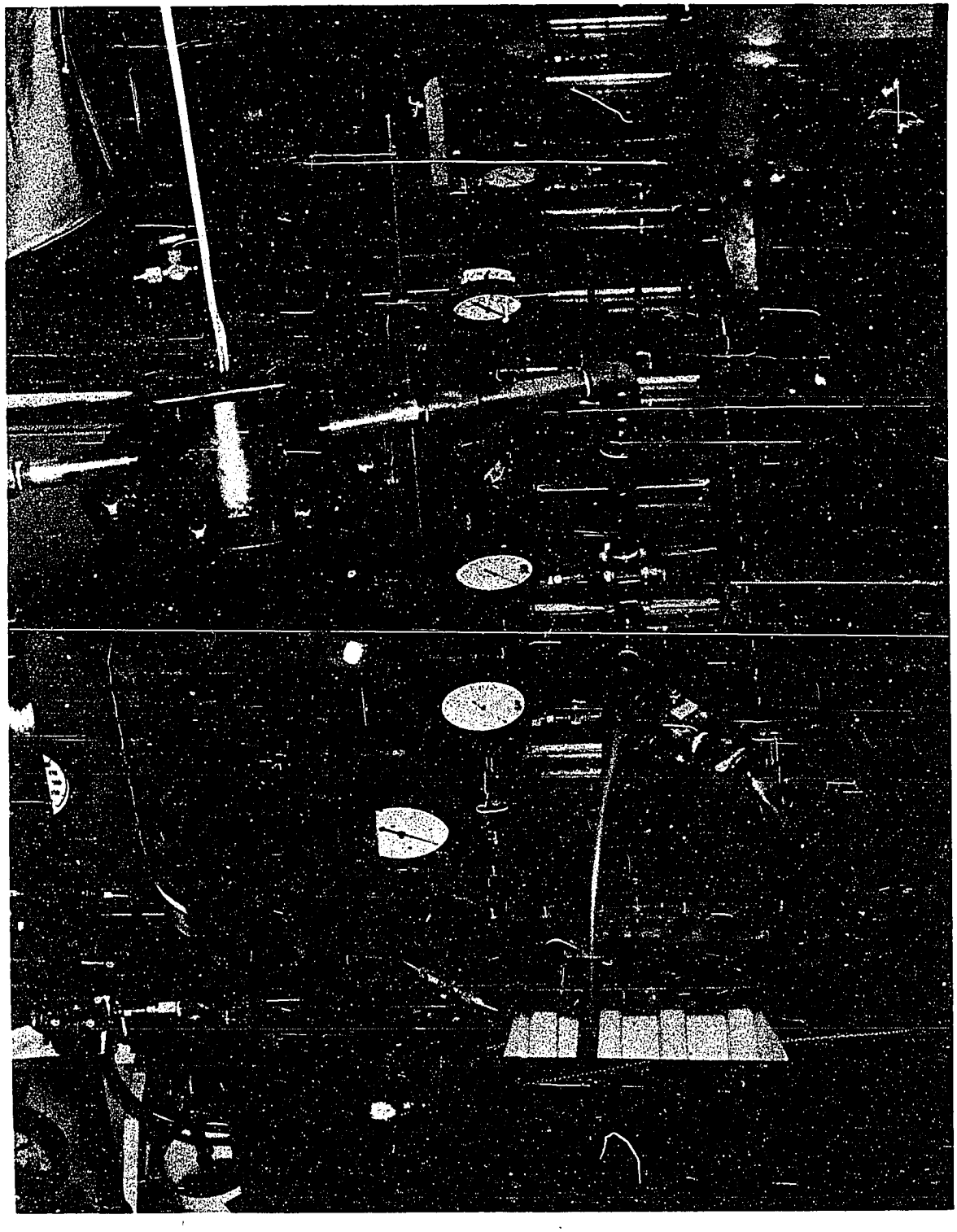

FIGURE 5 VIEW OF TEST EQUIPMENT

sand at the entrance. The triangular header, shown in Figure 5, provided a gradual change from the circular pipe to the rectangular conduit. The width of the channel at the bottom of the header was equal to the width of the flow channel in the model and was 1/4 inch thick. An opening of these dimensions extended through the frame of the upper entrance section. In order to aid in the transition of a vertical flow to a horizontal flow a trough with a radius of 1/2 inch was provided in the bottom entrance section. A smaller trough was also provided at the upper surface immediately before entering the model. These details are shown in Figure 4. Bolts were used to attach the header to the model and a 1/16-inch gasket material was used to obtain a fluid seal.

Despite the measures to insure uniform entrance of the slurry, entrance anomalies were observed at moderate and low flow rates using the lighter oils. The entrance would sand up in the center with flow occurring at the sides of the model entrance. Various obstructions were placed in the header to combat this problem. The common V-shaped flow splitters were not successful. Although a uniform entry was never attained at low flow rates, a 3-point entry was eventually achieved. In this case, the slurry entered the simulated fracture at both sides of the model and also in the center. Uniform flow distribution was obtained within the first one-half panel. This was accomplished by using a reinforced strip of wire screen to channel the entering slurry to the sides of the model while allowing clear fluid to flow downward and to sweep out the sand deposited continually in the center of the trough.

Slurry Flow System

To obtain more usable results, these tests were performed

under conditions of constant flow rather than conditions of constant pressure drop. The latter posed a much simpler problem from a design standpoint. It was important that not only bulk flow rate of slurry but also the concentration of the solid phase in the stream be held constant. Preliminary tests indicated that a wide variation of sand concentration existed when pumping blended slurries. Except for high viscosity oils and/or small solid particles, it was impossible to maintain a uniformly suspended slurry in the mixing tank. Ideally, the best system is the injection of sand into the fluid stream immediately ahead of the model entrance. This eliminates the problem of sand drop out in the flow lines leading to the model. No commercial equipment was available for this type of system; therefore the solids injection equipment was constructed.

Sand injection was accomplished by advancing a floating piston in a cylinder at a constant linear velocity. This forced the liquid-saturated solids placed above the piston into the fluid stream at a constant rate. The cylinder wall was made of a 4-foot long, 7 1/2-inch I.D. precision bore pipe. Only a light buffing was required to condition the interior surface of the cylinder for the floating piston. The piston was constructed of aluminum alloy and was 1/32 inch smaller in diameter than the pipe. Two O-ring seals provided fluid seals at the top and bottom of the piston. A pump cup with a bolted upper surface helped prevent the solids above from fouling the sealing action of the O-rings. The sand injection equipment is shown in Figure 5.

The floating piston was constructed from aluminum alloy not only because this material was very machinable but also because it

protected the cylinder walls. Any propping agent particles that worked down between the piston and the cylinder wall would scratch the piston rather than the steel. This was desirable since it would be easier to replace the piston than the injection cylinder.

To advance the piston, SAE 50 lubricating oil was forced at a constant rate into the cylinder below the piston. This was accomplished using various Zenith gear pumps driven by a 1/4-horsepower electric motor. A Graham variable speed transmission controlled the output to the pump. Calibration of pump rate against transmission speed was obtained for five pumps against varying discharge pressures. In both the calibration runs and test runs, a pressure of 150 psig was applied at the suction side of the gear pumps to prevent air suction when pumping the viscous drive fluid recommended by the pump manufacturer. A surplus air force oxygen tank was used as the drive fluid reservoir.

The head of the sand injection cylinder could be attached or removed from the precision bore pipe using slotted bolt flanges. The head was formed by constructing a hollow equilateral cone from heavy sheet metal. Its base was welded to a slot bolt flange and the upper one-third of the cone was removed to provide a window. The 4 1/2-inch square, 1/2-inch thick, lucite window was bolted to the top of the head using a flange arrangement. The actual viewing area was approximately three inches in diameter. The fluid stream was introduced into the header through a 3/4-inch diameter pipe nipple located near the base of the cone. Identical piping, separated by 180°, was provided for the exit of the flowing stream.

A pressure tap was provided in the lucite window so that a

vacuum could be pulled within the cylinder. In addition, a hole and sealing arrangement was provided so that a 1/4-inch metal rod attached to the floating piston could move vertically as the floating piston was advanced. A metal measuring tape attached to the rod indicated the position of the piston within the cylinder at any given time.

Fluid flow was instigated by forcing liquid under pressure from an 80-gallon reservoir tank using bottled nitrogen gas. Fluid flow rates were set and held constant using one of two Kates regulators. The regulators were self-contained and self-acting. Flow rates were set by opening or closing an adjustable metering orifice within the unit. The unit contained an automatic internal regulating valve which held the pressure drop at a single fixed value for all flow rates and all variations in line pressure within its operating range. The manufacturer claimed three per cent accuracy. These self-contained regulators were selected over a fixed orifice system because of the savings in money and space. The ranges of the two regulators were 0.2 to 1.6 gallons per minute and 2.0 to 16 gallons per minute. A Y-type strainer was placed in the flow line leading to the regulators so that contaminating materials would be removed from the stream.

The necessary piping and valves were installed so that the flow regulators and/or the sand injection cylinder could be bypassed. These lines were assembled from 3/4-inch line pipe and 3/4-inch copper tubing. A discharge line was provided between the sand cylinder and the model header so that slurry flow rate and solids concentration could be calibrated before the stream was introduced into the model. A three-way valve installed at this point facilitated the switching of the flow stream to the model entrance.

Flow discharged from the end of the model into an inclined sheet metal trough. It facilitated discharge sampling during the test runs. A 50-gallon open sheet metal tank, placed beneath the trough, collected the simulated fracturing fluids. Solids were separated from the liquid phase by placing a box constructed from 100 mesh screen material directly under the discharge trough. A pump was provided so that fluid could be transferred from the open discharge tank back to the fluid reservoir tank at the end of the test.

Test Procedure

A major factor in obtaining usable results from these tests was the ability to establish and maintain fluid flow rates and solid concentrations at the desired level. Flow rates and solids concentration were calibrated at the beginning and end of the sand placement phase of each test. Solids concentration was measured in terms of pounds of propping agent per gallon of clean liquid.

The initial step consisted of flowing clean liquid through the Kates flow regulators into the model header, bypassing the sand cylinder. The proper flow regulator was adjusted until the required flow rate was obtained at the discharge end of the model. The required flow rate was equal to $Q(1 - C\phi)$ since the void spaces between the solid particles were filled with liquid. The oil used during the fluid calibration was then transferred back to the reservoir tank.

Next, flow was directed through the sand cylinder and out the discharge line immediately upstream of the model header. Fluid flow and advance of the floating piston within the sand cylinder were initiated almost simultaneously. The accuracy of the settings on the

variable speed transmission regulating the gear pump output was found to be excellent. Seldom did the required setting deviate from the value determined from the pump calibration curves. This, coupled with the initial fluid flow calibration, made this phase of the calibration only a waiting game. Time was required for the stripping action within the sand cylinder to reach equilibrium. Normally, the sand and fluid flow rates checked within three per cent without adjustments. Several 2,000-milliliter graduates were used to catch and measure the samples.

This procedure was changed for the highest fluid flow rate. Because of the limited supply of fluid, there was insufficient time to adjust the flow and transmission setting if the initial settings were in error. Therefore, calibration checks were made only at the end of the model during these tests. However, 15 to 20 gallons of slurry was discharged to establish equilibrium within the sand cylinder prior to switching flow into the model.

Similarly, for the most viscous fluid, there was normally insufficient time to permit adjustments in the amount of solid phase. This was the result of the low settling velocity of the propping agents in the viscous fluid. However, samples were taken and sand volumes were recorded later.

The pressure behavior, position of the sand front, and time were recorded during the sand placement phase of the tests using a camera data recording system described in a later section. Steady state flow conditions existed once the sand front reached the end of the model. One to two-gallon samples of the discharge stream were caught and measured. Normally, the volumes of liquid and sand checked within five

per cent at this point. If the error on either quantity was greater than five per cent, the test was usually rerun. The data on the first test were always discarded.

During the steady-state and overflush portions of the tests, pressures were the only quantitative data obtained although a description of the sand movement was noted. The technique of overflushing consisted of simply stopping solid injection into the fluid stream and bypassing the sand cylinder. The latter was necessary since the liquid would continue to strip sand from the source. Thus, the fluid flow rate during overflush was equal to the liquid flow rate times $(1 - C\phi)$.

Inasmuch as the overflush could last several hours, it was sometimes necessary to transfer fluid from the discharge tank back to the reservoir tank while the test was in progress. No change in fluid flow rate occurred, provided the driving pressure in the reservoir tank did not change. A constant pressure was maintained by directing part of the return stream back to the pickup tank so that the return rate was slightly lower than the liquid flow rate to the model.

At the conclusion of a test run, any solids remaining in the model were cleared by high rate fluid flushing. Although large volumes of fluid were sometimes required, this method was far more desirable than disassembling the model. In the test with the 1/2-inch spacer a loop of polyethylene welding rod was used to agitate the deposited beads during this step. Considerable time was consumed when large flush volumes were necessary due to the low output of the transfer pump.

Pressure Measurements

One-sixteenth inch diameter pressure taps were provided along

the length of the model so that pressure data could be obtained. These taps were located in the metal crossbars separating the glass plates in a line two inches off the center line of the model. The five pressure taps were located at the first, second, fourth, sixth, and eighth crossbars. The pressure at the discharge end of the model was atmospheric. In general, 1/8-inch copper tubing was used to connect the gauges to an elbow screwed into the pressure taps. These lines ran almost horizontally over the metal cross piece to the gauges resting on top of the bolts used around the periphery of the model. The only exception was the USG gauge reading from 0 to 60 inches of water. The bellows type pressure element in this gauge was too massive to rest on the bolts. Therefore, 1/8-inch diameter nominal pipe resting on the metal crossbar was used in lieu of the 1/8-inch copper tubing.

Two major corrections were necessary to obtain the true pressure within the flow model. One was associated with pressure gauge calibration. The gauges were calibrated at the beginning of and three times during this study. For three of the gauges, recorded pressures differed slightly from the actual values. Inasmuch as these errors were essentially constant over the range of the gauges, the correction consisted of adding a constant to the gauge reading. The other correction took into account the head of oil present in the pressure tap and associated lines leading to the gauges.

Additional gauges were utilized at various points within the system upstream of the model itself. These gauges were required for control purposes. Gauges were located at the regulator to the nitrogen bottle, both fluid reservoir tanks, at the model header and upstream and

downstream of the Kates flow regulators.

An ordinary drugstore variety electric clock was used as the timing element during the test runs.

Camera Recording Devices

The number of elements to be recorded and the short test intervals expected during some runs made an automatic data recording system desirable. The instrument selected for this purpose was a Beattie-Coleman 70 mm sequence camera. A camera had distinct advantages over other methods in that it would not only read the instrument dials but would also record the position of the sand front and the mode of sand transport occurring within the model. The 70 mm film magazine, the largest size offered, was obtained. The resultant image size on the film was 2 1/2 inches by 3 3/8 inches. Large image size was important since the detail retained on the film increased as the image size increased. The magazine roll held 100 feet of 70 mm film. Over 300 shots could be taken before replacing the roll in the magazine.

The automatic film advance was operated by a 115 volt AC 50-60 cycle electric motor synchronized with the shutter. Approximately 3/4 of a second was required to advance the film. This time limitation was well below the expected shot frequency in the study. Another limitation of the camera was that the tripping shutter speed was fixed at 1/50 of a second. Thus proper lighting was imperative.

A 75 mm Wollensak lens was obtained for the camera which was bolted to the ceiling over the approximate center of the model. In this position the first 1 1/2 windows in the model were recorded on the film.

The manufacturer's provision for activating the shutter consisted of a button device on a 6-foot long cord. In order to automate data recording as much as possible a Sanenco Interval Timer was used. The interval timer was designed to take delayed sequence shots with motion picture cameras. A relay was installed so that the interval timer would activate the tripping device on the Beattie-Coleman camera. The timing interval range of this instrument varied from 1 to 120 seconds. Once the timer was set, the shutter would trip at the end each time interval until it was switched off. A counter was installed so that the number of frames taken on a given roll would be recorded.

Lighting was the primary factor in obtaining good pictures. Although some reflected light was necessary, it was found that transmitted and diffused light from below was very effective in distinguishing the glass beads. The bottom of the simulated fracture had been constructed with windows specifically for this purpose. A bank of fluorescent lights placed in a white shadow box supplied sufficient lighting. The bank consisted of four rows of tubes twelve feet long. The combined wattage of these lights was 464. Fluorescent lights were used in lieu of flood lights because of the amount of heat given off by the latter. The generated heat could result in a change of viscosity during a test run. It also presented a definite safety hazard when flowing light blended oils.

In order to obtain a bright even background, tracing paper was placed directly beneath the model to diffuse the light from below. The paper was found to be superior to ground and opaque glass in that it transmitted a greater percentage of the light. The main disadvantage

of this material was the changes in light transmission when it became oil soaked.

The data read from the sequence camera film included pressure from the gauges along the line of flow, position of the sand front, and time. Unless the sand movement resulted in the formation of a fairly full sand pack, the front could not be picked up from the film. Therefore, the front had to be recorded manually in many test runs. These readings were taken simultaneously with the sequence camera shots and distance was estimated to the nearest 1/10 of a panel.

In obtaining these data from the 70 mm film, a microfilm reader was used. With a 30 mm lens a magnification of 13 was obtained. Thus, the transparent section of a single panel on the film was enlarged to 9.9 centimeters. Front position could be determined to the 1/100 of a panel by this method. In cases where the front was irregular, an average distance was estimated. Compensation was made for the distortion on the film at the ends of the model.

After missing sand front position in run 16, this quantity was recorded manually in every run in which suspended flow was likely to occur. Overlap of visual and photographic recordings occurred in several runs. Data from both methods were in close agreement.

A 16 mm Paillard Bolex motion picture camera focused on the ninth panel in the model recorded the details of the sand movement. All shots were taken at a speed of 24 frames per second, using Tri-X black and white film. This film proved invaluable in the short test runs when there was insufficient time to make complete notes on the sand transport mechanism. The camera was started and stopped manually.

Scaling

During the experimental design of this study, preparations were made for scaling the sand transport mechanism. This was considered imperative since the unsteady state behavior of slurry flow is unknown. No references covering this aspect of slurry flow, regardless of the type of flow channel, were available. There was a distinct possibility that the sand concentration within a given element in the flow channel would be a function of its location with respect to the moving sand front. Thus, both the pressure gradient and rate of sand front advance would not be constant, but would change as the front progressed toward the end of the model. If this occurred, length would be a parameter and large distances would have to be simulated by the model in order to duplicate the distances found in the prototype.

Basically, there are two distinct scaling techniques. In one, the significant dimensionless parameter groupings, as determined by dimensional techniques and a fairly complete understanding of the process, are scaled. This approach has the advantage of permitting a greater latitude in selecting the values of the individual parameters. Because of lack of knowledge of the basic mechanics involved in slurry transport, this method could not be applied with any confidence. In short, no one has found the "Reynolds number" for slurries.

The method used in this study consists of scaling the individual parameters in terms of mass, length and time. For example, if it is desired to let length in the model, L, represent four times its length in the prototype, the L'/L ratio is 4. Since gravitational forces cannot be altered, the time ratio, T'/T, is fixed at 2. If

the mass of materials used in the model are identical to those assumed to exist in the prototype, the mass ratio, M'/M, is 64. From these three basic relationships, scaled values for the pertinent variables in this problem can be determined. A partial list of the scaling ratios includes: $\mu'/\mu = 8$; $v'/v = 2$; $P'/P = 4$; $Q'/Q = 32$.

While this work showed that the pressure gradients and sand front advance were constant during the unsteady state sand placement, a series of runs was made using the L'/L ratio of 4. The tests were designed to duplicate previous runs in the basic test series using the 58 cp oil. Since the viscosity scaling ratio was 8, the 7 cp oil was used as the fracturing fluid. The propping agent was 70-140 mesh glass beads. These beads were one quarter the size of the 20-40 mesh beads used in the original runs and also had a sphericity of almost 1.0. If a natural sand had been used in the basic test series, it would have been difficult to match both size and angularity. A 1/16-inch spacer was used to simulate the 1/4-inch fracture.

The results of these tests are given in Table I. The numbers in parentheses are the data obtained in the tests being simulated. The sand front velocities obtained in the scaled runs have been multiplied by 2, the velocity scaling ratio, for purposes of comparisons. The pressure gradients shown are identical to the values obtained in the tests.

TABLE I

RESULTS OF SCALING EXPERIMENTS

Run No.	Flow Conditions (gpm-lb/gal)	v_s (ft/min)	$\frac{\Delta P}{L}$ (oz/in^2/ft)	
47 (31)	8 - 8	20.9 (23.8)	5.12	(5.81)
48 (27)	4 - 8	13.4 (13.4)	3.91	(4.23)
49 (28)	1 - 8	6.04(6.24)	3.23	(3.24)
50 (25)	1 - 1	1.13(1.30)	1.68	(1.79)
51 (26)	4 - 1	4.10(3.93)	2.44	(2.76)

Differences between the two sets of figures are within the estimated experimental error. In addition the modes of sand transport were identical. These results are encouraging and indicate the scaling procedure outlined may be realistically applied to slurry flow in horizontal fractures. This concept was used to interpret and correlate the results of test runs outside the basic test series. Moreover, these principles may prove useful in extensions of this work, particularly if a radial flow system is studied.

CHAPTER III

MODES OF FLOW

One of the most important sources of information in these tests was derived from the ability to visually observe the movement of the solid particles in the slurry. At the initiation of this study, there was some doubt whether the measurable parameters, such as pressure and rate of sand front advance, would be sufficiently consistent and meaningful for correlation. The description of the movement of the solid particles in the slurry was considered an important contribution to the knowledge in this area and equally important in analyzing the other recorded data. This was particularly true in the case of pressure since others (3,8) have observed that minimum head loss occurred in the transition from the deposit to the nondeposit flow regime.

Flow Regimes in Basic Test Series

The basic test series investigated the viscosity of the oil, the rate of fluid flow, and the volumetric concentration of the propping agent as the primary variables. Fracture thickness was set at 1/4 inch and 20-40 mesh round glass beads were used as the propping agent. The solid concentration was varied from 1/4 to 8 pounds per gallon. In this work, concentration is expressed either in true volumetric concentration or as pounds of solids in a gallon of pure liquid.

The flow rate was varied from 1/4 gallon per minute to 8 gallons per minute. For the 1/4-inch spacer, the average bulk velocities in the model ranged from 1.68 to 53.7 feet per minute.

Most of these runs were performed using three different oils. The viscosity of the oils at room temperature was 6.96, 57.8, and 487.9. The density of the oils was essentially constant in the range of 0.85-0.88 gram per cc.

Figure 6 illustrates the different regimes devised to describe the transport mechanisms observed. The regions in which the flow regimes dominate are described in terms of the three basic test parameters. Bulk flow rates are expressed in terms of average bulk velocities. The total flow pattern may be basically divided into two regimes—deposit flow and suspended flow. Suspended flow may be defined as that flow regime wherein each particle is primarily propelled by the direct action of the fluid acting on its surface. This definition does not preclude the presence of a vertical solids concentration gradient in the liquid stream. Deposit flow, on the other hand, is defined in this study as that flow regime wherein the solid particles settle to form at least a single monolayer "pack" at the bottom of the fracture. The rate of advance of the leading edge of the sand deposit is normally much less than the superficial velocity of the transporting fluids. Although the movement of the solid is a function of the movement of the fluid, the front either moves because of the sand flowing above or along the solid surface with eventual deposition at the front edge or by the movement of the solid deposit itself.

The lines shown in Figure 6 represent the general position of

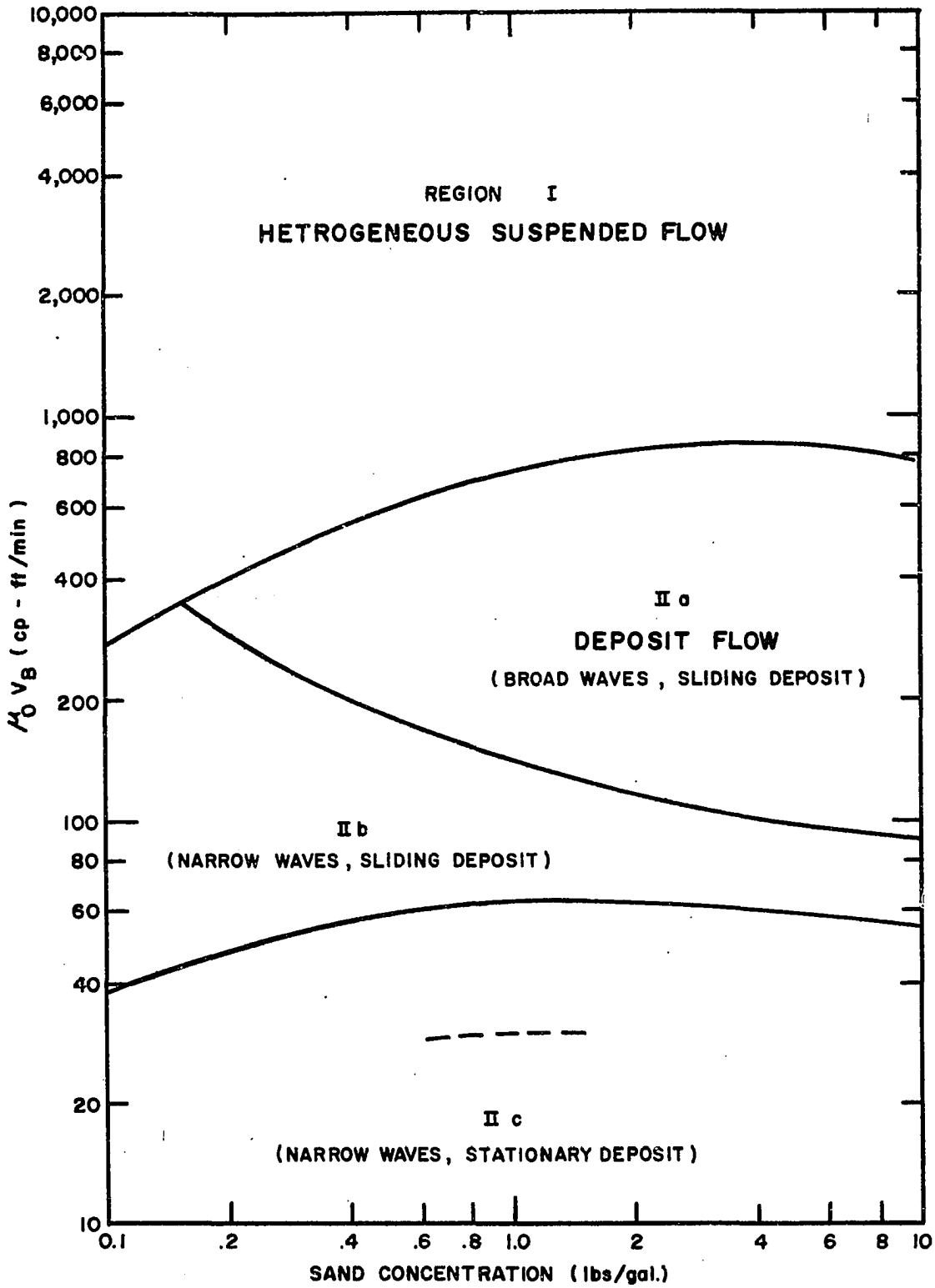

FIGURE 6 FLOW REGIMES IN THE BASIC TEST SERIES
(b = 1/4", 20-40 MESH BEADS)

the transition zone between regimes and not unique values. No tests were made specifically to define the transition from the various regimes. This figure was constructed from observation during tests designed primarily to obtain quantitative data. The numbers used in Figure 6 are based on this specific study and would apply only to the particle size and fracture thickness used. However, the general relationship of the areas to each other should apply to a wide range of particle sizes and fracture thicknesses.

A better understanding of the transport mechanisms is afforded by considering a concentration of 1 pound per gallon and describing the change in the flow characteristics as the "$\mu_o v_B$" ratio increases. Region IIc in Figure 6 represents that area of the deposit flow regime wherein the sand body either does not move or its motion is erratic. The deposit is extended primarily by beads moving along the solid surface to the leading edge of the front, at which point they are incorporated into the deposit. Bead movement to the front is in the form of narrow particle waves. A detailed description of this mechanism will be given later.

The dashed line shown in the middle of Region IIc represents the point, at the specified concentration, where the sand body itself starts to pulsate. These pulsations increase in frequency and intensity until Region IIb is reached. At this point a slow but steady advance of the sand deposit is attained.

Region IIb represents the general area wherein narrow particle waves are active in the movement of the solid over the sliding deposit. As the "μv" product is increased, the breadth of these waves increases

until Region IIa is entered. This region represents the deposit flow regime where broad waves are transporting solids over a moving solid deposit.

Region I represents truly heterogeneous suspended flow of the solids in the slurry. There is a definite concentration gradient in the vertical direction but the flow satisfies the definition for suspended flow.

A third regime of flow was never attained in this work—homogeneous flow. Homogeneous flow would be defined as that flow regime wherein the conditions for suspended flow were satisfied without a vertical concentration gradient.

With every combination of flow rate and sand concentration tested with the 7 cp oil, some form of deposit flow occurred. With the 488 cp oil, only suspended flow was observed. The glass beads were transported by the intermediate viscosity oil in both the deposit and the non-deposit flow regimes, depending upon the specific test conditions.

Tests with the 7 cp Oil

The initial tests were performed using 7 cp oil. According to Beal (1) this is the average viscosity of continental crudes. However, the average includes some light condensate production. Because of this, the viscosity of a typical crude used as a fracturing fluid may be slightly higher.

The bead deposits formed during these tests normally were not stationary, but moved along the bottom of the fracture. Only at 1/4 gallon per minute, the minimum flow rate tested, was the bead or sand pack definitely stationary. At flow rates of 1 gallon per minute the deposit

moved in a pulsating manner. This action was more exaggerated at moderate solids concentrations. At high sand concentrations, the sand deposit tended to advance at fairly constant velocities. Uniform advance of the deposited sand occurred at the higher flow rates, regardless of concentration.

The presence of deposited sand altered the flow conditions in the fracture and increased the superficial velocity of the sand slurry flowing above it. Sufficient sand was deposited on the bottom of the fracture to permit the transport of sand in varying degrees along the surface of the sand deposit and in the open section above. It was generally transported to the leading edge of the sand bank where the velocity is reduced and the sand became part of the sand bank. Except for the test at 1/4 gallon per minute the sand pack may be considered as being propagated by the addition of sand at both ends.

The transport of beads above the settled layer followed a general pattern. The beads were seldom transported as individual particles in suspension. An important means was the rolling and/or sliding of particles along the top of the sand deposit. This mechanism was present in all tests in the deposit flow regime.

In the transport of beads as a slurry in the open section of the flow channel, interaction between particles played a very important role. This interaction manifested itself by the formation of particle waves which advanced relatively fast downstream. The general character of these waves is illustrated through a series of pictures taken from the overhead sequence camera.

Figure 7 shows the wave action of the glass beads in four test

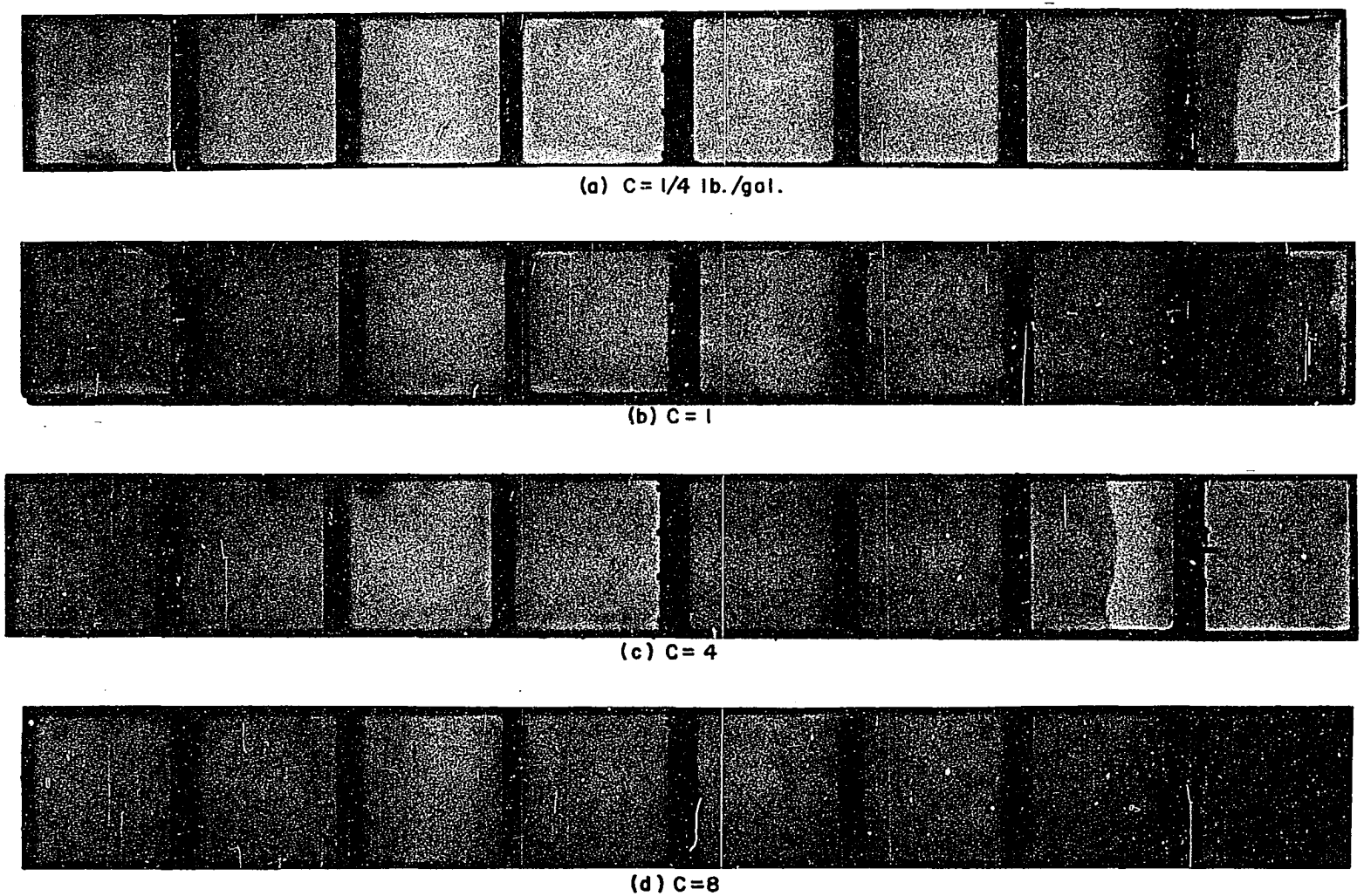

(a) C = 1/4 lb./gal.

(b) C = 1

(c) C = 4

(d) C = 8

FIGURE 7 MODEL VIEWS SHOWING THE INCREASE IN WAVE ACTION WITH INCREASING SAND CONCENTRATION

(μ_o = 7 cps., Q = 1 gpm , b = 1/4 in., 20-40 mesh beads)

runs while using 7 cp oil. In these overhead views of the model, the first and last panels are not shown. The tests were all performed at a liquid flow rate of 1 gallon per minute with sand concentrations of 1/4, 1, 4, and 8 pounds per gallon. At the low concentration (Figure 7a), the waves are barely noticeable. As the concentration increases, the frequency and intensity of the wave action increase.

At the low flow rate used in Figure 7 the waves did not extend across the full breadth of the model. They were localized and tended to be confined to a given width. However, as the waves reached the leading edge of the sand pack they spread out, distributing sand over large segments of the front.

As the waves advanced downstream, a furrow of beads was formed on both sides of its line of flow. A relatively loose sand pack or channel was left directly behind the waves. As shown at the higher concentrations, the waves tended to move through the channels created by previous waves. Between waves, beads were transported as individual particles or small groups of particles along the top of the sand pack and into these channels. Bead transport between waves tended to close the channels, but wave action reopened them before closure occurred.

At 1/4 pound per gallon sand concentration there was a slight but definite wave action that is not apparent in Figure 7. Still pictures are basically inferior to motion pictures and actual observations because the motion of the beads draws the observer's attention to the transport mechanism. Photographs must rely on light contrast obtained with various degrees of bead packing. If the contrast is slight, it may be lost during reproduction. In Figure 7(a), the contrast is

sufficient to show the channeling within the bead pack. The channels were formed as a result of the wave action transporting the beads to the edge of the sand front.

In Figure 8, the effect of flow rate on the mode of flow of the beads is demonstrated. The four runs shown were made at a bead concentration of 1 pound per gallon. The fluid flow rates were 1/4, 1, 4, and 8 gallons per minute. At the low flow rate the wave action occurring above the stationary bead deposit was similar to that observed in Figure 7(b). This picture, depicting flow at 1 gallon per minute with 1 pound per gallon sand, was repeated in this series.

When the flow rate was 4 gallons per minute the character of the wave action changed. As seen in Figure 8(c), the waves were no longer narrow but generally extended across the entire panel. They had more of a rolling action and a fairly constant frequency which was lacking in the runs shown in Figure 7. The sand pack moved downstream at a substantially constant velocity. A few particles were transported in suspension in the open section of the fracture.

In this test, portions of the wave front near the sides of the model advanced ahead of the center section. This V-shaped configuration may be caused by the two-point slurry entry near the sides of the model, with the center of the entrance blocked with beads. At this flow rate, an increase in sand concentration increased the intensity of the wave action. Flow described in Region IIb occurred when the sand concentration was reduced to 1/4 pound per gallon.

Figure 8(d) was obtained at a flow rate of 8 gallons per minute. Here, suspended flow conditions were being approached. Although the

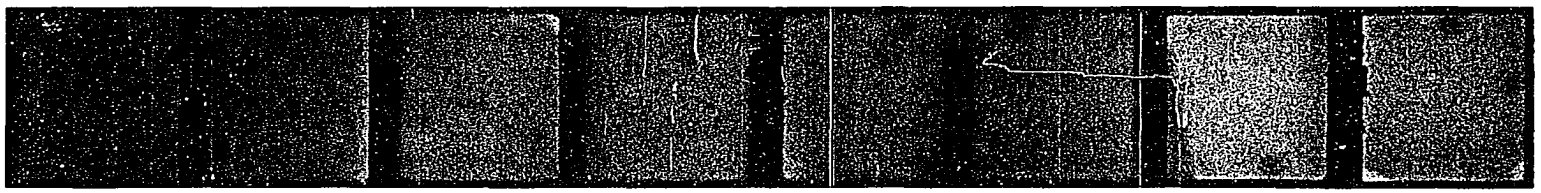

(a) Q = 1/4 gpm

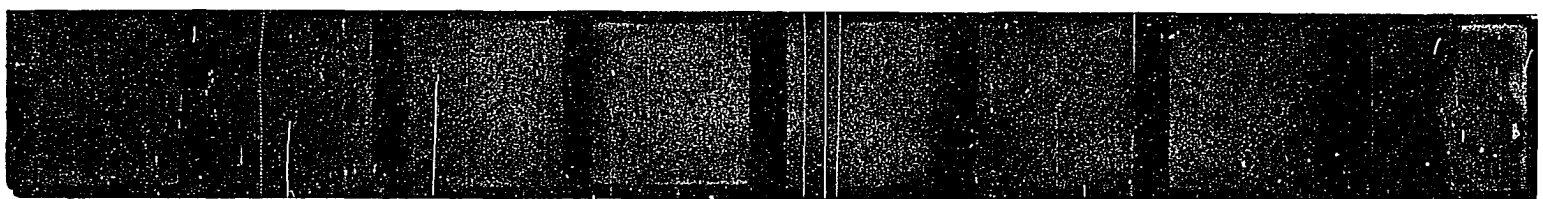

(b) Q = 1 gpm

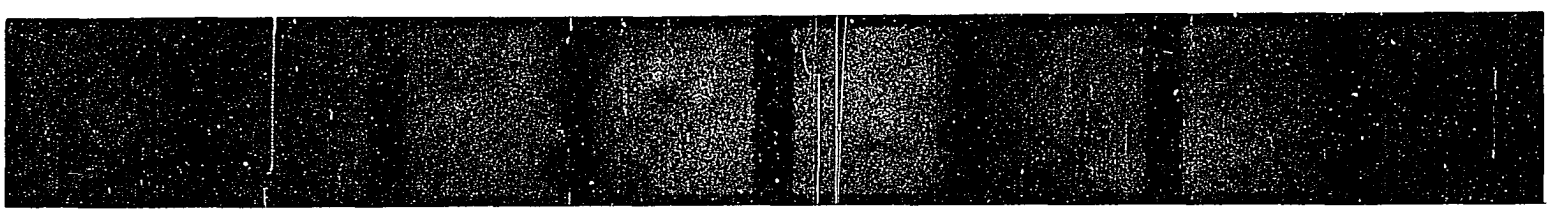

(c) Q = 4 gpm

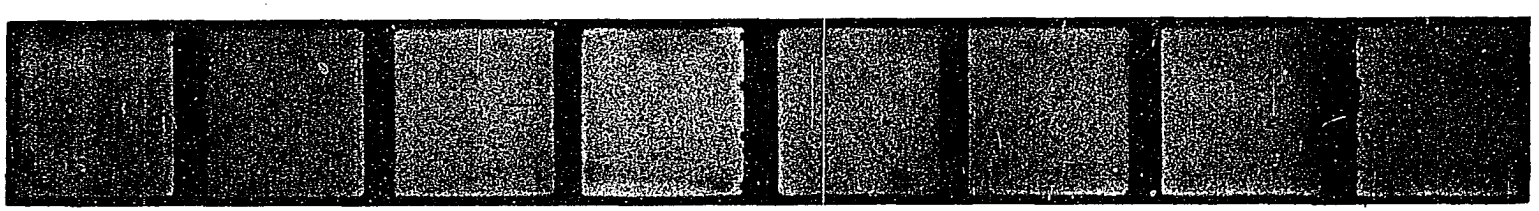

(d) Q = 8 gpm

FIGURE 8 MODEL VIEWS SHOWING WAVE ACTION AT VARIOUS FLOW RATES
(μ_o = 7 cps., C = 1 lb/gal., b=1/4 in, 20-40 mesh beads)

character of the waves had again changed, this transport mechanism still persisted. The details of the wave action cannot be distinguished in the still photograph but there was the underlying broad rolling wave action that normally preceded the advent of suspended flow. This test was performed at 8 pounds of sand per minute, the maximum sand injection rate. Larger sand flow rates were possible but presented a definite safety hazard. Thus, the propping agent concentration was not increased above 1 pound per gallon at this high flow rate. Tests at lower concentrations resulted in diminishing the wave action even further. With 1/4 pound of sand per gallon it was difficult to distinguish any wave action. A few ripples were formed on the surface of the moving, loosely packed bead deposit.

Tests with the 58 cp Oil

The majority of the flow conditions in the experiments described above were duplicated in tests using 58 cp oil. At the lower flow rates a bead deposit was associated with the transport mechanism. However, as rates increased, suspended flow was obtained even under these laminar flow conditions.

Figure 9(a) shows a test run using 58 cp oil at flow conditions of 1 gallon per minute and 1 pound per gallon bead concentration. It was noted that the wave action over the sand pack was not narrow and localized as obtained using 7 cp oil under identical test conditions. The waves were broad and generally covered the whole width of the panel. The appearance of this run was more analogous to the action obtained at 4 gallons per minute using the light oil. However, the waves were stronger and better defined. This picture demonstrates that increases in fluid

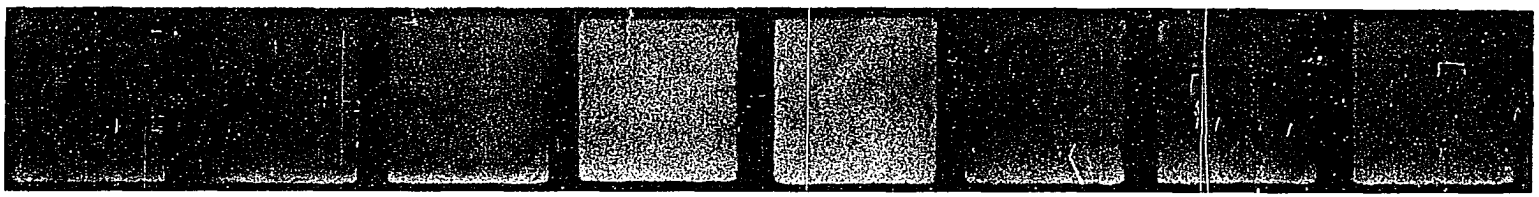

(a) REPEAT OF 7(b) USING 58 cps. OIL

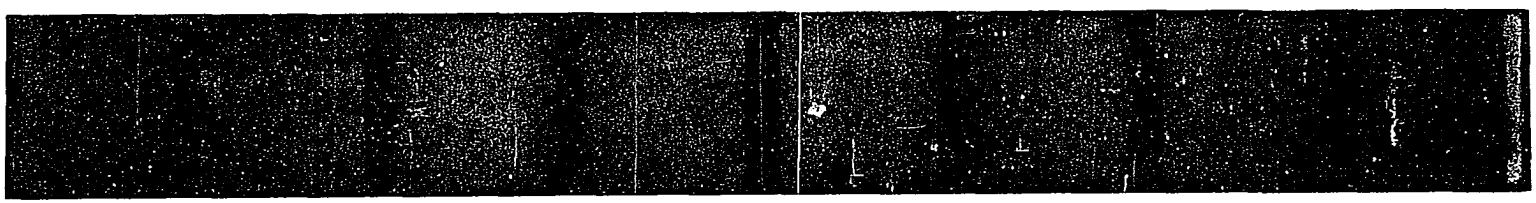

(b) REPEAT OF 7(b) USING 20–40 MESH OTTAWA SAND

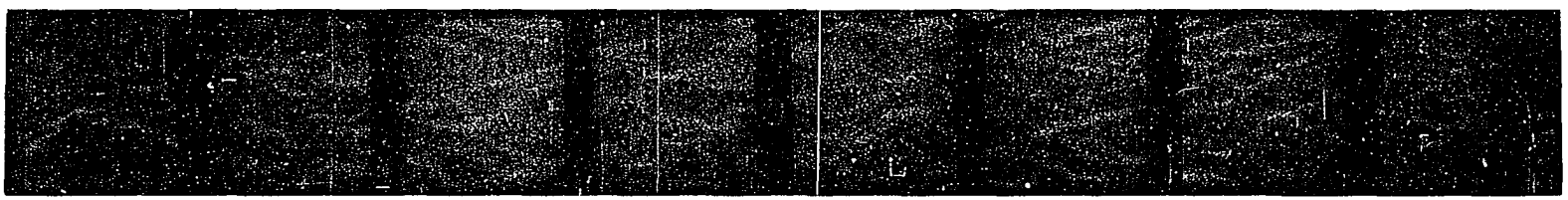

(c) OVERFLUSH OF 9(b), TIME - 2 MINUTES

FIGURE 9 MODEL VIEWS AT VARIOUS TEST CONDITIONS

viscosity have the same effect on the transport mechanism as increases in fluid velocity.

At this flow rate of 1 gallon per minute, a decrease in sand concentration caused the frequency and strength of the waves to greatly diminish. Increasing the sand concentration to 8 pounds per gallon also decreased the wave action. The sliding sand deposit appeared to have only a few ripples of beads along its surface.

In subsequent tests at flow rates of 4 and 8 gallons per minute, suspended flow was obtained. Although it was easy to differentiate visually between the bead-laden slurry and the clear fluid contact, it could not be distinguished on the overhead sequence camera film. Therefore, no pictures are shown.

Homogeneous suspended flow was never obtained in these tests. Heterogeneous suspended flow was expected, since laminar flow persisted even at the highest flow rates tested. Homogeneous flowing suspensions are obtained only with fine particles and under turbulent flow conditions. The turbulent eddies associated with the flow tend to disperse the solids and keep them suspended. Chien (4) has demonstrated that a major factor affecting distribution of solids at turbulent stream is the ratio of the terminal settling velocity of the solid particles to the friction velocity at the wall. The general form of the equation is

$$\left(\frac{C_2}{C_1}\right) = f\ \left(\frac{y_2}{y_1}\right)^{-v_t/kv_w^*} \tag{35}$$

where C_1 and C_2 are the concentrations at elevations y_1 and y_2, respectively, and the coefficient of k is considered the universal constant with a value of 0.4. Development of this equation was based on the

assumption that the settling due to gravity is balanced by the upward transport due to turbulence.

Because of the presence of the concentration gradient in these tests it was difficult to distinguish between flow with a thin deposit and heterogeneous suspended flow. The criterion used in these tests was whether or not at least one nearly complete monolayer of beads was associated with the flow. If a monolayer was formed, flow was considered to be in the deposit flow regime.

Under these laminar flow conditions, transport in Region I was characterized by a form of layer flow; that is, the beads within a given vertical increment would move at substantially the same, constant velocity. The number of layers varied from 2 to 5 and was confined to the lower half of the fracture. The velocities of these layers increased as the distance from the lower boundary of the fracture increased. There was very little, if any, exchange of beads from one level to another. However, as beads from the faster moving upper layers reached the sand front, they would be distributed within the lower layers. Thus, even under suspended flow conditions, the sand was not distributed in chronological order. The number of beads within a given layer varied with vertical position, with the bottom layer containing the most beads. The bead concentration within a given layer remained constant as the flow progressed downstream. The relative position of the beads within a given horizontal layer did not change to any great degree. Although no supporting data were obtained, it appeared as if the sand was distributed so that the layers would transport equal amounts of sand during a given time increment.

Tests with 488 cp Oil

In tests using the 488 cp oil, heterogeneous suspended flow occurred in every case. Neither fronts nor the detailed sand movement could be distinguished from the sequence camera film. Therefore, none of these pictures were included.

Four tests using this heavy oil were made at a fluid flow rate of 1 gallon per minute. The concentrations were 1/4, 1, 4, and 8 pounds of sand per gallon of liquid. The notes obtained during the visual observations of these tests indicated that the degree of packing in the bottom layers varied from 40 to 70 per cent, depending on sand concentration. In the upper layers the beads were more widely dispersed. At 1/4 and 1 pound per gallon one layer was flowing over the bottom layer. At 4 pounds per gallon two upper layers were present. At 8 pounds per gallon it was difficult to distinguish the number of layers or the degree of packing within the layers. However, there were approximately four upper layers in this test.

At 2 gallons per minute flow rate, the number of upper layers involved in the flow mechanism was also a function of the sand concentration. The bead concentrations tested were 1/4, 1, and 4 pounds per gallon which resulted in three, four, and five layers, respectively.

The final runs of this test series were performed at a flow rate of 4 gallons per minute. Tests at 8 gallons per minute were not made because of the pressure limitations of the flow model. Tests at 1/4, 1, and 2 pounds per gallon of glass beads resulted in three, four, and five-layered flow. In the test at 1/4 pound per gallon concentration, the beads were more widely dispersed than in any previous test.

It was estimated that if flow had been stopped upon reaching steady state flow conditions a 50 per cent partial monolayer of beads would have been distributed in the fracture. Calculations based on rate of advance of the sand front confirm this observation. For a given oil, the amount of sand distributed in the fracture increased as sand concentration increased and/or flow rate decreased.

Other Basic Series Tests

Two runs made using a 3.2 and a 14.2 cp oil were included in this basic test series. Both tests were performed at a fluid flow rate of 1 gallon a minute and at a sand concentration of 1 pound per gallon. The other test conditions were identical to those set forth in this series of tests. Doubling the viscosity did not appreciably affect the mode of flow observed under these flow conditions using the 7 cp oil. However, the waves were slightly more consistent. Reducing the viscosity by half greatly affected the mode of flow. With this low viscosity oil, the wave action became much more erratic and inconsistent. Except for occasional sliding action associated with a few larger waves, the deposit at the bottom of the fracture was stationary. The mode of flow was identical to that obtained with the 7 cp oil at a flow rate of 1/4 gallon per minute. At these low $\mu_o v_B$ values a high degree of choking or clogging of the flow passage was required to transport the sand.

Effects of Other Parameters on the Modes of Flow

A cursory scan into the effects of propping agent angularity, fracture thickness, and size of the propping agent on sand transport was made. These tests were performed using the 7 cp oil. The flow conditions

were normally set at 1 gallon per minute fluid at 1 pound per gallon sand concentration. For the most part the parameters were investigated individually with the remainder of the variables being held constant at the value designated during the basic test series. These variables were only scanned since the number of runs required for an extensive study was prohibitive.

Sand Angularity

Two commonly used propping agents were utilized to study the effect of sand angularity on its movement in horizontal fractures. They were 20-40 mesh round Ottawa sand and a 20-40 mesh angular sand (Figure 3). One run was made with each sand. Test conditions were identical to those in Figure 7(b).

A sand deposit was formed and advanced steadily downstream during the test with the round Ottawa sand. However, no wave action was associated with the transport to the leading edge of the front. Instead, flow channels were formed within the pack, as shown in Figure 9(b). The bulk of the sand transported to the front was carried in these channels with very little in the open section above the pack and along the top of the banks between channels. A few panels upstream from the sand front the sand pack contained fewer and wider channels. However, near the front the channels became narrower and more numerous and gave a cross-hatched appearance. This channel configuration distributed the sand evenly over the entire model width and resulted in a straight even front. The character of these flow channels is more easily distinguished in Figure 9(c). This picture was obtained by "overflushing" the sand pack with clean liquid at the same flow rate used for its implacement.

One important factor in wave formation is the rolling and sliding of the beads or sand along the surface of the sand pack. During this motion, beads become randomly aligned which alters the localized flow conditions. Because of the interaction between particles and the localized increase in fluid velocity, additional particles on the verge of movement in the pack are incorporated in the wave. As the wave advances over the sand deposit, it catches up to and incorporates more particles. The wave grows and the previously opened section above the sand deposit becomes increasingly choked. Choking occurs to such a degree that part of the bead pack as well as the wave is pushed downstream and to the sides, leaving an open channel behind the wave. In the case of nonspherical particles, it is more difficult for the sand to slide or roll along the top of the sand pack, thus making it difficult, if not impossible, for the initial phase of wave formation to occur.

When this test was repeated using 20-40 mesh angular sand, the mode of transport was almost identical to that obtained with the Ottawa sand. The major difference was that the bead pack did not slide at a constant velocity but advanced in occasional jumps or pulsations. Bead transport to the edge of the front was again through channels. The channels were slightly narrower, more numerous, with a greater degree of cross-hatching.

Although the use of natural sands altered the mode of transport in these specific tests, the analysis of the quantitative data showed that the rate of advance of the sand front and pressure drop were only changed slightly.

Fracture Thickness

Three runs were made using the 1/16, 1/8, and 1/2-inch spacers to investigate the effect of fracture thickness on sand transport. Except for this parameter, the test conditions in Figure 7(b) were duplicated. The transport mechanism in these tests ran the full gamut from heterogeneous suspended flow to deposit-load flow.

The utilization of 20-40 mesh glass beads in these tests resulted in a change of the fracture thickness to bead diameter ratio directly proportional to the change in fracture thickness. The diameters of 20-40 mesh glass beads ranged from 0.84 mm to 0.42 mm with an average diameter of 0.63 mm. The changes in superficial bulk velocities were inversely proportional to fracture thickness.

In the test using the 1/16-inch spacer, it was possible for two of the larger size beads to bridge in the flow channel. However, this did not occur. The beads moved through the model in two-layer flow with the upper layer passing over the bottom layer. Although the beads in both layers were widely dispersed, the bottom layer contained the majority of the particles.

The mode of transport in Region IIa occurred when the fracture thickness was increased to 1/8 inch. The bead pack flowed along the bottom of the fracture at relatively constant velocity with a strong, broad wave action occurring above it.

A different mode of flow was observed in the test using the 1/2-inch thick fracture. A very thick bead deposit was formed within the fracture which moved en masse toward the discharge end of the model. There was no wave action or suspended flow in the open channel with

negligible bead movement along the surface of the bead pack. Additions to the pack were made near the entrance instead of additions of beads to the front. Solids transport under these conditions is described as deposit-load flow. This transport mechanism is unique in that the beads are distributed in the model in chronological order. The beads injected early are found at or near the leading edge of the front while the last beads injected are located at the entrance. A more or less reverse chronological order results when the bead pack is stationary. Chronological mixing occurs in varying degrees with the other bead transport mechanism deposit.

The distribution of beads with respect to the order of injection is important. In order to increase permeability of a fracture near the well bore, larger propping agents are sometimes used during the latter stages of the hydraulic fracturing treatment. Mixing is undesirable since this results in a permeability less than the permeability of the smallest size sand used. Near the well bore where the velocities are high, suspended flow is likely to occur. As the distance from the well bore increases, flow described by Regions IIa and IIb will be attained. Since severe mixing occurs in these regimes, "tail-ins" with larger size propping agents should be limited to relatively small volumes. The amount of sand should be equal to approximately that required to prop the portion of the fracture area governed by suspended flow. As a precaution, a preflush prior to this operation would be advisable.

Size of Propping Agent

These tests studied the effect of changing the fracture thickness to the bead diameter ratio by varying bead size while holding the

fracture thickness at 1/4 inch. Again the test conditions in Figure 7(b) were duplicated except for this parameter. In the first test, 40-70 mesh round glass beads were used in the slurry. This mesh size range was one-half that of 20-40 mesh beads. The results of the sieve analysis indicated that the average mean diameter of the particles was 0.31 mm. The smaller particles caused the flow regime to shift from IIc to IIa. Bead transport was in the deposit flow regime. The broad wave action was not readily apparent from the overhead sequence camera film, but was shown clearly on the motion picture film.

This test was repeated using 12-20 mesh glass beads, which were about twice the size of the 20-40 mesh beads. In this run a two-layer pack was formed at the bottom of the fracture and moved downstream at a constant velocity. Packing was so close that it gave the appearance of a miniature mosaic tile floor. There were only a few widely scattered beads on top of this pack and deposit-load flow was approximated.

An anomaly occurred in this run that had not been previously observed. A few widely separated beads advanced ahead of the leading edge of the monolayer pack. The distance from the most advanced beads to the front, as well as the number of beads, increased steadily as the front progressed downstream. These beads reached the end of the model approximately one panel ahead of the recorded sand front. Although the advanced beads were widely dispersed, there was a concentration gradient which decreased with distance from the bead deposit. Both large and small beads were present in this anomaly.

Additional Tests in 1/8-Inch Fractures

A series of tests was made using 12-20 mesh glass beads and a 1/8-inch fracture spacer. The tests were designed primarily to determine whether bridging would occur at moderate and low flow rates since two of the largest particles could bridge in the flow channel. This condition also existed in the test with 20-40 mesh beads and the 1/16-inch fracture. However, at the flow rate tested two-layered suspended flow occurred. It was doubted that two-layered suspended flow could be obtained with the heavy beads except at very high velocities.

The sand transport mechanism at a flow rate of 1 gallon per minute resulted in a single monolayer on the bottom of the fracture with a few beads moving slowly over it. Again, a few widely dispersed beads were present beyond the leading edge of the sand pack. At the end of the test the advanced beads were approximately 2 1/2 panels ahead of the full monolayer pack. The concentration of beads in this area was approximately 5 per cent of a full monolayer.

In the next run the fluid flow rate was decreased to 1/2 gallon per minute. The superficial fluid velocity in this test was equivalent to that in the 1/4-inch fracture. There was no visable change in the mode of transport except that the distance from the bead front to the leading advanced beads was approximately 1 1/2 panels.

The mode of flow did not change when the flow rate was reduced to 1/4 gallon per minute. Individual beads were located up to 8 inches ahead of the sand pack. Upon overflush, definite evidence of bridging was observed. Columns comprised of two to three beads bridging the flow channel remained. Each panel contained from 10 to 15 such

pillars or columns. Had the rate been reduced further, the bridging might have resulted in a "sandout".

No quantitative data were recorded during the tests at higher flow rates. Only notes on the mode of transport were taken. At a fluid flow rate of 1.75 gallons per minute, the bead pack at the bottom of the fracture was no longer a full monolayer. Gaps between groups of beads began to appear. As the flow rate was increased, the beads began to disperse as individual particles. At 8 gallons per minute, bead flow was still primarily restricted to the bottom layer. Because of their weight, very few beads were present in the upper section of the fracture.

Two tests were made with the 40-70 mesh beads and 1/8-inch fracture. Again, the sand concentration was held constant at 1 pound per gallon and 7 cp oil was used. At fluid flow rates of 1/2 and 1 gallon per minute, the regime of flow was in Region IIc. Since the b/d ratio was identical to the ratio in the basic test series, these two tests provided a check on the scaling techniques set forth in Chapter II. The tests simulated μv products of 188 and 376 cp-feet per minute in a 1/4-inch fracture. The regime of flow predicted from Figure 6 was identical to those observed, Region IIc.

Scaling Tests

The final series of tests was an investigation into the feasibility of scaling sand transport in thin rectangular flow channels. Five runs were made. All five were scaled to duplicate previous tests in the basic test series using an L'/L ratio of 4. The scaling procedure, description of the tests, and comparison of quantitative data are given in Chapter II.

In each case, the regime of flow observed was identical to the sand transport mechanism acting in the tests being simulated. Duplication of tests in Region IIc resulted in a broad wave action extending the full width of the model. This also occurred in original runs. However, the width of the model in these last tests represented four feet in the prototype. This indicates that broad wave action would extend indefinitely for flow between infinite parallel plates.

Overflushing

Overflushing is commonly practiced in the field. However, the volumes are normally quite small. The primary objective is to pump sufficient fluid at the end of the treatment to clear the well of sand. The volume of fluid pumped in excess of the amount necessary to clear the flow line varies with the operator.

In each test slurry was injected into the model until steady state conditions were reached; that is, until the mass flow rate of the solids out the end of the model was equivalent to the amount injected. Even in deposit flow regime, steady state conditions occurred almost immediately after the sand reached the end of the model. This was confirmed by obtaining discharge samples of the stream.

After these samples had been taken, the drive mechanism actuating the floating piston in the sand cylinder was shut down. The fluid was then bypassed around the sand cylinder to eliminate the stripping of sand from this source. Thus, during the overflush portion of the test, the fluid flow rate was maintained at a rate identical to that used in placing the sand. The superficial bulk fluid velocity in the model was

reduced because the bulk flow rate of the sand was no longer part of the flow stream.

The effects of overflushing under these conditions can be correlated to the mode of sand transport during the initial sand placement phase. In cases where the sand was transported in suspension, this flow mechanism persisted during the overflush. The model was quickly cleared of all sand.

In tests where the initial transport was in Region IIa, the broad wave action continued in the early stage of the overflush. In the latter stages a thin V-shaped pack remained in the center of the flow channel. This behavior is illustrated in Figures 10(a) and 10(b). The initial sand placement phase of this test is illustrated in Figure 9(a).

The first picture in Figure 10 was taken approximately three minutes after the overflush had begun. Here sand is still being transported over the sand pack by the broad wave action existing during the initial placement of the sand. Two waves are found in panels 8 and 9. The sand deposit is present throughout the entire length of the model. This may not be apparent because of the staining of the diffusion paper beneath the model caused by a slight oil leak around the O-ring seal and the center gasket joining the two sections of the model. Staining causes the center two panels and the perimeter of the model to transmit more light.

Behind the waves, the thickness of the bead pack is reduced by the continual rolling and sliding of particles along the surface. This action diminishes as the pack becomes thinner and it almost terminates when only two or three layers of beads remain.

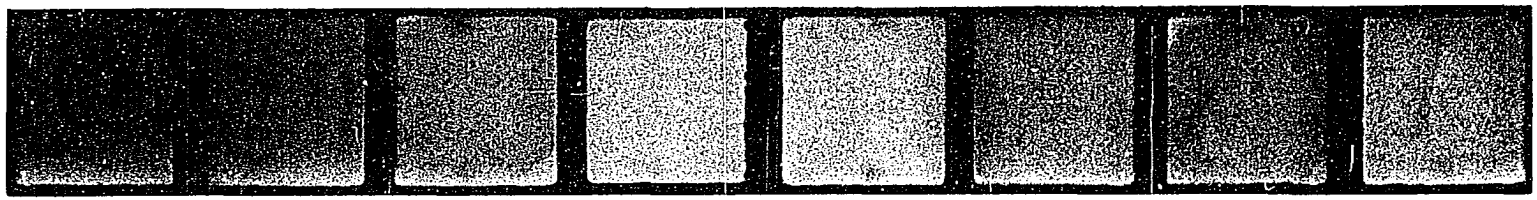

(a) OVERFLUSH OF 9(a), TIME-3 MINUTES

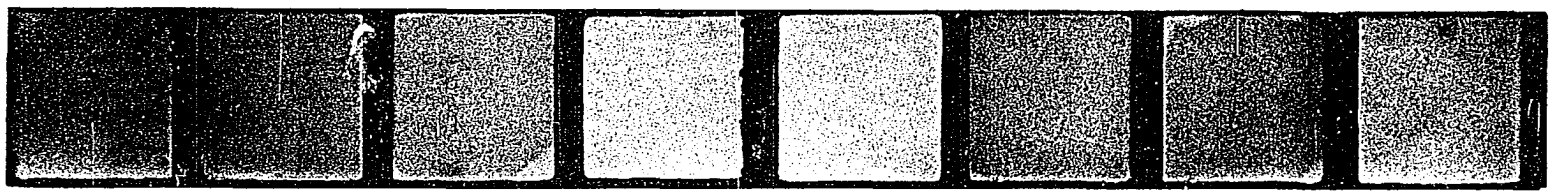

(b) OVERFLUSH OF 9 (a), TIME - 60 MINUTES

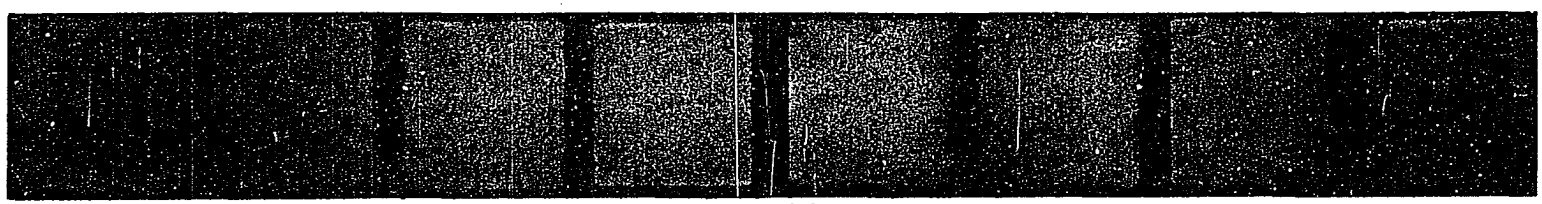

(c) OVERFLUSH OF 7(b), TIME - 2 MINUTES

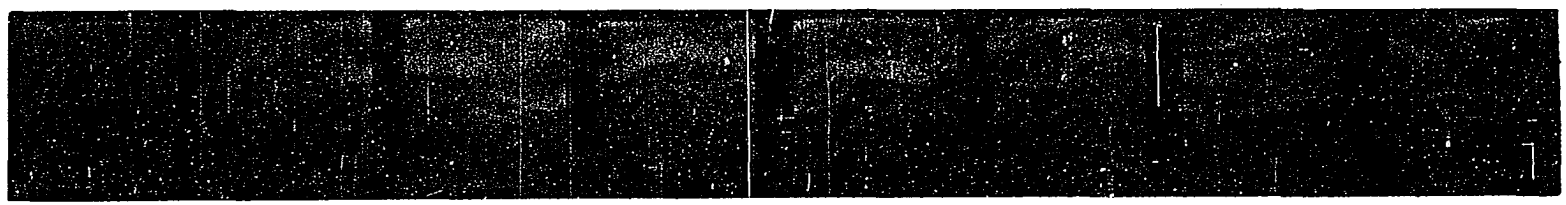

(d) OVERFLUSH OF 7(b), TIME - 52 MINUTES

FIGURE 10 MODEL VIEWS DURING OVERFLUSH

Figure 10(b) shows the progress made in sand removal after a time lapse of one hour. A 2 and 3-grain V-shaped pack remained in the center of the flow channel. The width of the open flow channels flanking the pack decreases as distance from the header increases until they are nonexistent approximately half way down the length of flow. Superimposed upon this pack is another layer of beads having similar configuration. Its peak starts slightly downstream from the crossbar separating the fourth and fifth panels. Particle movement along the top of the sand pack in the upstream half of the model has almost terminated. This mode of transport is still occurring downstream on the thicker deposit. Narrow waves are present in the ninth panel, where the sand concentration in the flow channel is still fairly high.

The V-shaped configuration of the sand deposit may be due to the irregularity of slurry entry into the flow channel. Entry was primarily at the sides of the flow channel. In the initial phase of the overflush, sand along the sides was stripped out faster than in the center. Because of this action, the open channels were formed at the sides of the model. These open channels carried a large portion of the flow and continually stripped sand from the sides of the sand pack. It is conceivable that, had the entry been primarily at the center of the model, an open channel would have formed in this area.

Overflushing of tests originally in Regions IIb and IIc resulted in a rapid termination of the localized wave action and deposit movement. Instead, many narrow randomly aligned channels were quickly developed because of irregularities along the surface and within the sand deposit. Certain channels began to dominate the flow and were

widened and deepened as flow continued. This is illustrated in Figures 10(c) and 10(d). The mode of sand transport occurring in the sand placement phase of this test is shown in Figure 7(b).

Figure 10(c) was taken two minutes after the flush was initiated. Fluid entry was primarily on the right side even though staining of the diffusion sheet gives the appearance that fluid is entering also on the left side. In this stage of the overflush the channels are not well defined and have a cross-hatched appearance near the center of the flow channel.

The last picture in this series of photographs shows the development of the channel 52 minutes after initiation of the overflush. The strong fluid entry on the left side is now quite evident. The principal channels are broad and meandering with numerous smaller channels leading into them. The channels are located primarily on the right side near the model entrance. However, as the flow moves downstream, the channels distribute themselves more or less evenly to cover the full width of the sand pack.

Figure 9(c) shows channel formation occurring 102 seconds after the initiation of the overflush of the test performed with 20-40 round Ottawa sand. In this run a sliding sand deposit containing channels was obtained during the initial sand placement phase. Sand was transported to the leading edge of the front primarily through channels within the pack. During the overflush, the existing channels within the pack were widened and deepened giving them a well-defined appearance in this print. The interlocking network of channels especially prevalent near the end of the model is analogous to those existing near the front in Figure 9(b).

Similar results were obtained in the overflush of the angular sand test.

Data pertaining to the rearrangement of sand in a fracture during overflush indicate that sand which had been transported in suspended flow may be transported or completely removed from the area dominated by this flow mechanism. From a theoretical standpoint this is advantageous since an open flow channel containing no sand has the highest flow capacity. However, if the sand is removed from a sufficiently large area, closure around the well bore may result when the treating pressure is released.

Even without overflushing, suspended flow may present a problem. If the area dominated by this flow mechanism is sufficiently large, the bead concentration in this area may not be adequate to hold the fracture open. Complete closure could result if the beads crush or imbed in the formation. This is more of a problem with the thicker, more viscous crude oils and the gels than it is with a standard crude. Sufficient propping around the well bore may be insured by using a lighter oil or by reducing pump rates near the end of the treatment.

One of the most desirable configurations of sand placement is the wide channel shown in Figure 10(b). Here the channels are sufficiently wide that a high capacity flow channel would exist after fracture closure. With the narrow channels generally obtained by overflushing at low flow rates with the 7 cp oil, fracture closure may completely level out the highs and lows of the sand bank.

The results of these tests indicate that the desired increases in fracture flow capacity by overflushing with large fluid volumes is feasible provided they are carefully designed. The design may consist

of successive overflushes followed by sand slurry tail-ins. These can be performed with various oils and/or rates to yield a high fracture flow capacity and insure fracture-well bore connection. The possibility that induced fractures extend primarily in one or more directions increases the feasibility of overflushing.

One important aspect of overflushing is the reduction in sand cost. The expenditure for the sand is a major cost item with multi-layer sand propping. Overflushing not only distributes the sand in such a manner that the fracture flow capacity is increased, but it extends the radius without a proportionate increase in this cost item.

CHAPTER IV

BASIC QUANTITATIVE DATA

The quantitative information desired from these tests was the rate of sand front advance and pressure behavior along the line of flow. This chapter deals with the analysis of the experimental findings and their conversion into the convenient engineering parameters.

Rate of Sand Front Advance

Rate of sand front advance was obtained by plotting sand front position readings versus elapsed time for each run. Without exception this resulted in a straight line on coordinate paper, i.e., sand velocity was a linear function of time. Figure 11 shows such a typical plot of the data (Run 49). This run was performed using 7 cp oil, 70-140 glass beads, and a 1/16-inch thick spacer. The flow rate was 1/8 gallon per minute with a sand concentration of 8 pounds per gallon. The slope of the straight line portion of this curve is defined as the rate of frontal advance. In this case it is 3.02 feet per minute. The superficial bulk fluid velocity is 4.09 feet per minute. The resulting sand transport efficiency, v_s/v_B, is 0.74.

The important implication of the straight line section of these curves is that except for possible irregularities at the sand front and model entrance the degree of packing within the sand bank is

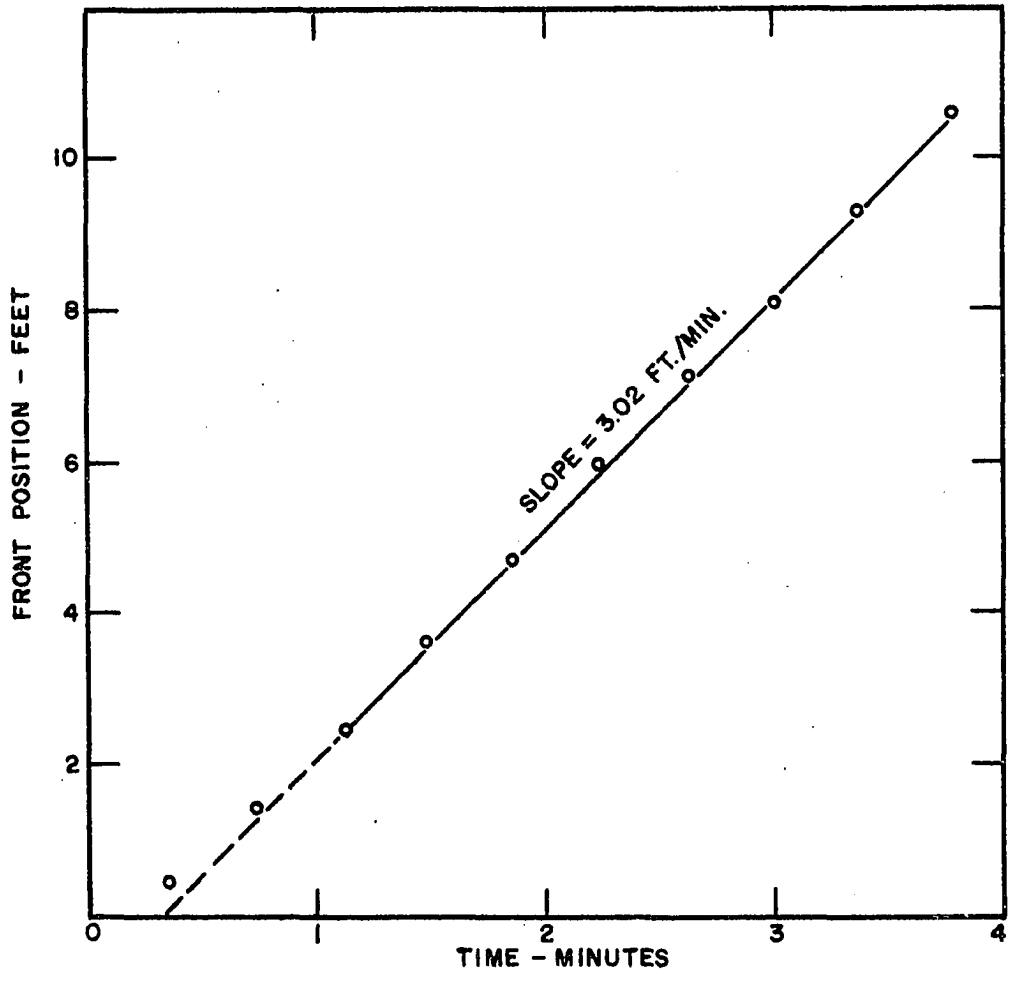

FIGURE 11 DETERMINATION OF RATE OF SAND FRONT ADVANCE

constant and not a function of time. Straight line relationships obtained in the suspended flow regime shows that concentration of the sand behind the leading sand particles also does not vary with time. The continual recurrence of the straight line is a clear indication that it is unnecessary to physically lengthen the model or to "scale" length to properly interpret the results for application to long horizontal fractures, provided the model length is sufficient to minimize end effects.

The dashed line in Figure 11, the extrapolation of the straight line portion of the curve, intersects the abscissa at 19 seconds. The time intercept was common among the other runs and was a result of the inherent delay representing the time required for the sand to reach the fracture entrance. As part of the test procedure, the clock was started as the 3-way valve was turned to direct flow into the header. There was approximately a 14.5-cubic inch holdup volume in the model header and associated flow channels leading to the fracture slit. The bulk flow rate in this test was 36.8 cubic inches per minute. Therefore, 19 seconds was within the expected time differential. In this run the delay time was exaggerated not only by the low flow rate but also by the narrow fracture thickness and high sand transport efficiency.

The first two data points in Figure 11 indicate channeling within the model header, i.e., sand enters the model prematurely. This anomaly is corrected as the test proceeds.

Pressure Behavior

While rate of frontal advance data is by definition limited to the initial sand placement phase of the tests, pressure data were obtained during the entire test interval. Figure 12 shows the total

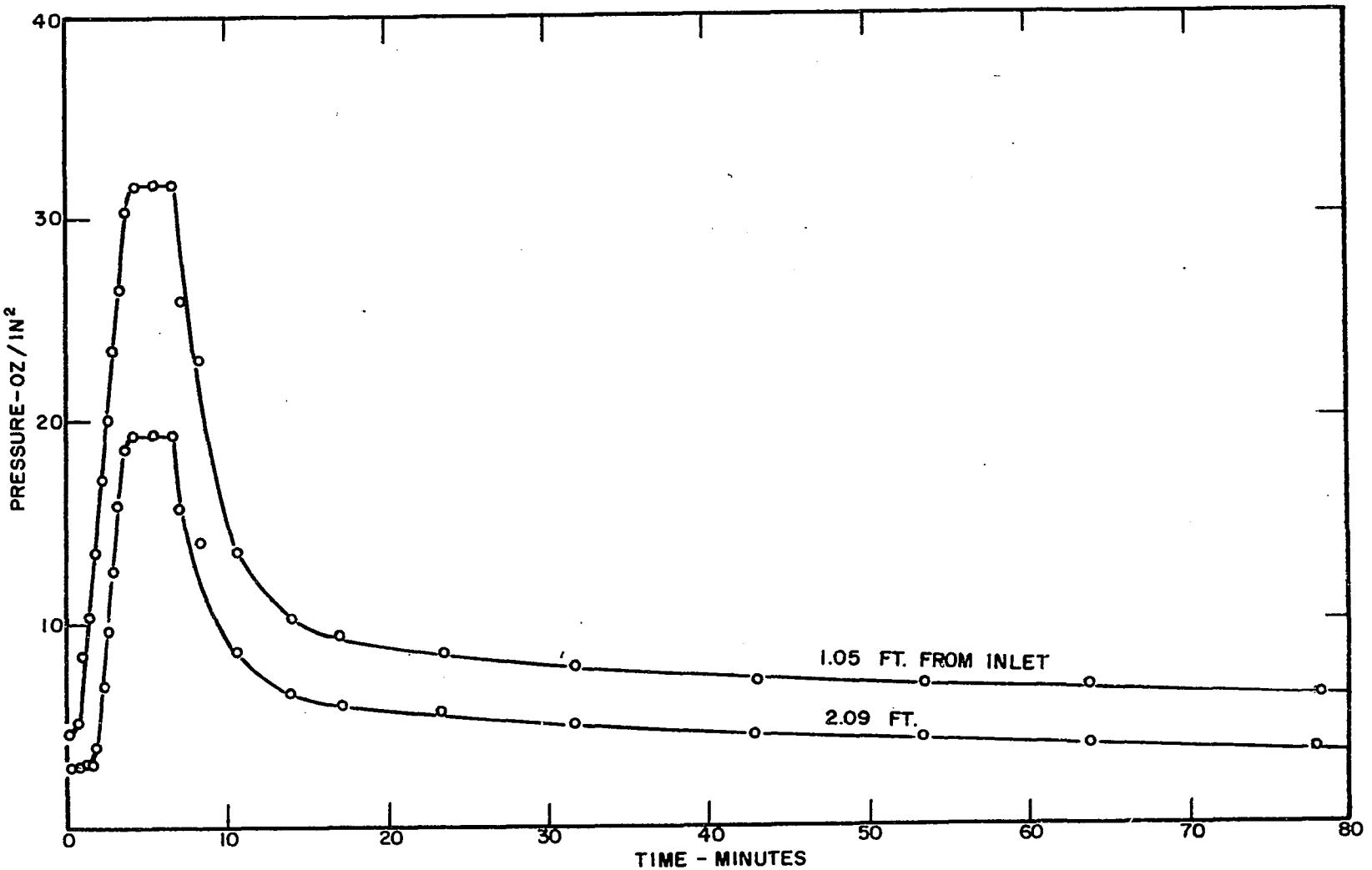

FIGURE 12 TOTAL PRESSURE BEHAVIOR

pressure behavior during the same Run 49. For clarity, data from only two gauges were plotted. These gauges were located at the first and fourth crossbars of the model. The pressure readings were corrected for gauge error and oil head.

The various test phases—sand placement, steady state flow, and overflush—are readily distinguished from this plot. During sand placement, pressure rose sharply and was a linear function of time. Steady state flow conditions resulted in straight line parallel to the time axis. A rapid decline in pressure was experienced during the early stages of the overflush. The rate of decline decreased and eventually degenerated into a gentle slope. The pressure was still dropping slowly as the test was concluded at 78 minutes.

This behavior was typical of other tests except for the latter stages of the overflush. This section of the curve was unique to tests in the deposit flow regime.

The intersection of the ordinate represents the pressure differential necessary to flow clean liquid through the model at the bulk flow rate of the slurry. The pressure remained at this value until shortly after the arrival of the sand front. For tests in the suspended flow regime, this pressure was essentially duplicated at the conclusion of the overflush operation. Although the flow rate was reduced somewhat by the curtailment of solids injection, suspended flow persisted during the overflush and the model was quickly cleared of sand. However, overflush pressures never stabilized in tests where a sand deposit was formed during sand placement. In some tests solids removal was still occurring even after several hours. This contradicts the conclusion of Izymova

and Shan'gin (17) that sand movement terminates after a critical amount of overflushing.

Interest is focused on the pressure behavior during the sand placement phase of these tests. An enlargement of this portion of Run 49 is shown in Figure 13. The four gauges plotted are located on the first, second, fourth and sixth crossbars of the model. The portion of the curves obtained prior to sand front arrival is represented by the horizontal dashed lines. A rapid pressure increase then occurs almost immediately and a straight line relationship is obtained. The slopes of these lines are identical. This occurs in all experimental runs using two or more gauges.

The clear liquid pressure drops measured in the early stage of this test are all slightly lower than the pressure drops calculated theoretically. This is illustrated by the table below:

TABLE II

COMPARISON OF THEORETICAL AND EXPERIMENTAL LIQUID PRESSURE DROPS (RUN 49)

Gauge Position (Ft from Header)	Calculated Pressure Drop (Oz/In^2)	Experimental Pressure Drop (Oz/In^2)
1.05	4.6	4.2
2.09	4.1	3.7
4.17	3.1	2.8
6.31	2.1	2.0

A major problem in this and other tests is associated with the magnitude of pressure differences being measured. With only liquid

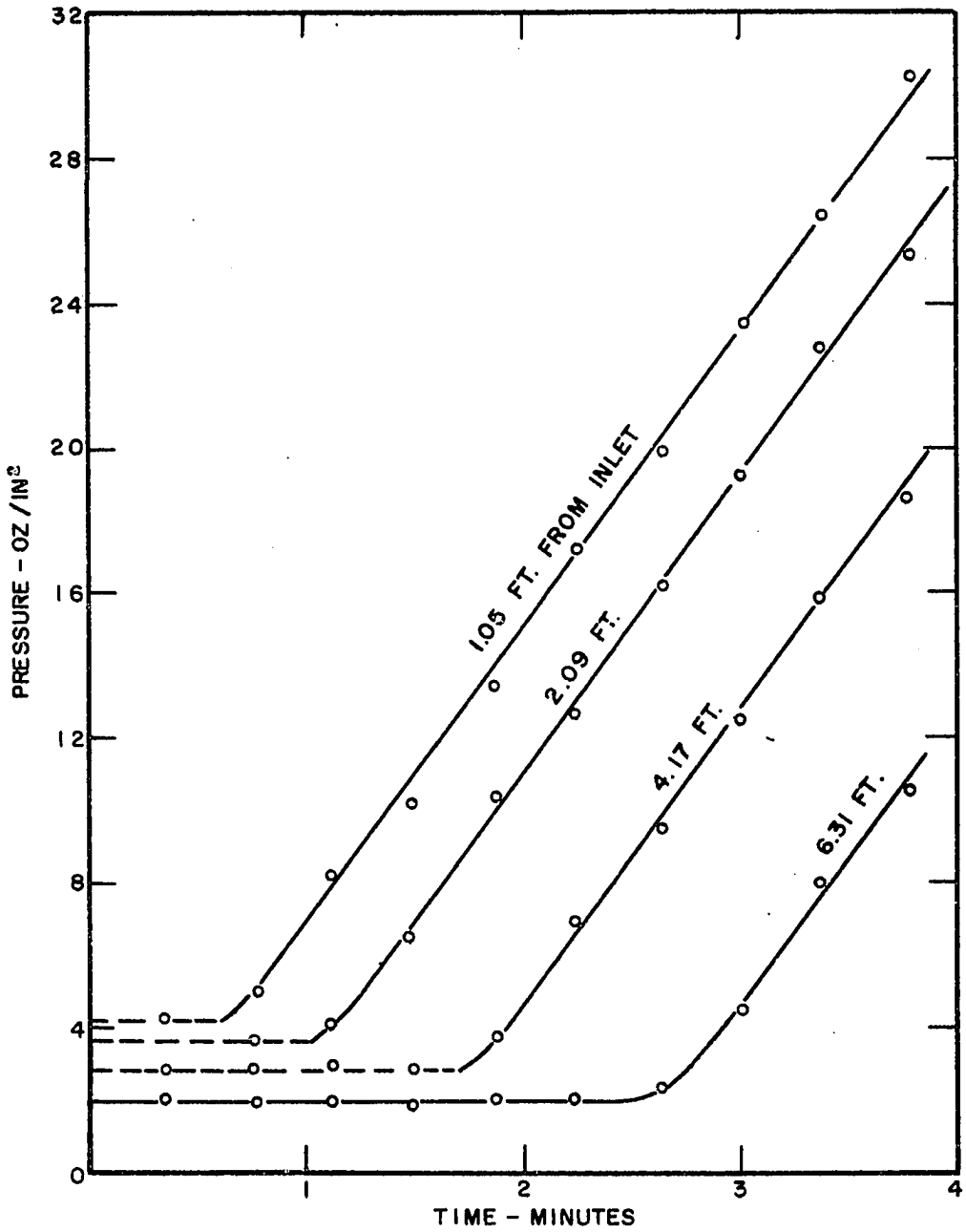

FIGURE 13 PRESSURE BEHAVIOR DURING SAND PLACEMENT

flowing, just a small portion of the total scale is utilized. The gauge readings are the least consistent in the low scale range. As the sand and slurry pass each gauge, the pressure rises and this error is reduced. However, the low values could be due to the thickness of the flow channel being larger than the nominal spacer thickness. Only a slight deviation in fracture thickness would result in a significant error because of the thin spacer used in this run. The data also show that the pressure drop at the end of the model is nearly equal to the theoretical value. This deviation from the low reading trend could be due to end effects.

To evaluate these possibilities, a series of tests was performed by flowing clear 7 cp oil through the model. These tests were made with the 1/16-inch and the 1/4-inch spacers using manometers as the pressure measuring devices. Fluid rates were varied from 1/4 gallon to 1 1/2 gallons per minute in the 1/16-inch thick flow channel and from 1/4 gallon to 6 gallons per minute with the 1/4-inch spacer. The results of the tests with the 1/16-inch fracture are shown in Table III.

TABLE III

PRESSURE BEHAVIOR OF CLEAR LIQUIDS

	GAUGE POSITION				
	1	2	3	4	5
P-Pressure, oz/in^2	26.14	23.29	17.63	12.04	6.18
L-Distance Between Gauges, ft	1.04	2.08	2.12	2.09	2.11
ΔP Between Gauges, oz/in^2	2.85	5.66	5.59	5.86	6.18
$\frac{\Delta P}{L}$	2.73	2.71	2.64	2.78	2.94
Calculated Thickness, in	0.0649	0.0650	0.0656	0.0646	0.0634

The first line represents the average pressure reading obtained in five tests based on 1 gallon per minute fluid flow rate. Maximum deviation between readings was 1.8 per cent after correcting for the capillary rise in the manometers.

The fourth line shows the variation in pressure drop per unit length, $\Delta P/L$, expressed in ounces per square inch per foot. The maximum deviation among these figures is on the order of 10 per cent. Some differences were expected because of the construction of the model, despite the extreme care taken to insure smooth flow surfaces.

From these pressure data an average fracture thickness along the line of flow may be calculated. Equation (10), derived for flow between infinite parallel plates, was used. Although the measured pressures varied as much as 10 per cent, the differences in fracture thickness were found to be small. This result was expected since pressure

drop is a function of plate separation to the third power.

The last line in Table III shows the fracture thicknesses calculated from these data. These figures represent the average thickness downstream to the next pressure tap. For each section, the calculated thickness is slightly higher than the nominal thickness of the fracture spacer. The values range from +0.001 to +0.003 of an inch. The lowest value is obtained in the last two panels of the model. The increased pressure drop across this section gives the appearance of an end effect. These tests not only confirm Equation (10) but attest to the careful construction of the model.

The accurate pressure measurements of the manometers afforded the observation of an anomaly which effects pressure drop along the line of flow. It was stated earlier that the normalized pressure drops obtained in these clear fluid tests deviated slightly. These deviations were not random but followed a general pattern. At high flow rates the normalized pressure differentials were all lower than those observed at reduced rates. These deviations could be due to the bowing of the model across its breadth. The supporting metal crossbars were designed to permit a deflection of less than .01 inch at a flowing pressure of 25 psi. At the lower pressures experienced in these tests, the observed deviations are within the range expected.

The average fracture thickness of the last 9 panels in the flow model was calculated to be 0.0647 inch. Therefore, the model thickness may be considered 0.002 inch larger than the nominal thickness of the spacer. An identical value was obtained in the test using the 1/4-inch spacer. Thus, the error was due to inaccuracies in fabricating the

model rather than deviations in the spacer thickness. While this error was sufficient to cause measurable differences in pressure drop along the line of flow for the 1/16-inch spacer, the error was negligible for the 1/4-inch fracture.

Since the plot of both sand front position and pressure against time results in a straight line during the unsteady state sand placement phase of these tests, it is logical that the same result is obtained when plotting pressure drop versus sand front position. Such a plot is shown in Figure 14. The data obtained in Run 49 are again shown. As expected, the pressures remain constant until the sand front passes the gauge. They then increase and a straight line relationship between the two quantities is obtained. The straight line sections of each curve are parallel.

The slope of these curves, once the sand front has passed, represents the increased pressure gradient due to the sand. This quantity is designated in this work as the $(dP/dL)_s$. This is an important quantity and has been used by investigators of slurry flow in pipelines in their correlations. The $(dP/dL)_s$ may be measured directly from this curve. To obtain the actual pressure gradient of the flowing slurry, the pressure gradient due to the liquid must be added to this quantity. Similar graphs were obtained for all tests in this study.

The pressure gradients used in subsequent correlations were determined in this manner. The method had two distinct advantages— (1) no corrections were necessary for constant gauge error and gauge elevation and (2) errors associated with entrance effects, end effects, and anomalies at the sand front were eliminated. The errors listed in

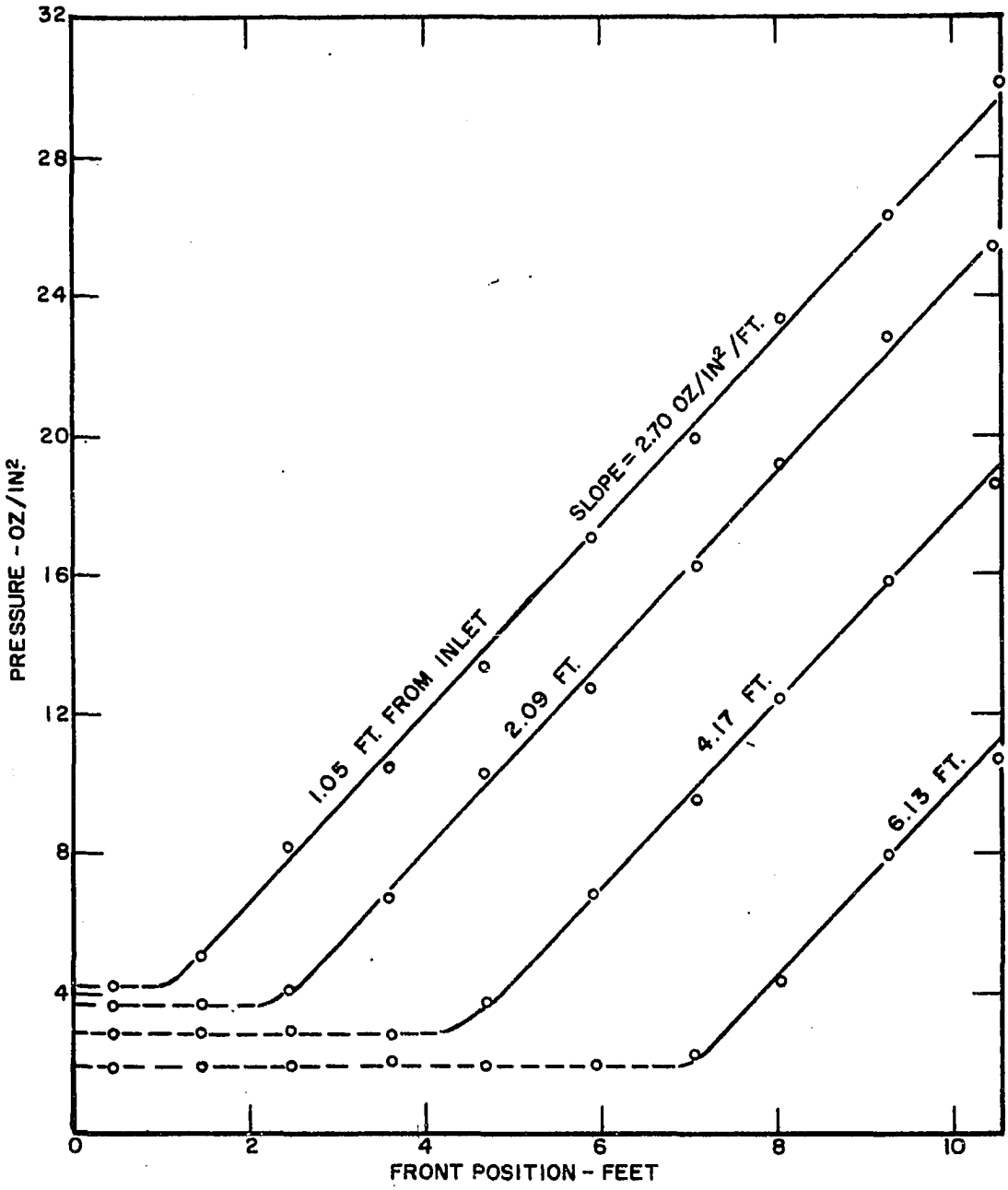

FIGURE 14 DETERMINATION OF $\left(\frac{dP}{dL}\right)_S$

(2) above did exist to some degree in these tests. Entrance effects were discussed in the section dealing with model header design. End effects have been shown to be negligible when flowing clear liquid. However, in slurry flow, particularly in the deposit flow regime, pressure readings were frequently low at the end of the model. This was attributed to a difference in sand deposit configuration and degree of packing at this discontinuity. Similar pressure behavior had been observed near the sand front. In both instances the extent of this anomaly was less than 6 inches.

CHAPTER V

DISCUSSION OF RESULTS

The conversion of the raw experimental data into the pertinent parameters to be correlated was discussed in Chapter IV. In the case of pressure, the basic data was expressed in terms of the increased pressure gradient due to the solid phase $\left(\frac{dP}{dL}\right)_s$. By adding the pressure gradient of the liquid phase, the total pressure gradient $\frac{\Delta P}{L}$ is obtained. For sand front advance the raw data were reduced to a velocity term, v_s, for each test.

The basic test series consisted of a detailed investigation into the effects of liquid viscosity, slurry flow rate and solids concentration on the sand transport mechanism. The development and discussion of the results will initially be restricted to this area of investigation. The trends established for the effects of fracture thickness, size of propping agents and sand angularity are presented in later sections of this chapter.

Pressure Behavior

In the majority of the reported studies on slurry flow in pipes, pressure was the only dependent variable measured. In slurry pipeline design, optimum flow conditions are based on the energy required to transport the solids. For a given solids concentration, the

amount of power consumed is at a minimum when pressure loss is at a minimum. In hydraulic fracturing treatments the amount of energy consumed in transporting the sand in the fracture is relatively unimportant. Pressure losses through the flow string and across the perforations, and the treating pressure required to create and extend the fracture overshadow the frictional losses within the fracture. These three quantities plus the head of fluid in the well have been successfully used in determining the hydraulic horsepower requirements.

Pressure behavior is important in relating the results of this study to those obtained in circular conduits. However, the primary purpose is to provide the pressure data needed to estimate fracture thickness under dynamic flow conditions. Perkins and Kern (25) in their investigation of fractures created in brittle and plastic material concluded that the fracture thickness is controlled by the pressure drop within the fracture. The results of their study can be applied provided clear fluid is pumped or when the propping agent is transported in homogeneous suspended flow. In these two cases pressure behavior is known. Inasmuch as there are no data for the deposit flow regime other than those presented here, they are of particular engineering value.

In fixing the liquid flow rate and sand concentration at given values, the flow rate of the slurry was fixed. Inasmuch as the other variables were held constant, the following expression for the pressure gradient within the fracture may be written:

$$\frac{\Delta P}{L} = f(\mu_o, Q_B, C) \tag{36}$$

From an analysis of these data and those available for the multiphase flow of liquids, it seems apparent that the system behavior involves a

transfer of momentum between phases. Consequently, it has been deduced that the expression of flow rate in terms of velocity is desirable, or

$$\frac{\Delta P}{L} = f(\mu_o, v_B, C) \tag{37}$$

Because of the lack of fundamental knowledge in this area, it was necessary to correlate the data empirically. There are numerous dimensionless groupings which contain the three variables investigated. It has been determined that several combinations of these could be used to correlate the data. However, such groups contained other variables that were held constant in the basic investigation. To use them would involve implications that could not be supported by the data proper. Such a procedure, though common, is not a sound one. Therefore, correlation was made on a dimensional basis.

It has been found that a plot of $\mu_o v_B$ versus $\frac{\Delta P}{L}$, as shown in Figure 15, yields an excellent correlation. This combination of viscosity and velocity appears desirable since the theoretical pressure drop for clear liquid is a straight line function of this grouping. The fact that pressure drop increases with an increase in either velocity or viscosity shows that a Reynolds number alone would not be a suitable replacement, since viscosity appears in the denominator of that expression.

The equation of the clear fluid line in Figure 15 is

$$\frac{\Delta P}{L} = (1.069 \times 10^{-3})\mu_o v_B \tag{38}$$

The parameter in Figure 15 is sand concentration in pounds per gallon. Curves are drawn for 1/4, 1 and 4 pounds per gallon. These data points as well as those obtained at concentrations of 1/2, 2 and 8 pounds per gallon are shown. The solids concentration of each test may be determined from the symbols used to plot the data.

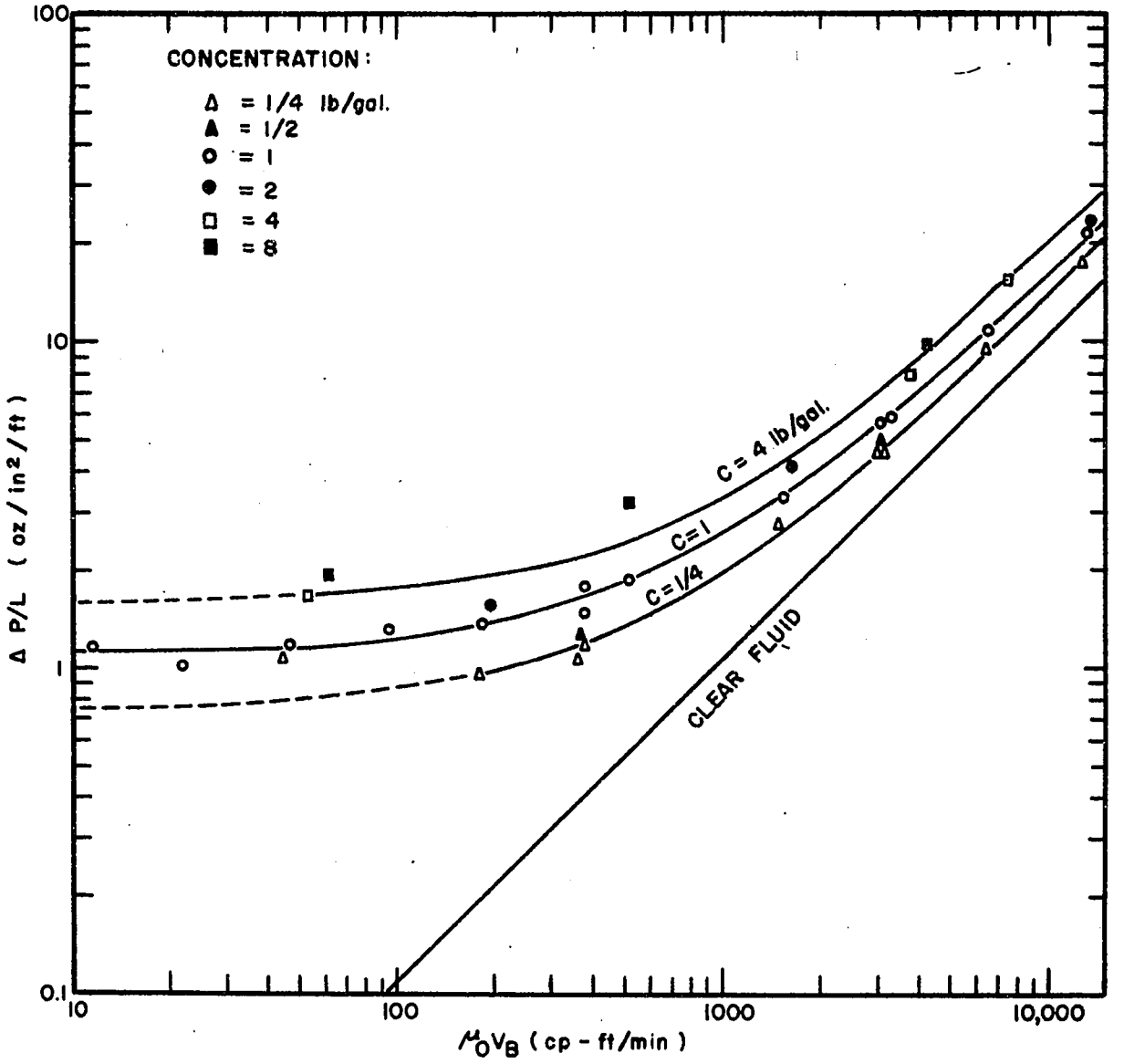

FIGURE 15 PRESSURE BEHAVIOR IN THE BASIC TEST SERIES
(b = 1/4 " , 20 - 40 MESH BEADS)

Changes in test oils occur at "μv" values of approximately 400 and 3000. The utility of this correlation is enhanced by the fact that continuous curves were obtained for a given sand concentration even though the points represent widely varying oil viscosities and flow rates.

Although the general character of these curves is similar to those obtained by Durand and others for solid transport in pipes, there are distinct differences. First, concentration of the solids does not affect pressure drop to the degree reported in those investigations. Second, these curves do tend to flatten out and reach a minimum value at low values of "μv". No rise in pressure was obtained at low values of "μv". One point obtained in this area at a sand concentration of 1/4 pound per gallon is relatively high. However, supporting data are required before any significance can be given to this point.

According to previous work in hydraulic conveyance, the transition between deposit and suspended flow should exist near the minimum head loss value occurring somewhere between 10 and 100 cp-feet per minute. However, this transition occurred at an approximate rate of two gallons per minute with the 58 cp oil. These conditions correspond to a "μv" product of approximately 800. Thus, the change from the deposit to the suspended flow regime deviates significantly from the value observed in circular pipes.

As viscosity and/or superficial bulk velocity increases, the pressure gradients for the various concentrations tend to reach a parallel asymptote to the clear fluid line. There is no indication that these lines will eventually coincide with the clear fluid line. Additional data are required to clarify this.

Straight line relationships are obtained on Cartesian coordinate paper. Log-log paper is used in Figure 15 because detail is not lost at low values of "μv". Data on slurry flow in pipes indicate that the pressure gradient should increase at lower values of "μv"; however the data obtained in these tests are insufficient to support this hypothesis. Therefore, it is assumed that the pressure gradient at low flow rates reaches a constant minimum value. These minimum values are equivalent to the ordinate intercept of the straight lines obtained on Cartesian coordinate paper. The general equation of these curves is:

$$\frac{\Delta P}{L} = a + m\ (\mu_o v_B) \tag{39}$$

The values of both a and m may be evaluated graphically. An equation for each constant concentration curve was obtained expressing pressure gradient as a function of oil viscosity and bulk velocity.

It was found that the value of "m" was constant and had a value of 1.35×10^{-3}, provided that the viscosity of the slurry was used rather than the viscosity of the oil. There are several correlations available expressing slurry viscosity as a function of solids concentration. Most of these correlations assume that the particles are spherical and interference between particles is negligible. However, Einstein's relationship (9) as modified later (10) is simple and basically as good as any available within the concentration range investigated. It is

$$\mu_s = \mu_o\ (1 + 2.5\ C) \tag{40}$$

where C is the volumetric concentration of the solid phase in the slurry. Concentrations of 1/4, 1 and 4 pounds of sand per gallon of pure liquid are equivalent to volumetric concentrations of 0.0118, 0.0456, and 0.1606,

respectively. At these low values of concentration, Einstein's equation yields almost identical results as the more sophisticated methods. (31)

In order of increasing concentration, the values obtained for the constant "a" were 0.75, 1.10, and 1.60. These values readily lend themselves to expressions in terms of volumetric concentration. The general form used was a constant times concentration raised to power. It was found that $a = 2.79\ C^{0.30}$. Thus, the general expression for the pressure gradient under these test conditions is:

$$\frac{\Delta P}{L} = 2.79\ C^{0.30} + (1.35 \times 10^{-3})\mu_s v_B \qquad (41)$$

This empirical equation is only valid for the specific conditions of this test series in the range of values of C, v, and μ tested. A limitation is readily seen when considering clear fluid flow. When $C = 0$ and $\mu_s = \mu_o$, the expression obtained for the pressure gradient is simply $\frac{\Delta P}{L} = 1.35 \times 10^{-3}\mu_o v_B$. The constant (1.35×10^{-3}) does not correspond to the value calculated theoretically and given in equation (10), which was confirmed experimentally. At extended values of the "μv" product, the predicted pressure gradients should be fairly accurate. However, the pressure drops calculated at μv values lower than those tested may introduce appreciable error.

The pressure increase due to the presence of the sand divided by the clear fluid pressure drop $\left(\frac{dP}{dL}\right)_s \Big/ \left(\frac{dP}{dL}\right)_l$ is plotted against the superficial fluid velocity and fluid viscosity product in Figure 16. The ordinate is equivalent to the term ψ used by Durand in his correlations.

It can be seen in Figure 16 that a straight line relationship is obtained at low values of "$\mu_o v_B$". At high values each curve approaches

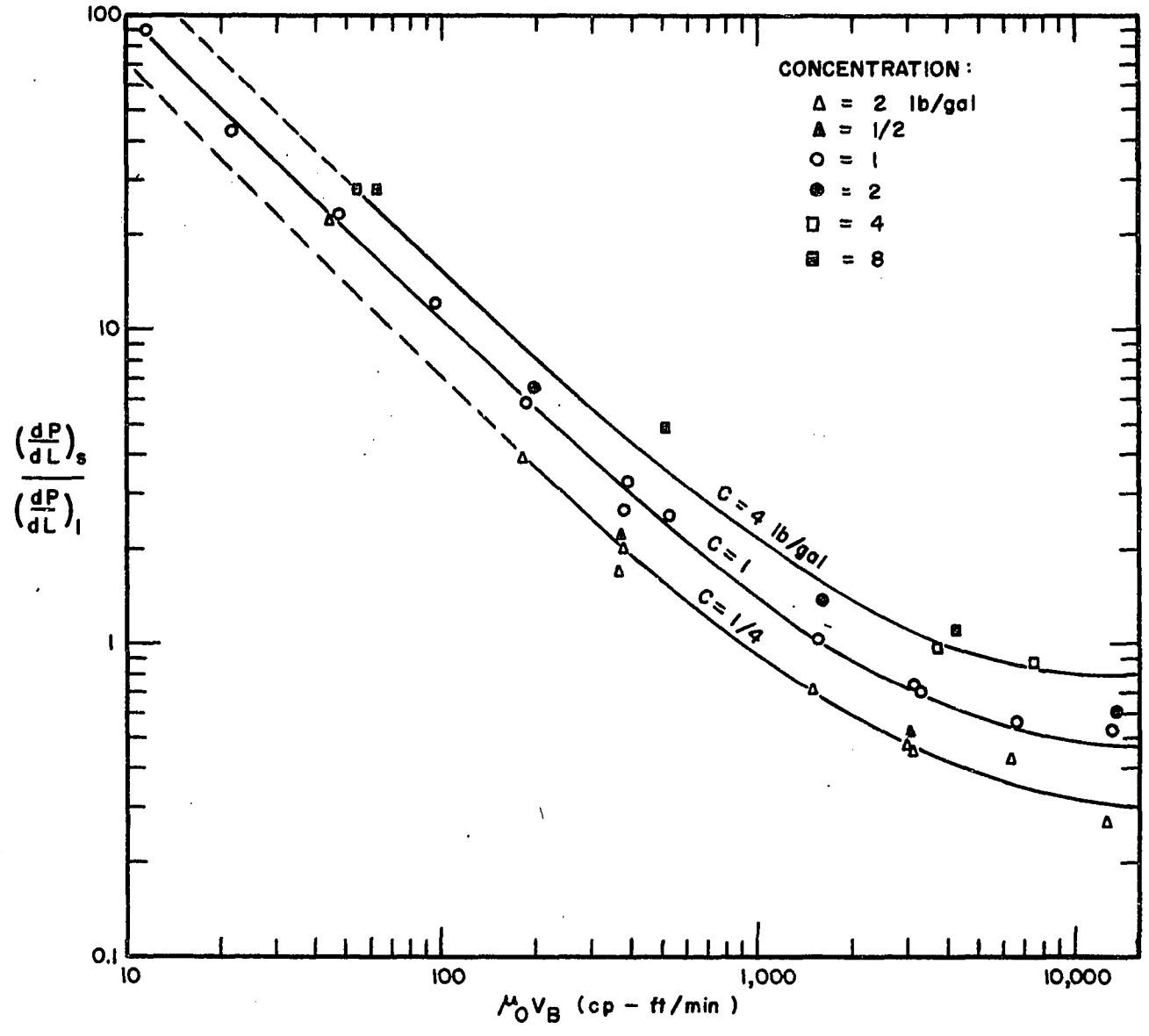

FIGURE 16 THE EFFECT OF SOLIDS ON PRESSURE BEHAVIOR

a constant value of ψ. In order of increasing concentration, these values are 0.290, 0.402, and 0.75. This characteristic arises from the fact that at high flow rates the pressure gradient curves approach a parallel asymptote of the clear fluid line, as shown in Figure 15. This feature of slurry flow with coarse sands and gravel in pipes was also observed by Durand but ignored in his correlation. The discrepancy in Durand's correlation is probable due to the number of variables and the wide range of data correlated. The data points were widely scattered in his work. Either the asymptotic characteristic could not be observed in the spread of data or it was assumed unimportant when considering the full range of the investigation.

Figure 16 may be used as an alternate to Figure 15 for the calculation of slurry pressure drop if one chooses to calculate $(dP/dL)_L$ from equation (10). Its primary purpose, however, is to illustrate how the slurry pressure drop compares with that of a clear liquid for varying values of μ_o and v_B.

Rate of Sand Front Advance

The most significant quantity obtained from the experimental data is the rate of advance of sand in the fracture. In the deposit flow regime, this quantity, v_s, is the rate of advance of the sand pack formed on the bottom of the fracture. In heterogeneous suspended flow regimes, v_s denotes the rate of advance of the leading solid particles in the slurry.

The rate of sand advance is important from two standpoints. First, the ratio of v_s to the bulk velocity v_B yields an efficiency

factor for the sand transport mechanism. This factor, coupled with knowledge of fracturing fluid leak-off to the formation, may be used to estimate the portion of the created fracture area containing a propping agent. Secondly, the rate of advance of the sand in the fracture, for a given flow rate and sand concentration, fixes the amount of sand distributed in the fracture. The areal extent of the sand pack and its thickness are important quantities in fracture design procedures.

As in the case of pressure behavior, the sand velocity data are correlated against dimensional parameters rather than dimensionless groupings. Thus, for the basic test series, the following general expression may be written.

$$v_s = f(v_B, C, \mu_o) \tag{42}$$

The initial phase of correlating the data consisted of plotting v_s versus the superficial bulk velocity on log-log paper. As expected, there was a high degree of scatter among the points, although for a given concentration and a given oil, a straight line relationship was definitely indicated. These lines were generally parallel and had slopes from 1.30 to 1.40. Thus, at constant oil viscosities and sand concentrations,

$$v_s = A_n v_B^{\,d} \tag{43}$$

where A_n are constants and d is approximately 1.36.

The most reliable data were obtained for glass bead concentrations of 1 pound per gallon since more tests were made at this concentration. Also, the experimental error was lower because the test equipment was designed to handle moderate sand concentrations.

In order to incorporate sand concentration into equation (43)

it was assumed that the form C raised to an exponential power x was applicable. The values of x would not necessarily be constant, but could be a function of one or more variables. In this correlation scheme, each oil was considered separately. For each individual data point, the value of x was calculated such that $(v_B C^x)_i = (v_B C^x)_1$ at equal values of v_s. Thus, the line at 1 pound per gallon sand concentration was considered the base line in this collapsing technique.

It was found that the value of x was essentially constant for each specific oil. The variations of x were not a function of flow rate or sand concentration. The average values calculated for the 7, 58, and 488 cp oils were 0.61, 0.45, and 0.33, respectively. A significant feature of these calculations was that a plot of v_s versus $v_B C^x$ on log-log paper (Figure 17) resulted in a single straight line correlation rather than individual lines for each oil. The slope of the line best matching the points is 1.35. This single line correlation indicates that solids concentration and fluid viscosity are interrelated. The exponent x may be expressed as a function of μ_o. The expression obtained is $x = 0.791\mu_o^{-0.143}$, and

$$v_s = 0.705\ v_B^{1.35} C^{1.07} \mu_o^{-0.143} \qquad (44a)$$

There is another alternative in deriving an expression for x. Under these test conditions a correlation can be obtained by using v_t, the terminal velocity of the 20-40 mesh glass beads, rather than oil viscosity. These two correlation techniques are compatible since the rates of fall in the intermediate and heavy oils are governed by Stokes' law, while terminal velocity in the light oil is reasonably approximated by Stokes' law.

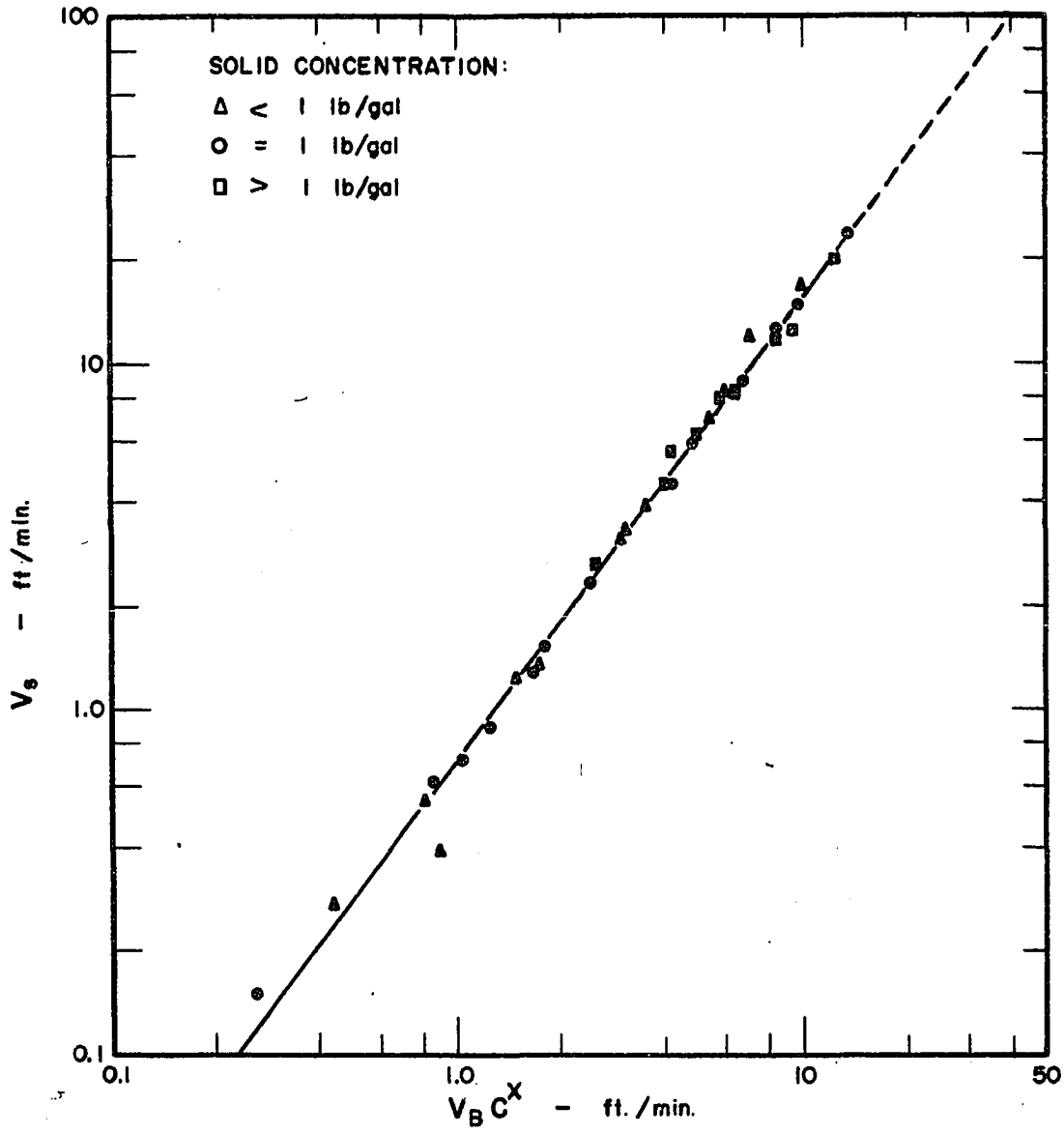

FIGURE 17 CORRELATION OF DATA ON RATE OF SAND ADVANCE

The average terminal velocity of the 20-40 mesh beads in each of the three oils was determined experimentally. At least 50 beads were timed in each liquid. The values obtained were 0.129, 0.0193, and 0.00239 feet per second. The diameter of the testing cylinder was sufficient to eliminate the necessity of correcting for wall effects.

The data were re-analyzed using terminal velocity as a parameter. The expression, $x = 0.782v_t^{0.142}$, was obtained for the concentration exponent, and

$$v_s = 0.705v_B^{1.35}C^{1.05}v_t^{0.142} \qquad (44b)$$

The differences obtained using these two equations are small. Based on these data there is no real advantage in using v_t as a parameter. Tests with a low viscosity fluid, such as water, would clarify the relative merit of the two equations.

Figure 17 shows the degree of scatter of the individual data points using this correlation scheme. The majority of the points are within 10 per cent of the correlating line. This level of accuracy is considered quite good. The data on the individual tests outside this range are given below:

TABLE IV

MAXIMUM DEVIATIONS FROM SAND FRONT ADVANCE CORRELATION

Run No.	Q_o (gal/min)	Conc. (lb/gal)	μ_o (cp)	v_s exp (ft/min)	v_s calc (ft/min)	% Error
29	1	1/4	58	0.392	0.601	-35
7	1/4	1	7	0.151	0.114	+32
30	8	1/4	58	12.01	9.91	+21
5	1	1/4	7	0.272	0.233	+16
34	1	4	488	5.54	4.82	+15
46	4	1/4	7	1.35	1.51	-11

It is significant that the solids concentration in four of these tests was 1/4 pound per gallon. At low sand concentrations experimental error is increased because of the small volumes of solids measured. For example, in Run 30 the desired calibration reading at the header was 153⅓ cc total volume with 29 cc of beads in 3 seconds. The steady state calibration at the end of the sand placement phase indicated errors of +6.1 per cent and +13.4 per cent on slurry volume and sand concentration, respectively. Equation (44a) predicts that this alone would result in a 17.6 per cent error in v_s.

Another major source of error is associated with $\pm$ 3 per cent accuracy of the liquid flow regulators. The regulators must adjust for increase upstream pressures as the tests progress. Fluctuations in liquid flow rates will also cause fluctuations in the sand concentrations of the stream since the equilibrium conditions within the sand cylinder head are disturbed.

The magnitude of errors in Runs 30, 5, 34, and 46, although substantial, is not out of line. However, the 35 and 32 per cent errors in Runs 29 and 7 are too high. Deviations from the desired fluid flow rates and solids concentrations are significant, but they do not account for this level of error. It is possible that during the long sand placement phase of the tests (27 and 70 minutes) there was a malfunction of the flow regulators. The test at 1/4 gallon per minute is at the lower limit of the flow regulator range. It is also possible that the straight line correlation may not be valid at low flow rates where stationary solid deposit is formed in the fracture.

In analyzing data, there are many possible ways to obtain a correlation. Several attempts were made to obtain a realistic representation of the experimental results. In the initial attempt to correlate these data, it was assumed that the general form of the equation was $v_s = A\, v_B^{d1}\, \mu_o^{d2}\, C^{d3}$ where A, d_1, d_2, and d_3 are constants. The constant on the viscosity term was calculated by collapsing the 1 pound per gallon concentration lines of the three oils. The equation best fitting the data was

$$v_s = 0.0306\, v_B^{1.36}\, \mu_o^{0.279} \qquad (45)$$

Using the procedure described above, the value of d_3 was calculated for each of the remaining data points. This exponent was found to be a function of oil viscosity. The values obtained were 0.60, 0.44, and 0.31, which correspond to the values obtained in developing equation (44a). Had this correlation scheme been pursued to its conclusion, it would have ultimately yielded the relationship described in equation (44a).

A correlation based on the linear equation described above was obtained. The best fit of the experimental data occurred for

$$v_s = 0.235\ v_B^{1.32}\ \mu_o^{0.273}\ C^{0.606} \qquad (46)$$

However, the per cent deviation in the ratio of experimental to predicted values of v_s is substantially increased. The average deviation is approximately 15 per cent contrasted to 7 per cent for equation (44). A comparison of the experimental and predicted values for both equations is tabulated in Appendix B.

In other correlation attempts, an equation of the form $v_s/v_B = A\ C^{a\mu_o{}^b}$ was investigated. This form is desirable since the predictions of v_s are restricted between 0 and v_B. However, the deviations obtained were not acceptable. Other approaches to limiting the value of v_s include the use of the parameter, v_D. This quantity is equal to $v_B - v_s$. At low sand front velocities, v_D is essentially equal to the bulk velocity. However, as the rate of sand advance increases, v_D decreases. Under ideal transport conditions the value of v_D approaches zero. Of the ten attempts to incorporate this term in a correlation scheme, not one satisfactory fit was obtained. Within the experimental range of these data, equation (44) yielded the best correlation.

Sand Placement Efficiency

The analysis of the results obtained in this phase of investigation is best accomplished by expressing the rate of sand movement in terms of the efficiency factor, v_s/v_B. The following expression for sand placement efficiency during the basic test series is obtained from equation (44a):

$$\frac{v_s}{v_B} = 0.705\ v_B^{0.35} C^{1.07} \mu_o^{-0.143} \qquad (47)$$

A similar expression may be obtained from equation (44b).

Figures 18, 19, and 20 demonstrate the effect of sand concentration, oil viscosity, and flow rate on the value of $\frac{v_s}{v_B}$. The points shown are experimental while the curves were constructed using equation (47). In Figure 18, this efficiency ratio is plotted against sand concentration at various flow rates for 7 cp oil. This figure shows that concentration has a marked effect on the $\frac{v_s}{v_B}$ ratio. Assuming a radial flow pattern, the superficial bulk velocities in these tests would exist 17, 35, and 133 feet from the well bore for a pump rate of 20 barrels per minute. Fluid loss during a hydraulic fracturing treatment would cause these velocities to be attained nearer the well bore.

Figure 19 demonstrates the effect of viscosity on $\frac{v_s}{v_B}$ at a flow rate of 4 gallons per minute. Again, sand placement efficiency is plotted against sand concentration. High efficiencies are obtained at high sand concentrations with the more viscous oil. In fact, equation (47) predicts over 100 per cent efficiency at a sand concentration of 4 pounds per gallon. This region of the curve is beyond the range of the test data. This is not unexpected since the equation is empirical and only applies rigorously within the test range.

As a matter of physical practicality the maximum efficiency cannot exceed 100 per cent. Therefore, equation (47) has as its effective upper limit a value of $\frac{v_s}{v_B} = 1.0$. The value of $C^{1.35x}$ must be between 0 and 1. The limiting values of v_B are therefore zero and the value $v_B^{0.35}$ that yields a value of $\frac{v_s}{v_B} = 1.0$. Consequently, any value of $\frac{v_s}{v_B}$

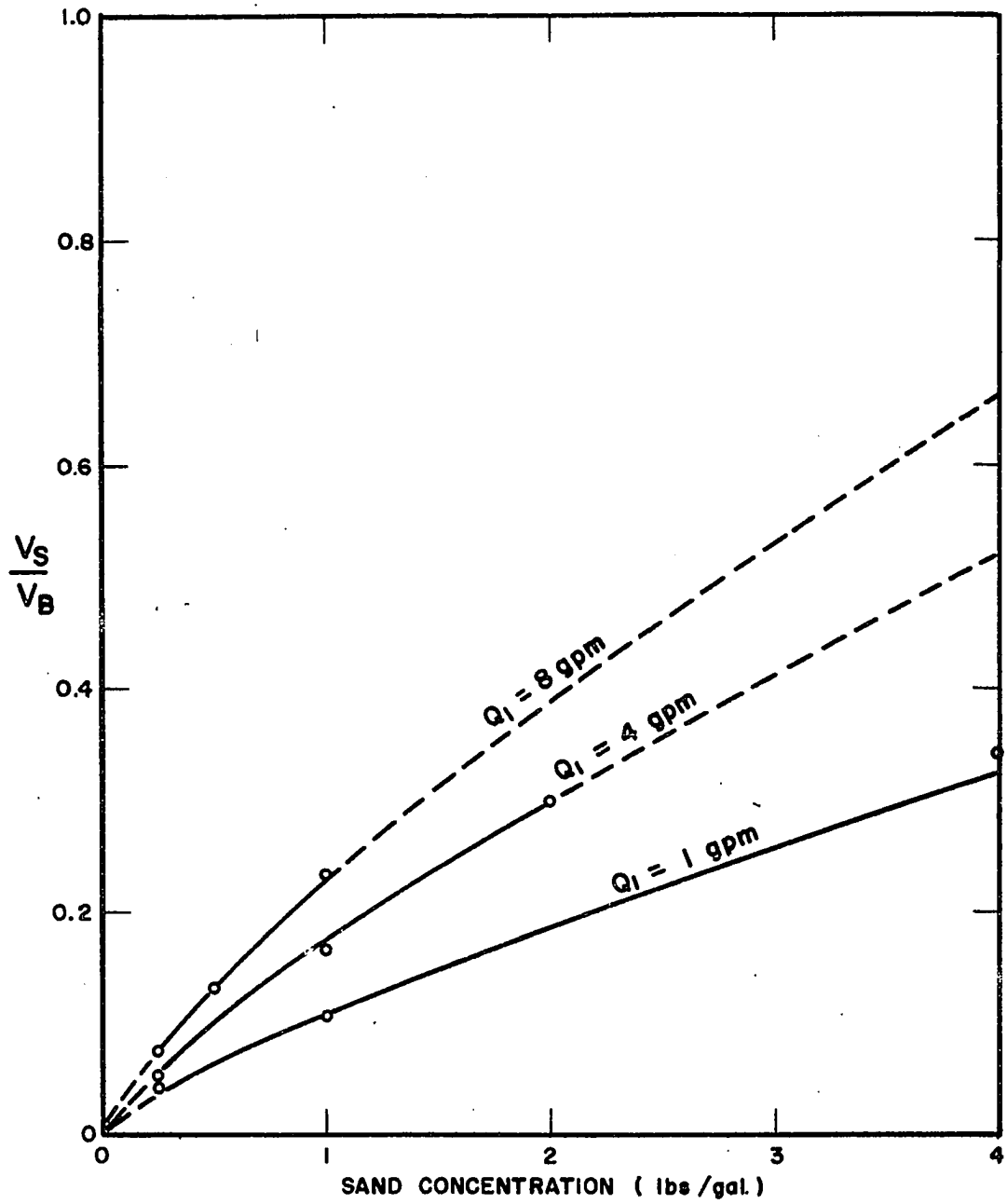

FIGURE 18 VARIATION OF SAND PLACEMENT EFFICIENCY WITH SAND CONCENTRATION AND LIQUID FLOW RATE FOR A 7 cp OIL
(b = 1/4", 20-40 MESH BEADS)

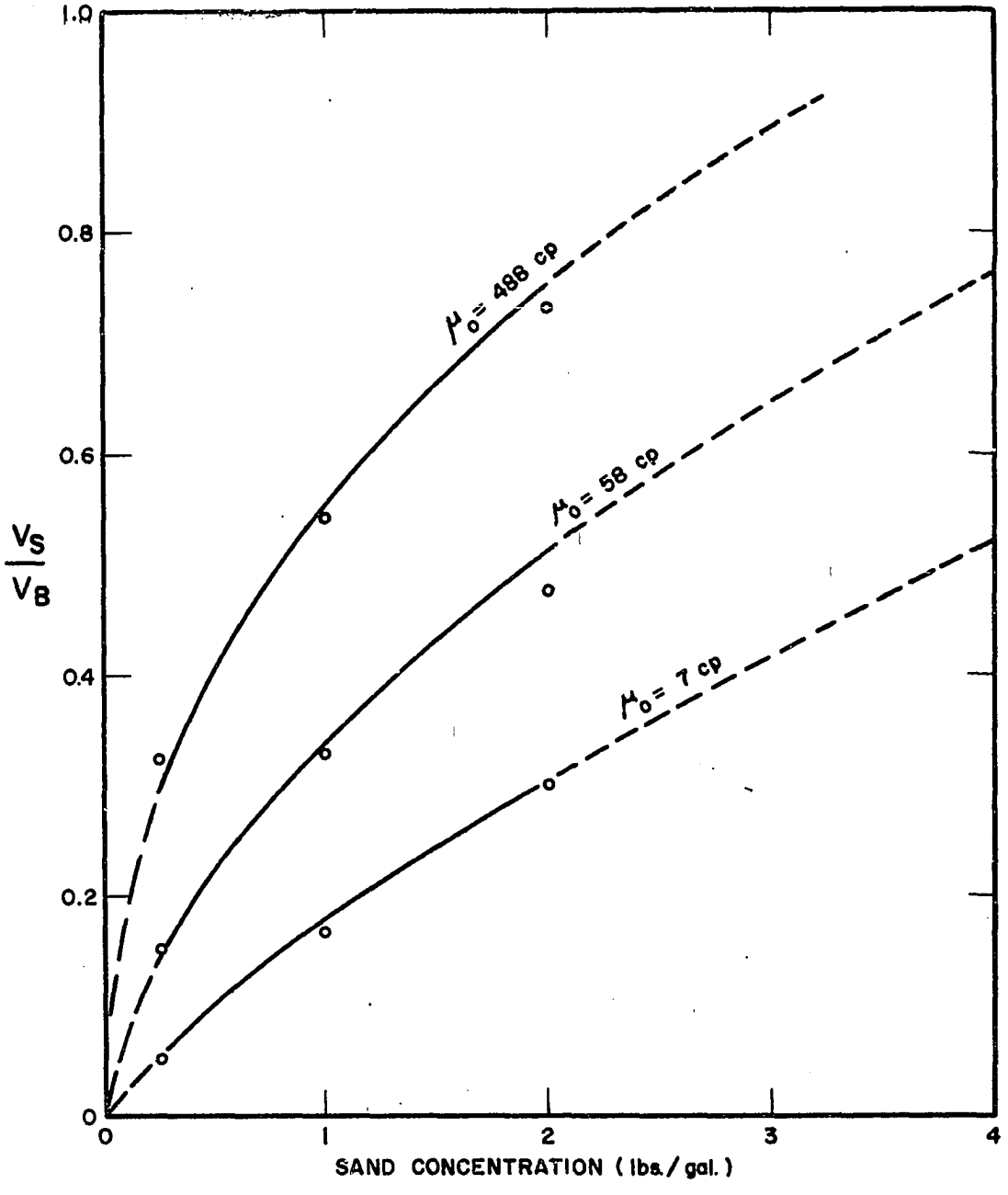

FIGURE 19 VARIATION OF SAND PLACEMENT EFFICIENCY WITH SAND CONCENTRATION AND OIL VISCOSITY AT A LIQUID FLOW RATE OF 4 gpm
(b = 1/2", 20-40 MESH BEADS)

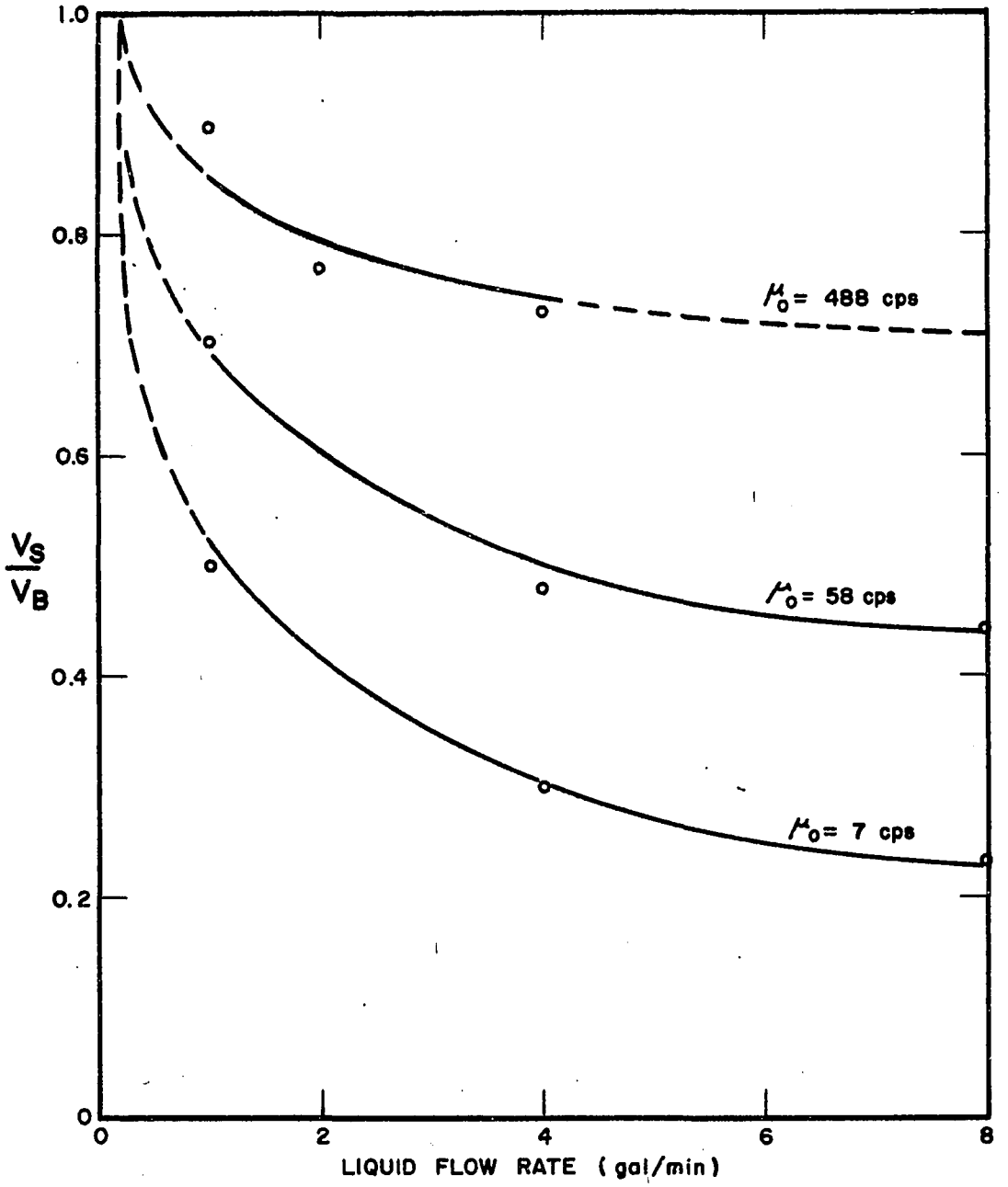

FIGURE 20 VARIATION OF SAND PLACEMENT EFFICIENCY WITH LIQUID FLOW RATE AND OIL VISCOSITY AT A MASS FLOW RATE OF 8 lbs/min
(b = 1/4", 20-40 MESH BEADS)

over 1.0 generated from this correlation may be considered to represent ideal sand placement conditions. Extrapolation of empirical correlations outside the test range is, at best, risky. Placement efficiency of 0.727 is obtained for the 488 cp oil at a sand concentration of 2 pounds per gallon. This, plus the general trend of these data, supports the conclusion that ideal sand transport conditions are being approached for concentrations exceeding 4 pounds per gallon. Had tests been possible at high solids concentration, an asymptotic approach to $\frac{v_s}{v_B} = 1$ should have occurred.

Figure 19 shows that the sand placement efficiency is not directly proportional to the ratio of oil viscosities but that high sand placement efficiencies may be obtained with high viscosity oils. This means that the use of gels can be effective in placing sand, assuming that the non-Newtonian behavior does not greatly alter the flow characteristics of the slurry. From a practical standpoint, increasing slurry injection rates is an expensive method of improving sand placement during a hydraulic fracturing treatment. High sand placement efficiencies are particularly critical in the placement of partial monolayers. Attempts to place partial monolayer sand pack at these velocities with a 7 cp oil would result in a multilayer sand pack of limited extent.

In Figure 20, the effect of liquid flow rate and oil viscosity on transport efficiency is demonstrated. These curves were obtained for each oil at a constant sand injection rate of 8 pounds per minute. Thus, as flow rate increases, sand concentration decreases; and more fluid is used to transport the identical amount of sand.

By definition, $\frac{v_s}{v_B} = 1$ is obtained when liquid saturated sand

is pumped. An injection rate of 8 pounds of sand per minute is equivalent to a bulk flow rate of 0.606 gallon per minute. The volumetric concentration of the solid phase under this condition is 0.632. Transport efficiencies on the order of 1.0 are predicted by equation (47).

The three curves in Figure 20 originate at this common point. When small amounts of liquid are added to the slurries, the transport efficiencies drop rapidly. However, as more liquid is added and the flow rate increases, the rate of decline of $\frac{v_s}{v_B}$ becomes small. In this portion of the curves, an increase in flow rate will cause essentially a proportionate increase in the rate of sand advance.

Sand Pack Thickness

Sand distribution within a fracture is important in designing hydraulic fracturing treatments. This quantity, and data on embedment and crushing of the propping agent, may be used to estimate the flow capacity of an induced fracture. The concentration of sand within the simulated fracture during a test run is equal to $\frac{Cv_B}{v_s}$. This quantity is constant since the rate of sand front advance was constant and the tests are performed at fixed injection rates. If $\frac{Cv_B}{v_s}$ is multiplied by 1.58, the fraction of the fracture thickness occupied by the bulk sand, F, is obtained. Thus, from equation (47)

$$F = 2.24\ v_B^{-0.35} C^{1-1.07} \mu_o^{-0.143} \qquad (48)$$

The maximum and the minimum bead pack thickness occurred under identical flow conditions for the three oils tested. A maximum degree of packing was obtained at a flow rate of 1 gallon per minute and a sand concentration of 8 pounds per gallon. The minimum was obtained at a

flow rate of 8 gallons per minute and 1/4 pound per minute sand concentration. The values are given in the table below:

TABLE V

MAXIMUM AND MINIMUM VALUES OF F
IN THE BASIC TEST SERIES

Sand Conc. (lb/gal)	Flow Rate (gpm)	7 cp Oil	58 cp Oil	488 cp oil	Minimum Value
8	1	0.873	0.620	0.486	0.437
1/4	8	0.250	0.081	0.043	0.019

The figure for the minimum degree of packing using the 488 cp oil was calculated and was not confirmed experimentally because of the pressure limitations of the model.

For the particle size and fracture thickness in the basic test series, the thickness of a single layer of beads occupies approximately 10 per cent of the fracture thickness. Values of F less than 0.10 indicate that a partial monolayer pack is obtained. The last column in the table represents the thickness of the sand pack when the transport is 100 per cent efficient. These values represent a minimum possible thickness and are a function only of the concentration of sand in the injected slurry. These minimum values indicate that, although the sand pack is thicker at the highest sand concentrations, the transport mechanism is more efficient. The ratio of the minimum value divided by the actual sand deposit thickness equals the sand placement efficiency factor. This immediately provides an insight into one reason sand concentration has a great effect on transport efficiency. The minimum possible transport efficiency may be obtained by dividing the minimum sand pack thickness

by one. Therefore, at 8 pounds per gallon the transport efficiency must be at least 43 per cent, while at 1/4 pound per gallon the ratio is approximately 2 per cent.

It should be stressed that the calculated F values do not represent the fraction of the fracture width occupied by the bead deposit. This quantity is applicable to the fracture thickness obtained when the formation is allowed to heal. In the deposit flow regime, it includes the sand incorporated in the bead deposit and the sand being transported in the open section above. Deposit thickness during placement may be larger than the F values predicted by equation (48) since the experiments by Dorzhkin et al (7) indicate the sand concentrations within the deposits are on the order of 0.40 to 0.50.

The effect of liquid flow rate and input sand concentration on the value of F is illustrated in Figure 21. As in its counterpart, Figure 18, the oil viscosity is constant at 7 cp. The dashed lines indicate the behavior predicted by equation (48) and not confirmed experimentally. For the three experimental curves, the fraction of the fracture thickness occupied by the sand initially increases rapidly but tends to level out as sand concentration in the injection stream is increased. This characteristic is more dominant at the high liquid flow rates than at 1 gallon per minute. At a given sand concentration, the F values of the three lines are inversely proportional to $v_B^{0.35}$. Thus, as liquid flow rate increases, the solids concentration in the fracture decreases.

The values obtained under ideal transport conditions are essentially a straight line in this plot since $F_{ideal} = 1.58C$. Intersection of this line with the experimental curves would indicate that ideal

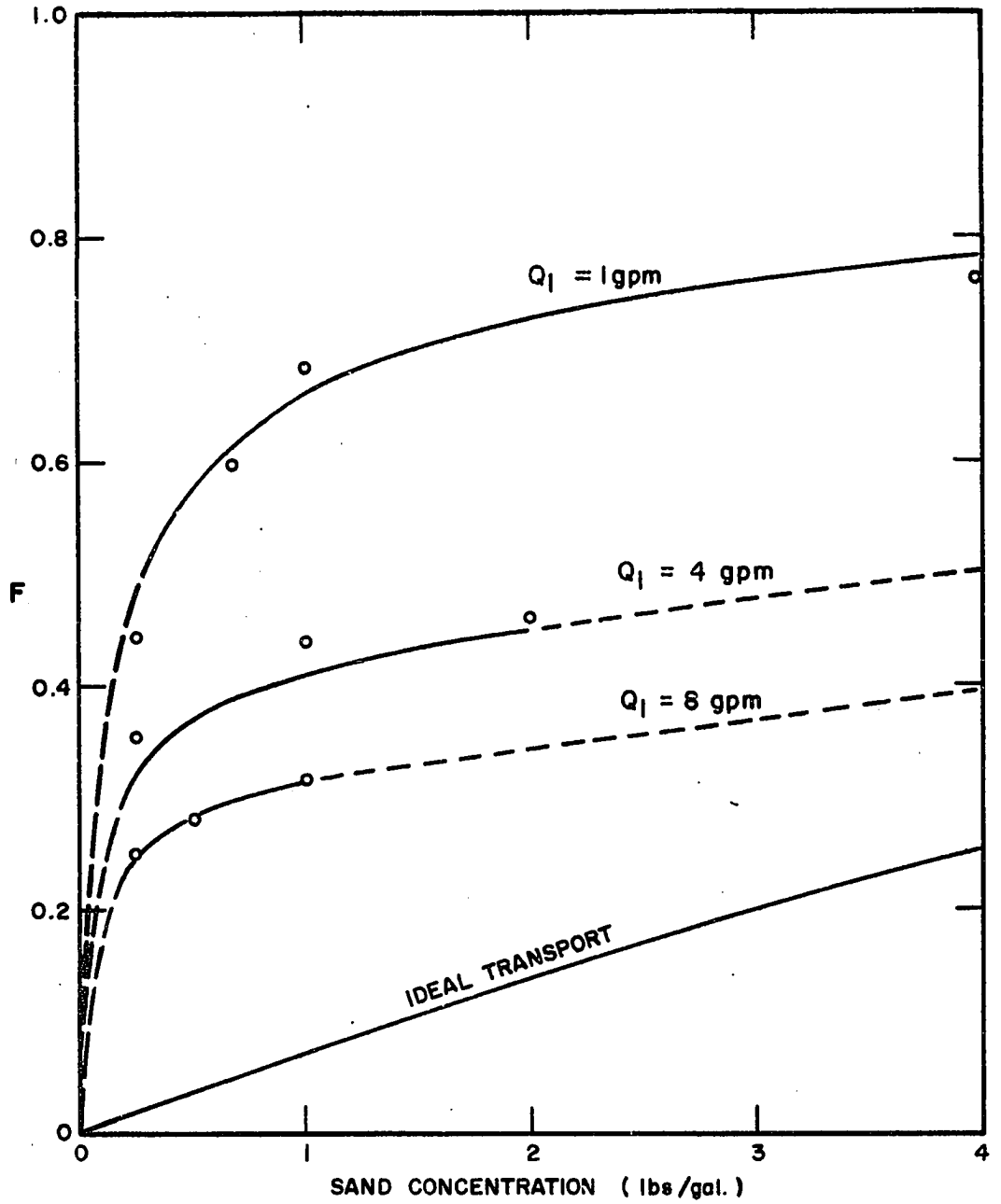

FIGURE 21 THE EFFECT OF LIQUID FLOW RATE AND SAND CONCENTRATION ON THE FRACTION OF SOLIDS IN THE FRACTURE.
(b = 1/4", 20-40 MESH BEADS, μ_0 = cps)

transport had been attained.

Figure 22 illustrates the effect of oil viscosity on sand placement at a liquid flow rate of 4 gallons per minute. As oil viscosity increases, the amount of sand per unit surface area in the fracture decreases. As the magnitude of the F values approach ideal transport conditions, the curves begin to assume the characteristics of the ideal line. The abrupt change in slope degenerates into a smooth curve as the oil viscosity increases.

Variations in F values obtained by increasing liquid flow rate while holding sand injection constant at 8 pounds per minute is demonstrated in Figure 23. As in Figure 20, curves are drawn for the three oils used in the basic test series. Initial increases in liquid flow rate cause a rapid reduction in sand pack thickness. However, as more liquid is used to transport the sand, the rate of decline of F decreases. This also occurs under ideal transport conditions since solids concentration is a function of the liquid flow rate. In fact, the curve for the 488 cp oil follows the ideal case closely.

The limitations of the straight line correlation described by equation (44a) at high $v_B C^x$ values have been discussed in this chapter. However, sand pack thickness calculations point out that irregularities may occur at low values of $v_B C^x$. Just as v_s/v_B ratio cannot exceed 1.0, the fraction of the fracture thickness occupied by the sand cannot be larger than 1.0. The minimum value of v_s equals $1.58Cv_B$, the bulk sand volume injected per unit time. For Run 7, performed at 1/4 gallon per minute and at a sand concentration of 1 pound per gallon, equation (48) predicts an F value of 1.06. The value obtained experimentally is 0.80.

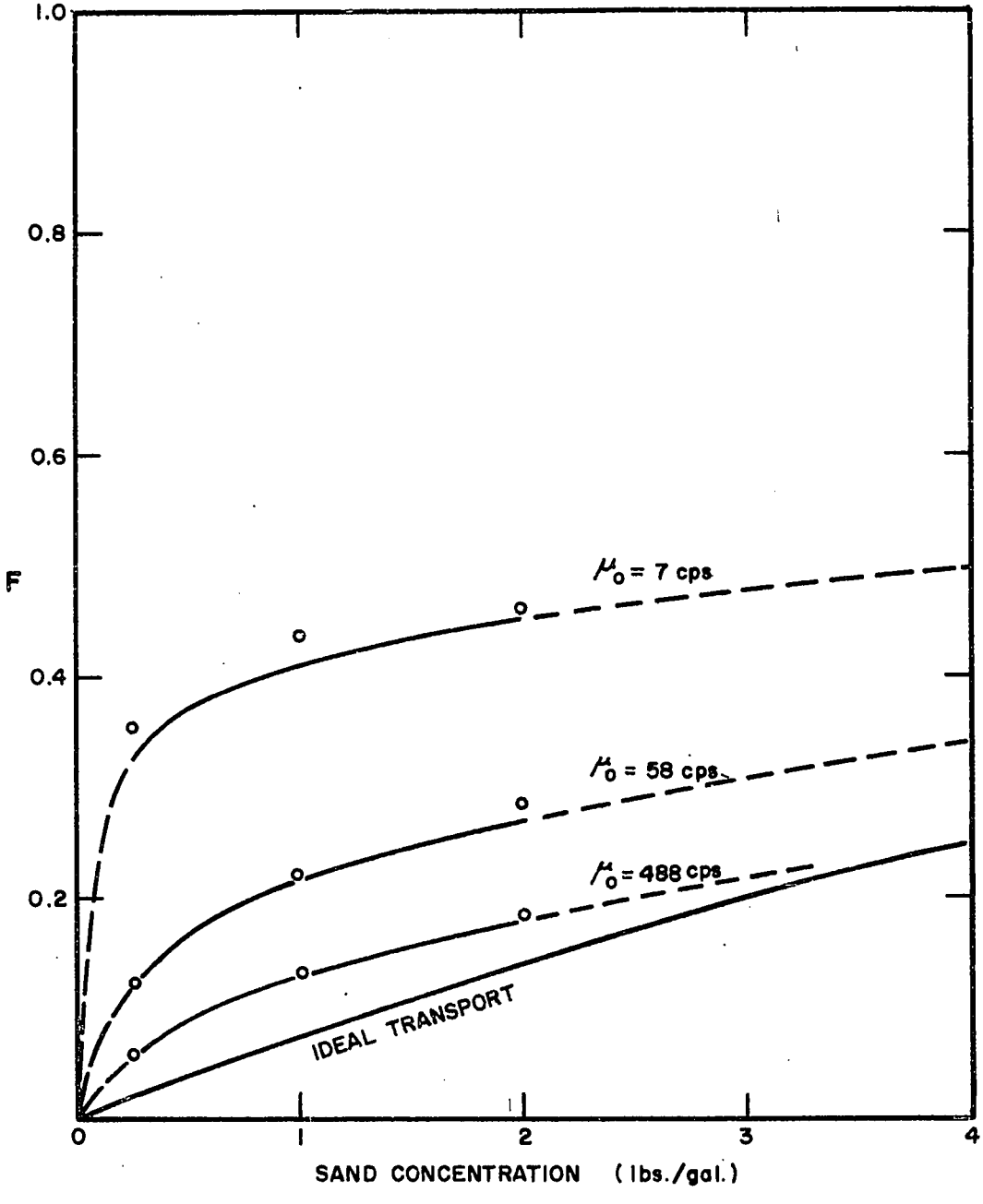

FIGURE 22 THE EFFECT OF OIL VISCOSITY AND SAND CONCENTRATION ON THE FRACTION OF SOLIDS IN THE FRACTURE.
(b = 1/4", 20-40 MESH BEADS, Q_i = 4 gpm)

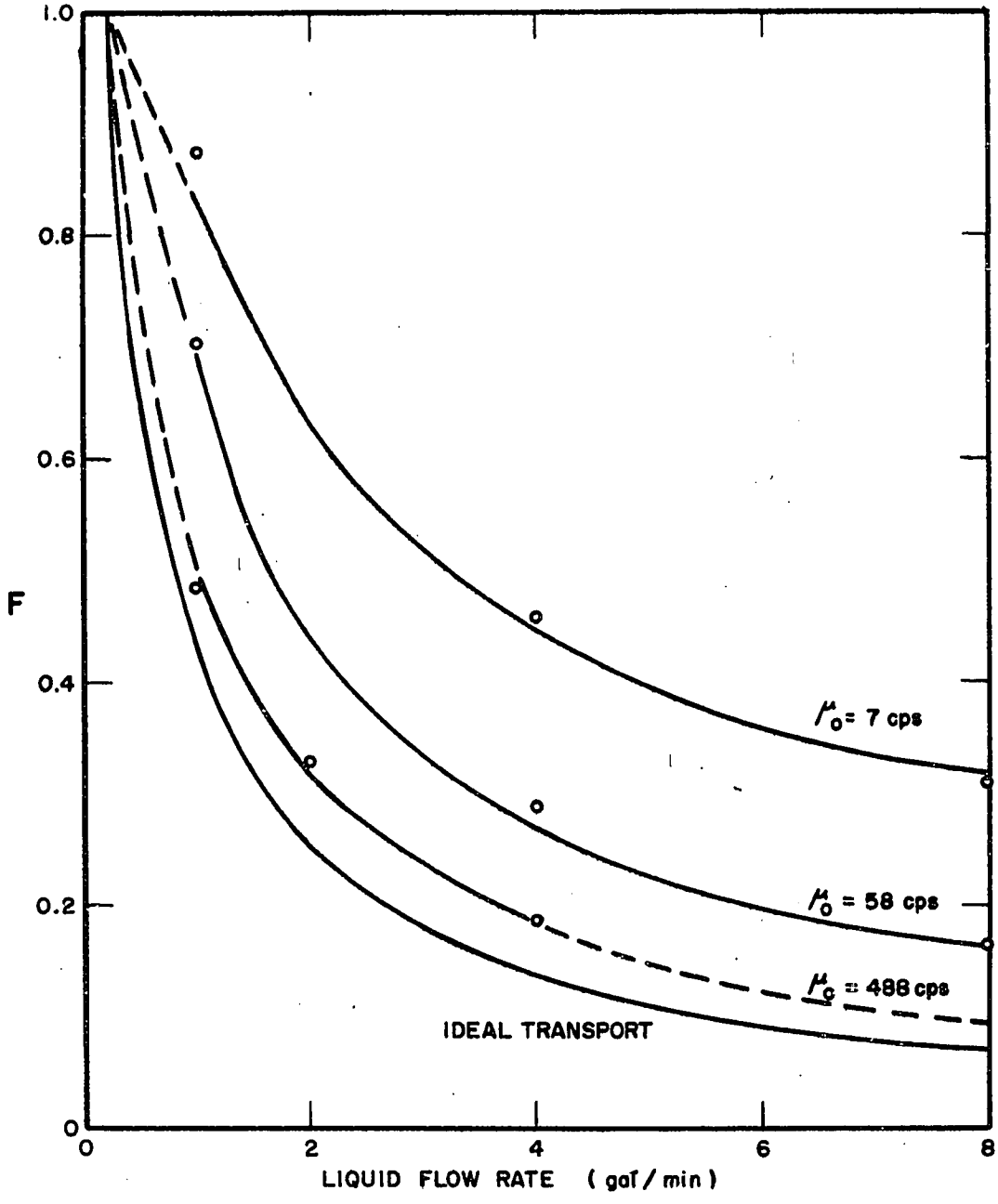

FIGURE 23 THE EFFECT OF OIL VISCOSITY AND FLOW RATE ON THE FRACTION OF SOLIDS IN THE FRACTURE (b = 1/4", 20-40 MESH BEADS, Q_s = 8 lbs/min.)

The difference in these figures was previously classified as experimental error. The actual experimental error may, in fact, be much lower. Equation (44a) does not take into account the restriction imposed on the minimum value of v_s. Had additional tests been performed at still lower flow rates, this practical limitation on the rate of sand front advance might have been demonstrated more dramatically.

Tests Outside the Basic Test Series

The purpose of the tests outside the basic test series was to gain an insight into the effects of some of the other parameters on the sand transport in fractures. A major source of information was derived from the visual observations during the tests. Detailed descriptions of the sand transport mechanisms are described in Chapter III. The quantitative data are presented in Appendix C. These data are insufficient to incorporate additional variables in the relationships developed from the basic test series. In some instances, however, definite trends were established.

The tests are grouped according to the new variables being investigated—fracture thickness, angularity of the propping agent, and particle size. Tests investigating the latter were principally confined to the determination of the flow conditions required to obtain bridging within the model flow channel.

Effect of Fracture Thickness

Intuitively, this parameter should greatly affect sand transport in horizontal fractures. This was verified in the tests on 1/16, 1/8, and 1/2-inch fractures. In these three runs, slurry flow

conditions were constant. Fluid flow rate was 1 gallon per minute with a sand concentration of 1 pound per gallon. Thus, as the fracture thickness decreased the superficial bulk velocities increased. The use of 20-40 mesh glass beads resulted in a change of the fracture thickness to bead diameter ratio directly proportional to fracture thickness. The quantitative results are shown in Figure 24. Both pressure gradient and sand placement efficiency are plotted against fracture thickness. A distinct similarity exists between the two curves. The values obtained with the 1/2-inch spacer are only slightly lower than those obtained with a 1/4-inch separation. However, the pressure and placement efficiency increase rapidly as fracture thickness is reduced.

The sand front position in the 1/16-inch fracture could not be distinguished on the sequence camera film. Therefore, the pressure gradient was calculated using the pressure readings under steady-state flow conditions. Sand positions were estimated from the pressure response along the line of flow during the initial sand placement phase of the test.

As pointed out in Chapter III, the transport mechanism was different for each run. In the 1/2-inch thick fracture the beads were transported primarily by deposit load flow. The test using the 1/4-inch fracture resulted in narrow wave action along the top of the bead deposit. Again reducing thickness by one-half, the wave action became more pronounced and covered the full width of the flow model. Suspended flow occurred in the thin fracture. Figure 24 demonstrates the order of magnitude of sand placement efficiencies and pressures obtained under the various transport conditions.

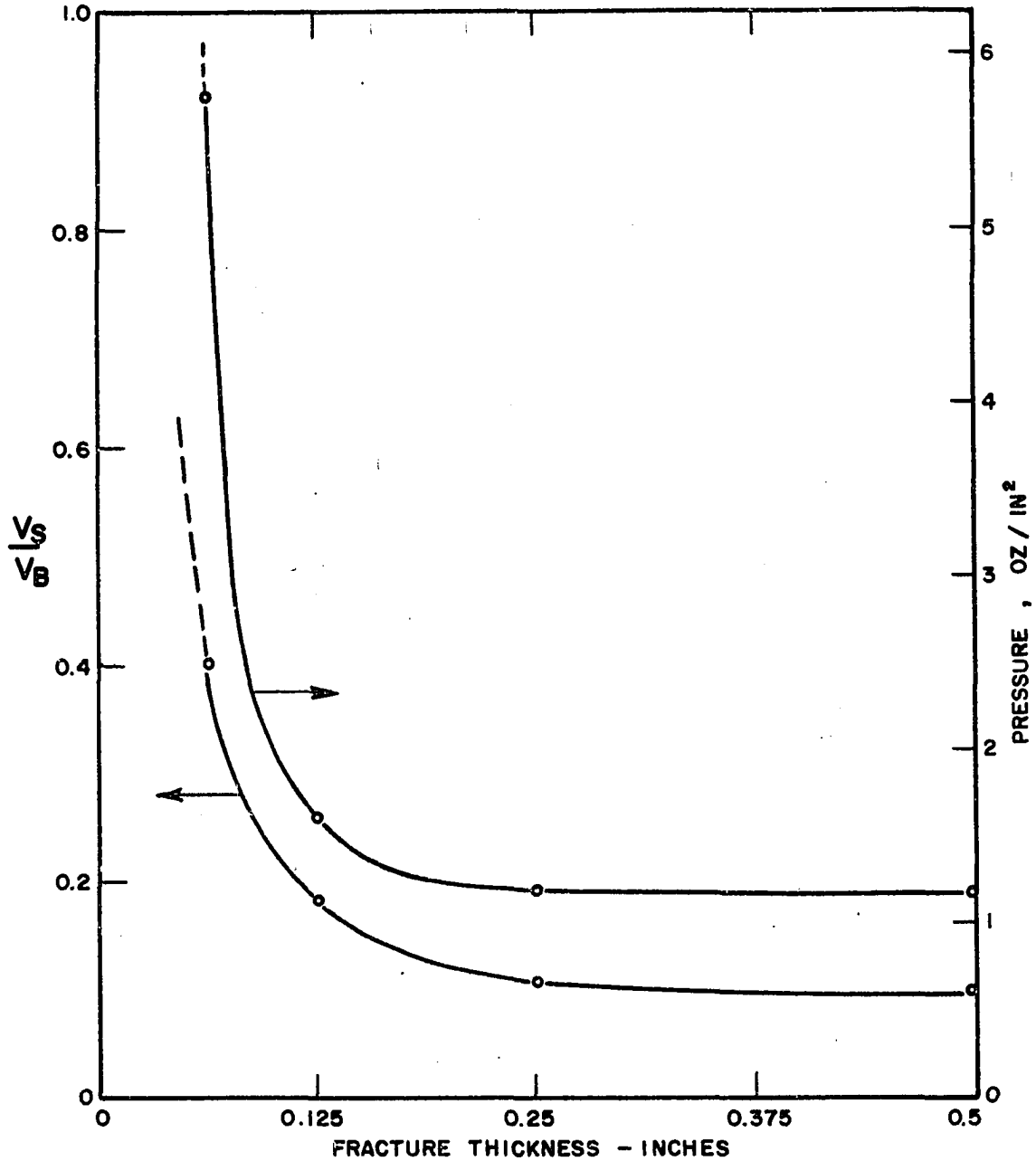

FIGURE 24 THE EFFECT OF FRACTURE THICKNESS ON SAND TRANSPORT BEHAVIOR
(20-40 MESH BEADS , Q_i = 1 gal/min, CONC. = 1 lb/gal)

If it is assumed that bead diameter has only a slight effect on flow behavior, the scaling procedure postulated previously may be used to compare the results of these tests with behavior in the basic test series. For example, if a 1/4-inch fracture is to be simulated by a 1/16-inch spacing, the $\frac{L'}{L}$ ratio equals 4. Thus, $\frac{\mu'}{\mu} = 8$ and $\frac{v'}{v} = 2$. These corrected values for viscosity and velocity may be used to predict the rate of sand front advance from equation (44a). The results of these calculations are given below:

TABLE VI

THE EFFECT OF FRACTURE THICKNESS ON TRANSPORT EFFICIENCY

Fracture Thickness	Simulated Test Conditions			Predicted v_s/v_B	Test v_s/v_B
	μ_o (cp)	v_B (ft/min)	v_s (ft/min)		
1/16	55.7	53.6	25.17	0.452	0.400*
1/8	19.6	19.0	4.46	0.235	0.182
1/4	6.96	6.72	0.749	0.111	0.107
1/2	2.46	2.36	0.134	0.057	0.100

*Determined from pressure response during test.

The trend of the experimental $\frac{v_s}{v_B}$ curve is predicted in these calculations. The calculated transport efficiencies for the small fracture spacings are higher than the measured values. This is expected since the 20-40 mesh beads simulate larger size particles in the two tests. The values for the 1/4-inch fracture were obtained in the basic test series. Here, the difference between the $\frac{v_s}{v_B}$ ratios only reflects the error obtained at this point using equation (44a).

Since the 20-40 mesh beads in the 1/2-inch fracture correspond to the 40-70 mesh size in the 1/4-inch fracture, the predicted value of $\frac{v_s}{v_B}$ should be larger than the experimental value. However, just the opposite occurred. This is due to the inability of equation (44a) to accurately predict sand transport velocities at low slurry flow rates. From the material balance of the amount of solids injected, v_s must be at least 0.236 feet per minute. This yields a minimum transport ratio of 0.072. Thus, the experimental value of 0.100 is within the expected range.

The trend of the pressure curve in Figure 24 is also predicted by the application of scaling techniques to the results obtained in the basic test series. In order of increasing fracture thickness, the predicted pressures are 7.58, 1.64, 1.20, and 1.11 $oz/in^2/ft$.

Effect of Particle Size

To test this parameter, glass beads in the 12-20 and 40-70 mesh range were used in conjunction with the 20-40 mesh beads employed in the basic test series. The average diameter of the beads varied by a factor of 2 between each group. Particle sphericity was essentially constant at 1.0.

The analysis of fracture thickness data indicates that under the simulated and actual test conditions propping agent size has a relatively minor effect on rate of sand advance. Of course, slurries comprised of extremely large or very small particles would alter the behavior of the system.

The flow conditions were held constant during this phase of the investigation. The liquid flow rate was 1 gallon per minute with a

solids concentration of 1 pound per gallon. Two series of tests were performed—runs using a 1/8-inch fracture and tests in a 1/4-inch fracture. The results are given in the table below:

TABLE VII

THE EFFECT OF PARTICLE SIZE ON SAND TRANSPORT

Bead Size	1/8-Inch Fracture			1/4-Inch Fracture		
	v_B (ft/min)	v_s (ft/min)	$\frac{v_s}{v_B}$	v_B (ft/min)	v_s (ft/min)	$\frac{v_s}{v_B}$
12-20	13.4	2.31	0.172	6.72	0.930	0.138
20-40	13.4	2.44	0.182	6.72	0.717	0.107
40-70	13.4	2.56	0.190	6.72	0.872	0.130

In the 1/8-inch fracture, a slight increase in the transport efficiency occurred as the bead diameter was reduced. In fact, a straight line relationship exists between these two parameters. The straight line correlation has no real significance due to the magnitude of the possible experimental error in these tests. The fact that the differences are small is significant. This trend in sand placement efficiencies did not occur in the 1/4-inch fracture. Although the differences in v_s were again small, the fastest sand rate was obtained with the 12-20 mesh beads. While this behavior may be explained by experimental error, the anomaly may lie in the difficulty of establishing multi-layer flow with the large particles. The mode of solids transport in this test consisted of a two-layer sliding deposit with very few particles moving along the surface. The eight-fold increase in bead mass made the formation of a thick deposit difficult. This factor may account for the apparent increase in transport efficiency.

The possible applicability of equation (44b) was checked since terminal velocity incorporates particle diameter as a parameter. The terminal velocities of the beads in the 7 cp oil were 0.386, 0.129, and 0.040 feet per minute, respectively, for the 12-20, 20-40, and 40-70 mesh beads. The calculated values of the concentration term in equation (44b) are 0.61, 0.091, and 0.130. These differences are considerably greater than the variations in the sand transport data. Thus, this method of incorporating particle diameter does not appear to be valid. Equation (44b) may yield a more satisfactory correlation in the suspended flow regime. This, however, was not determined experimentally.

In an extension of this work, additional tests were performed to determine whether bridging would occur at low flow rates with 12-20 mesh beads. Fracture thickness was set at 1/8 inch. The sand concentration in the 7 cp oil was constant at 1 pound per gallon. The flow rates tested were 1/4 and 1/2 gallon per minute. Evidence of bridging was observed at the lowest rate. A detailed description of this aspect of the tests is found in Chapter III. Primarily, the mode of solids transport consisted of a full monolayer of beads with a few particles in the channel above.

The characteristic single-layer deposit flow is reflected in the sand transport data given below:

TABLE VIII

VARIATION OF SAND TRANSPORT EFFICIENCY
WITH FLOW RATE
(b = 1/8 in, 12-20 mesh beads)

Q_o (gpm)	v_B (ft/min)	v_s (ft/min)	$\frac{v_s}{v_B}$
1	13.0	2.31	0.172
1/2	6.72	1.11	0.165
1/4	3.36	0.49	0.146

The value of v_s is essentially proportional to the rate of sand injection. At the lower flow rates more beads were located on top of the single-layer deposit. This accounts for the slight decrease in transport efficiency as the flow rate is reduced.

As expected, the pressure variations obtained in these tests are within the estimated experimental error. Generally, however, pressure increased slightly as the sand transport efficiency increased.

Effect of Particle Angularity

To investigate the effects of sand angularity on the transport mechanism, two commercially available sands were used in the 7 cp oil. Ten-fold magnifications of these materials and the glass beads used in the basic test series are shown in Figure 3. The flow conditions in the two bests were Q_o = 1 gallon per minute at a sand concentration of 1 pound per gallon.

When solids are classed according to sieve size, angularity reduces the average mass of the particles. The differences in average diameter, density, and shape are reflected in the values of the

terminal velocities. In order of increasing angularity, the terminal velocities of these propping agents are 0.129, 0.093, and 0.0812 feet per second. These values were obtained by timing 50 particles and averaging the results.

Although the basic flow mechanism was altered when the natural sands were substituted for glass beads, the change in quantitative results was small. The rate of sand front advance increased from 0.717 feet per minute to 0.780 for the Ottawa sand and 0.834 for the angular sand. These differences may even be less since equation (44a) indicates that the value of v_s for the glass beads under this set of flow conditions is 0.731. The pressure gradients increased from 1.20 $oz/in^2/ft$ to 1.50 and 1.54 for the Ottawa and angular sand, respectively. Because of the magnitude of the possible experimental error, the results of these tests are inconclusive. Additional tests are required to evaluate the effect of particle angularity on solids transport in horizontal fractures.

CHAPTER VI

SUMMARY AND CONCLUSIONS

This study makes a meaningful contribution to the knowledge of slurry flow in horizontal fractures. The correlations and visual observations presented here will not only enable the engineer to better design hydraulic fracture treatments but will provide a real insight into the physical mechanisms involved. Although the number of variables investigated had to be necessarily limited, the ramifications of the work extend beyond the specific investigation.

Consistent, meaningful data were obtained in this study. The level of precision attained during the experimentation is seldom achieved in the area of slurry flow and attests to an exacting experimental design. This success may be attributed to large degree to the accurate sand injection system devised for the tests.

Time lapse photography proved to be a powerful tool. This technique obtained information not possible by conventional means. The extensive photographic evidence proved valuable in defining the basic flow mechanisms. It is significant that the various regimes of flow observed during the tests could be systematically organized with respect to the test variables.

The results presented herein show that the variables studied

in detail—oil viscosity, sand concentration, and flow rate—are important parameters affecting sand movement. They are undoubtedly not the only parameters but within the framework of the basic test series, it has been demonstrated that they can adequately describe the behavior of the system.

Although the transport of solids in fractures is a complex process, a relatively simple empirical approach was successfully used to correlate the data. The pressure behavior observed in these tests exhibits the same general characteristics as slurry flow in circular conduits. The roles of the parameters are altered, but a basic equivalence exists. Despite the wide variation in sand transport mechanisms, a single expression for the rate of sand front advance was effective in correlating this quantity. This indicates that the mode of flow, in itself, is not a controlling factor in sand placement.

The tests performed to investigate the feasibility of scaling slurry flow were encouraging. The results indicate that the scaling procedure proposed in the text may be realistically applied to sand movement in horizontal fractures. These principles may prove useful in extensions of this work, particularly if a radial flow system is studied.

The basic test series shows that sand placement in horizontal fractures under normal treatment conditions is inefficient. However, increased efficiencies are obtained at increased sand concentrations, liquid viscosities, and flow rates. It is not economically feasible to substantially increase the latter. However, increases in the viscosity of the carrying fluid is feasible using gelling agents. This concept is even more attractive economically when the sand is pumped at high solids

concentrations. This reduces the amount of fluid to be gelled, thus holding costs down. Calculations show that the employment of high viscosity-high concentration treatments can increase propped fracture areas several-fold at no increase in treatment cost.

The above comments on fracture design are applicable to conventional treatments in which a multi-layer sand pack is placed. The results of this study show that the placement of partial monolayers in horizontal fractures is extremely difficult. However, it may be possible to achieve the desired increases in fracture flow capacities by overflushing.

A sound basis has been provided for future investigations in the area of slurry flow in fractures. The difficulty in selecting additional work lies not in defining aspects of the problem which have not been previously investigated but in selecting the area of investigation which should be studied first.

Although the detailed investigation was limited to the aforementioned three quantities, data on the scanned variables should be a valuable guide in extending this work. Two variables that were not discussed are conspicuous by their absence. They are the density of solid-liquid phases and surface roughness along the fracture-formation interface. These quantities should be investigated since they could have a pronounced effect on solid transport. Additional investigations must not be limited to the physical dimensions of the flow model used here. The effect of the diverging flow stream in a horizontal radial flow pattern must, from an engineering standpoint, be studied. Quantitative data on slurry flow in vertical fractures also would be valuable.

BIBLIOGRAPHY

1. Beal, C. "The Viscosity of Air, Water, Natural Gas, Crude Oil and its Associated Gases at Oil Field Temperatures and Pressures," Trans. AIME (1946), vol. 165, p. 94.

2. Bingham, E. C. Fluidity and Plasticity, McGraw-Hill Book Co., Inc., New York (1922).

3. Blatch, N. S. "Discussion: Water Filtration at Washington, D.C.," Trans. Am. Soc. Civ. Engrs. (1906), vol. 57, p. 400.

4. Chien, Ning. "The Present Status of Research on Sediment Transport," Trans. Am. Soc. Civ. Engrs. (1956), vol. 121, p. 833.

5. Condolios, E., and Chapus, E. E. "Designing Solids - Handling Pipelines," Chem. Eng. (July 8, 1963), vol. 70, no. 14, p. 131.

6. Davies, S. J., and White, C. M. "An Experimental Study of the Flow of Water in Pipes of Rectangular Section," Proc. Roy. Soc. (London) (1928), vol. 119a, p. 92.

7. Dorozhkin, V. S., Zheltov, Yu. V., and Zheltov, Yu. P. "O Dvishenii smesi Zhidkosti s Peskom v Skvazhine i Treschchine pri Gidravlicheskom Razryve Neftenosnogo Plasta," Akad. Nauk. SSSR, Izv., Otdel Tekh. Nauk. (November 1958), no. 11, p. 37.

8. Durand, R. "Basic Relationships of the Transportation of Solids in Pipes - Experiment Research," Proceedings Minnesota Hydraulic Convention, Part I (1953), p. 89.

9. Einstein, A. "Eine neue Bestimmung der Molekulardimensionen," Ann. Physik (1906), vol. 19, p. 289.

10. Einstein, A. "Correction: Eine neue Bestimmung der Molekulardimensionen," Ann. Physik (1911), vol. 34, p. 591.

11. Happel, John, and Byrne, B. J. "Motion of a Sphere and Fluid in a Cylindrical Tube," Ind. Eng. Chem. (June 1954), vol. 46, no. 6, p. 1181.

12. Harrison, E., Kieschnick, W. F., Jr., and McGuire, W. J. "The Mechanics of Fracture Induction and Extension," Trans. AIME (1954), vol. 201, p. 252.

13. Hazen, A., and Hardy, E. D. "Works for the Purification of the Water Supply of Washington, D. C.," Trans. Am. Soc. Civ. Engrs. (1906), vol. 57, p. 307.

14. Howard, G. C., and Fast, C. R. "Factors Controlling Fracture Ex-Tension," Paper at Spring Meeting, Petroleum and Natural Gas Div., CIM, Edmonton (1957).

15. Hughmark, G. A. "Aqueous Transport of Settling Slurries," Ind. Eng. Chem. (May 1961), vol. 53, no. 5, p. 389.

16. Huitt, J. L. "Fluid Flow in Simulated Fractures," AIChE Journal (June 1956), vol. 2, no. 2, p. 259.

17. Izymova, A. M., and Shan'gin, N. N. "Dvizhenie Peska v Gorizontal'noi Treschchine, Obrazovavsheisya, pri Gidrorazryve," Neftyanoe Khozyaistvo (April 1958), vol. 36, no. 4, p. 44.

18. Johnstone, R. E., and Thring, M. W. Pilot Plants, Models, and Scale-up Methods in Chemical Engineering, McGraw-Hill Book Co., Inc., New York (1957).

19. Kern, L. R., Perkins, T. K., and Wyant, R. E. "The Mechanics of Sand Movement in Fracturing," Trans. AIME (1959), vol. 216, p. 403.

20. Knudsen, J. G., and Katz, D. L. Fluid Dynamics and Heat Transfer, McGraw-Hill Book Co., Inc., New York (1958).

21. Lapple, C. E. Fluid and Particle Mechanics, Univ. of Delaware, (1951).

22. Newitt, D. M., Richardson, J. F., and Abbott, M. "Hydraulic Conveying of Solids in Horizontal Pipes," Trans. Instn. Chem. Engrs. (1955), vol. 33, p. 94.

23. Nickuradse, J. Forsch. Gebiete Ingenieurw Forschungsheft (Sept. - Oct. 1932), reprinted in Petroleum Engineer (1940), vol. 11, no. 6, p. 164; no. 8, p. 75; no. 9, p. 124; no. 11, p. 38; no. 12, p. 83.

24. Page, F., Jr., Corcoran, W. H., Schlinger, W. G., and Sage, G. H. "Temperature and Velocity Distributions in Uniform Flow between Parallel Plates," Ind. Eng. Chem. (1952), vol. 44, p. 419.

25. Perkins, T. K., and Kern, L. R. "Widths of Hydraulic Fractures," Trans. AIME (1961) vol. 222, p. 937.

26. Smith, R. A. "Experiments on the Flow of Sand-Water Slurries in Horizontal Pipes," Trans. Instn. Chem. Engrs. (1955), vol. 33, p. 85.

27. Spells, K. E. "Correlations for Use in Transport of Aqueous Suspensions of Fine Solids Through Pipes," Trans. Instn. Chem. Engrs. (1955), vol. 33, p. 79.

28. Streeter, V. L. Handbook of Fluid Dynamics, McGraw-Hill Book Co., Inc., New York (1961).

29. Thomas, D. G. "Minimum Transport Velocity for Flocculated Suspensions in Horizontal Pipes," AIChE Journal (September 1961), vol. 7, no. 3, p. 423.

30. Thomas, D. G. "Minimum Transport Velocity for Large Particle Size Suspensions in Rough Horizontal Pipes," AIChE Journal (July 1962), vol. 8, no. 3, p. 373.

31. Ting, A. P., and Luebbers, R. H. "Viscosity of Suspensions of Spherical and Other Isodimensional Particles in Liquids," AIChE Journal (March 1957), vol. 3, no. 1, p. 111.

32. Wahl, H. A. "Fracture Design in Liquid-Saturated Reservoirs," Journal of Petroleum Technology (April 1963), vol. 15, no. 4, p. 437.

33. Walker, J. E., Whan, G. A., and Rothfus, R. R. "Fluid Friction in Noncircular Ducts," AIChE Journal (December 1957), vol. 3, no. 4, p. 484.

34. Whan, G. A., and Rothfus, R. R. "Characteristics of Transition Flow Between Parallel Plates," AIChE Journal (June 1959), vol. 5, no. 2, p. 204.

APPENDIX A

PRESSURE BEHAVIOR IN THE BASIC TEST SERIES

Run No.	μ_o (cp)	Q_l (gpm)	Q_s (lb/min)	C	v_B (ft/min)	$\mu_o v_B$ (cp-ft/min)	$\left(\frac{dP}{dL}\right)_l$ (oz/in²/ft)	Experimental Results: $\left(\frac{dP}{dL}\right)_s$ (oz/in²/ft)	Experimental Results: $\frac{\Delta P}{L}$ (oz/in²/ft)	ψ	From Equation (41): $\frac{\Delta P}{L}$ (oz/in²/ft)	% Error	No. of Data Points
1	7	4	4	0.0456	26.88	187.1	0.200	1.18	1.38	5.90	1.37	+ 0.7	23
2	7	1	4	.1606	7.64	53.1	0.057	1.60	1.66	28.07	1.71	- 3.0	17
3	7	1	2/3	.0310	6.62	46.1	0.049	1.18	1.23	24.08	1.06	+16.0	13
4	7	8	8	.0456	53.76	374.3	0.400	1.06	1.46	2.65	1.65	-11.6	7
5	7	1	1/4	.0118	6.49	45.2	0.048	1.10	1.15	22.92	0.80	+43.7	12
6	7	1	1	.0456	6.72	46.8	0.050	1.15	1.20	23.00	1.17	+ 2.5	13
7	7	1/4	1/4	.0456	1.68	11.7	0.013	1.17	1.18	90.00	1.12	+ 5.3	20
8	7	1	8	.2767	8.85	61.6	0.066	1.84	1.91	27.87	2 04	- 6.4	13
43	7	8	2	.0118	51.92	361.6	0.387	0.65	1.04	1.68	1.23	-15.5	6
44	7	8	4	.0234	52.56	365.8	0.391	0.85	1.24	2.17	1.41	-12.0	6
45	7	4	8	.0873	28.10	195.6	0.209	1.37	1.58	6.56	1.65	- 4.2	6
46	7	4	1	.0118	25.96	180.8	0.193	0.75	0.94	3.89	0.99	- 5.1	12
24	58	4	4	.0456	26.88	1,554	1.66	1.69	3.35	1.02	3.38	- 0.9	5
25	58	1	1	.0456	6.72	388.5	0.415	1.37	1.79	3.30	1.67	+ 7.1	11
26	58	4	1	.0118	25.96	1,501	1.61	1.15	2.76	0.714	2.78	- 0.3	9
27	58	4	8	.0873	28.10	1,624	1.74	2.49	4.23	1.43	3.94	+ 7.4	7
28	58	1	8	.2767	8.85	511.3	0.547	2.69	3.24	4.92	3.04	+ 6.6	8
29	58	1	1/4	.0118	6.49	375.4	0.401	0.78	1.18	1.95	1.25	- 5.6	17
30	58	8	2	.0118	51.92	3,003	3.21	1.37	4.58	0.427	4.81	- 4.8	4
31	58	8	8	.0456	53.76	3,108	3.32	2.49	5.81	0.750	5.66	+ 2.6	4
32	58	8	4	.0234	52.56	3,037	3.25	1.65	4.90	0.508	5.14	- 4.7	6
33	488	1	1	.0456	6.72	3,280	3.51	2.45	5.96	0.698	5.91	+ 0.8	11
34	488	1	4	.1606	7.64	3,724	3.98	3.92	7.90	0.985	8.48	- 6.8	13
35	488	1	1/4	.0118	6.49	3,168	3.39	1.17	4.56	0.345	5.04	- 9.6	13
36	488	1	8	.2767	8.85	4,316	4.61	5.08	9.69	1.10	11.52	-15.9	11
37	488	4	1	.0118	25.96	12,670	13.55	3.65	17.20	0.269	17.93	- 4.1	6
38	488	4	4	.0456	26.88	13,120	14.02	7.51	21.53	0.536	20.35	+ 5.8	4
39	488	4	8	.0873	28.10	13,710	14.66	8.96	23.62	0.611	23.33	+ 1.2	4
40	488	2	2	.0456	13.44	6,559	7.01	3.97	10.98	0.566	10.72	+ 2.4	5
41	488	2	8	.1606	15.28	7,448	7.96	7.16	15.12	0.899	15.36	- 1.7	5
42	488	2	1/2	.0118	12.98	6,336	6.77	2.93	9.70	0.433	9.33	+ 3.9	11
13	3.20	1	1	.0456	6.72	21.6	0.023	0.99	1.01	43.04	1.13	-10.6	13
14	14.2	1	1	.0456	6.72	95.5	0.102	1.23	1.33	12.06	1.24	+ 7.2	11
23	76.0	1	1	.0456	6.72	510.9	0.546	1.40	1.95	2.56	1.85	+ 5.4	5

APPENDIX B

RATE OF SAND FRONT ADVANCE DURING BASIC TEST SERIES

Run No.	μ_o (cp)	Q_l (gpm)	Q_s (lb/min)	C	v_B (ft/min)	Experimental Results v_s (ft/min)	Experimental Results $\frac{v_s}{v_B}$	Experimental Results F	Prediction from Equation (44a) v_s (ft/min)	Prediction from Equation (44a) $\frac{v_s}{v_B}$	Prediction from Equation (44a) F	Prediction from Equation (44a) % Error	Prediction from Equation (46) v_s (ft/min)	Prediction from Equation (46) $\frac{v_s}{v_B}$	Prediction from Equation (46) F	Prediction from Equation (46) % Error	No. of Data Points
1	7	4	4	0.0456	26.88	4.49	0.167	0.432	4.78	0.178	0.405	- 6.1	4.78	0.178	0.405	- 6.1	23
2	7	1	4	.1606	7.64	2.60	.341	.740	2.45	.321	0.709	+ 6.1	1.95	0.255	0.995	+33.3	17
3	7	1	2/3	.0310	6.62	0.540	.082	.597	0.527	.080	0.613	+ 2.5	0.597	0.090	0.544	- 9.5	13
4	7	8	8	.0456	53.76	12.54	.233	.309	12.17	.226	0.319	+ 3.0	12.00	0.223	0.323	+ 4.5	7
5	7	1	1/4	.0118	6.49	0.272	.042	.443	0.233	.036	0.517	+16.7	0.324	0.050	0.372	-16.0	12
6	7	1	1	.0456	6.72	0.717	.107	.674	0.731	.109	0.661	- 1.9	0.768	0.114	0.632	- 6.6	13
7	7	1/4	1/4	.0456	1.68	0.151	.090	.801	0.114	.068	1.060	+32.5	0.124	0.074	0.974	+21.8	20
8	7	1	8	.2767	8.85	4.43	.501	.873	4.66	.527	0.830	- 4.9	3.29	0.372	1.175	+34.7	13
43	7	8	2	.0118	51.92	3.87	.074	.250	3.85	.074	0.251	+ 0.5	5.06	0.097	0.192	-23.5	6
44	7	8	4	.0234	52.56	6.92	.132	.280	6.85	.130	0.284	+ 1.0	7.80	0.148	0.250	-11.3	6
45	7	4	8	.0873	28.10	8.42	.300	.459	8.63	.307	0.449	- 2.4	7.56	0.269	0.513	+11.4	6
46	7	4	1	.0118	25.96	1.35	.052	.358	1.51	.058	0.321	-10.6	2.03	0.078	0.238	-33.5	12
24	58	4	4	.0456	26.88	8.83	.328	.220	9.23	.343	0.210	- 4.3	8.52	0.317	0.227	+ 3.6	5
25	58	1	1	.0456	6.72	1.30	.193	.374	1.42	.211	0.342	- 8.5	1.37	0.204	0.353	- 4.1	11
26	58	4	1	.0118	25.96	3.93	.151	.123	3.89	.150	0.124	+ 1.0	3.59	0.138	0.135	+ 9.5	9
27	58	4	8	.0873	28.10	13.40	.477	.289	14.50	.516	0.267	- 7.6	13.44	0.478	0.289	- 0.3	7
28	58	1	8	.2767	8.85	6.24	.705	.620	6.13	.693	0.630	+ 1.8	5.86	0.662	0.660	+ 6.5	8
29	58	1	1/4	.0118	6.49	0.392	.060	.308	0.601	.093	0.201	-34.8	0.577	0.089	0.209	-32.1	17
30	58	8	2	.0118	51.92	12.01	.231	.081	9.91	.191	0.098	+21.1	9.00	0.173	0.108	+33.3	4
31	58	8	8	.0456	53.76	23.76	.442	.163	23.50	.437	0.165	+ 1.1	21.30	0.396	0.182	+11.5	4
32	58	8	4	.0234	52.56	16.60	.316	.117	15.24	.290	0.128	+ 8.9	13.86	0.264	0.140	+19.8	6
33	488	1	1	.0456	6.72	2.32	.345	.209	2.32	.345	0.209	+ 0.0	2.47	0.368	0.196	- 6.1	11
34	488	1	4	.1606	7.64	5.54	.726	.350	4.82	.632	0.401	+14.9	6.18	0.809	0.314	-10.4	13
35	488	1	1/4	.0118	6.49	1.23	.190	.098	1.21	.186	0.100	+ 1.7	1.03	0.159	0.117	+19.4	13
36	488	1	8	.2767	8.85	7.96	.899	.486	7.51	.849	0.515	+ 6.0	10.44	1.180	0.371	-23.8	11
37	488	4	1	.0118	25.96	8.36	.322	.058	7.85	.302	0.062	+ 6.5	6.42	0.247	0.075	+30.2	6
38	488	4	4	.0456	26.88	14.54	.541	.133	15.02	.559	0.129	- 3.2	15.24	0.567	0.127	- 4.6	4
39	488	4	8	.0873	28.10	20.50	.730	.189	21.32	.759	0.182	- 3.8	23.94	0.852	0.162	-14.4	4
40	488	2	2	.0456	13.44	5.93	.441	.164	5.90	.439	0.164	+ 0.5	6.12	0.455	0.158	- 3.1	5
41	488	2	8	.1606	15.28	11.71	.767	.331	12.30	.804	0.316	- 4.8	15.48	1.013	0.250	-24.4	5
42	488	2	1/2	.0118	12.98	3.12	.240	.078	3.08	.237	0.079	+ 1.3	2.57	0.198	0.094	+21.4	11
13	3.2	1	1	.0456	6.72	0.620	.092	.781	0.565	.084	0.858	+ 9.7	0.618	0.092	0.784	+ 0.3	13
14	14.2	1	1	.0456	6.72	0.880	.131	.550	0.964	.143	0.504	- 8.7	0.908	0.135	0.534	- 3.1	11
23	76	1	1	.0456	6.72	1.51	.225	.320	1.55	.230	0.313	- 2.6	1.47	0.219	0.329	+ 2.7	5

APPENDIX C

EXPERIMENTAL DATA OBTAINED OUTSIDE THE BASIC TEST SERIES

Run No.	Q_I (gpm)	Q_S (lb/min)	C	Propping Agent	Mesh Size	b (in)	v_B (ft/min)	$\left(\frac{dP}{dL}\right)_I$ (oz/in²/ft)	Pressure Behavior: $\left(\frac{dP}{dL}\right)_S$ (oz/in²/ft)	Pressure Behavior: $\frac{\Delta P}{L}$ (oz/in²/ft)	Pressure Behavior: ψ	Sand Front Advance: v_s (ft/min)	Sand Front Advance: $\frac{v_s}{v_B}$	Sand Front Advance: F	No. of Data Points
9	1	1	0.0456	beads	12-20	1/4	6.72	0.050	1.06	1.11	21.2	0.930	0.138	0.522	16
10	1	1	.0456	beads	40-70	1/4	6.72	0.050	1.30	1.35	26.0	0.876	.130	.555	16
11	1	1	.0456	Ottawa sd.	20-40	1/4	6.72	0.050	1.45	1.50	29.0	0.780	.116	.622	22
12	1	1	.0456	ang. sand	20-40	1/4	6.72	0.050	1.49	1.54	29.8	0.834	.124	.581	22
15	1	1	.0456	beads	20-40	1/8	13.44	0.400	1.22	1.62	3.05	2.44	.182	.396	10
16	1	1	.0456	beads	20-40	1/16	26.88	3.20	2.52	5.72	0.79	10.8	.400	.180	0
17	1	1	.0456	beads	20-40	1/2	3.36	0.006	1.18	1.19	189.	0.337	.100	.714	12
18	1	1	.0456	beads	12-20	1/8	13.44	0.400	0.93	1.33	2.32	2.31	.172	.419	8
19	1/2	1/2	.0456	beads	12-20	1/8	6.72	0.200	1.13	1.33	5.65	1.11	.165	.437	10
20	1/4	1/4	.0456	beads	12-20	1/8	3.36	0.100	1.14	1.24	11.4	0.49	.146	.494	12
21	1	1	.0456	beads	40-70	1/8	13.44	0.400	1.33	1.73	3.32	2.56	.190	.379	9
22	1/2	1/2	.0456	beads	40-70	1/8	6.72	0.200	1.26	1.46	6.30	0.896	.133	.542	12
47	1	1	.0456	beads	70-140	1/16	26.88	3.20	1.92	5.12	0.60	10.47	.390	.185	9
48	1/2	1	.0873	beads	70-140	1/16	14.05	1.67	2.24	3.91	1.34	6.69	.476	.290	9
49	1/8	1	.2767	beads	70-140	1/16	4.42	0.526	2.70	3.23	5.13	3.02	.683	.640	10
50	1/8	1/8	.0456	beads	70-140	1/16	3.36	0.400	1.28	1.68	3.20	0.613	.152	.474	8
51	1/2	1/8	.0118	beads	70-140	1/16	12.98	1.55	0.89	2.44	0.57	2.05	.169	.110	7

APPENDIX D

NOMENCLATURE

a, d, m, A_n, B = empirical constants

b = fracture thickness - in

C = volumetric solids concentration in slurry - ft^3/ft^3

d = diameter of solid particles - in

D = pipe diameter

D_e = equivalent diameter of a conduit

f = Fanning friction factor

f_D = drag coefficient

F = fraction of fracture thickness occupied by sand

F_l = empirical constant of Durand

g = acceleration due to gravity

g_c = mass-force conversion factor

h = head loss

h_{min} = minimum head loss in slurry transport

H_o = height of open section in vertical fractures

H_s = height of settled sand in vertical fractures

K = proportionality constant for Stokes' and Newton's laws

L = length of flow channel - feet

P = pressure - oz/in^2

Q_B = bulk flow rate of slurry - gal/min

Q_l = liquid flow rate - gal/min

Q_o = oil flow rate - gal/min

Q_s = mass flow rate of sand - lb/min

Re = Reynolds number

S = distance sand deposit extends from well bore

t = time

v = velocity

v_B = average bulk velocity - ft/min

v_D = average bulk slurry velocity minus rate of sand front advance - ft/min

v_e = equilibrium velocity for vertical fractures

v_{max} = maximum velocity

v_m = minimum bulk velocity necessary for suspended flow

v_s = rate of advance of sand front - ft/min

v_t = terminal velocity - ft/sec

v_w^* = friction velocity at the wall

x = horizontal distance along the line of flow

y = vertical distance to boundary of fracture

y_c = vertical distance from center of fracture

Z = height of surface roughness

μ = viscosity

μ_o = oil viscosity, cp

μ_s = viscosity of solid-liquid slurry, cp

ρ_p = density of solid particles

ρ_l = density of liquid phase

ρ_s = density of slurry

τ = shear stress

τ_w = shear stress at the wall

ϕ = porosity of propping agents

ψ = ratio of the pressure gradient increase due to the solid phase to the pressure gradient of clear fluid